NON-PERTURBATIVE ASPECTS

OF

YANG-MILLS-HIGGS THEORY

Dissertation

for the acquisition of the academic title

doctor rerum naturalium (Dr. rer. Nat.)

submitted to the Council of the Faculty of Physics and Astronomy

Friedrich Schiller University

Jena

by **MSc. Tajdar Mufti**

born on 08.07.1981

dissertation submitted on 09-12-2014

Contents

Acknowledgments

I would like to use this opportunity to express my gratitude to everyone who contributed and supported throughout my research work as a PhD student. I am extremely thankful to their support, guidance, invaluable advices and constructive criticism which made it possible to complete my PhD thesis and in the meantime acquire experience and exposure i gained.

I am extremely thankful to my supervisor Prof. Axel Maas who supported, guided and advised me throughout my PhD work with immense patience, and Prof. Holger Gies for approving as a second supervisor. I am extremely thankful to Prof. Andreas Wipf and Prof. Gerhard Schäfer for giving me opportunity to take part in their offered courses as teaching assistant. Beside fulfilling a requirement for qualifying for PhD defense, it further increased my teaching experience and understanding the respective subjects. I am extremely thankful to Prof. Friedhelm Bechstedt for allowing me to take a course in Solid State Physics, which was a crucial requirement for qualifying for PhD defense.

I would like to thank Graduate School Jena (GRK 1523/1) and DFG (grant number MA 3935/5-1) for supporting me financially. Without their financing it would be impossible to do research, and gain international exposure and knowledge by attending and/or contributing in research activities, conferences, summer schools and other scientific meetings as a PhD student.

I would also like to express my extreme gratitude to the staff of the office of our faculty, specially Ms. Lisann Schmidt, for taking care of all small and important non-academic matters, which immensely facilitated my research activities throughout my time here as a PhD student.

Abstract

Yang-Mills-Higgs theory, being a part of the Standard Model, presents a great opportunity for investigation both from the point of view of theory and phenomenology. It contains regions in the theory's parameter space which are suitable for Higgs like Physics and QCD like Physics. At the same time it presents a chance to study spectrum of the weak sector. For this purpose the choice of the SU(2) gauge group and scalar field in fundamental SU(2) are considered.

The correlation functions are the key for investigation, because at least in principle knowing all the correlation functions gives us all the information about the theory under consideration. For the case of gauge dependent quantities, with the selection of minimal Landau gauge, propagators and three point vertices are considered for investigation in both regions of QCD like Physics and Higgs like Physics. It is found that even when scalar (Higgs) propagator and its vertices with the gauge fields are in agreement with what tree level perturbative calculations suggest, there is a considerable deviation in other propagators and other vertices.

For the purpose of exploring spectrum in the theory, 0^+ singlet and 1^- triplet channels are considered. The decay from 0^+ to 1^- channel is also studied. There also exists a duality between single particle states and bound states, which is also studied in detail. For the Higgs which is discovered at LHC, the duality is found to exist while for heavier Higgs the existence of duality is no longer observed. Overall, the explored spectra suggest that Yang-Mills-Higgs theory may be a weakly interacting theory possibly till the time when Higgs mass is in TeV scale and the naive picture of a weakly interacting theory breaks down anyway and the theory becomes non-perturbative.

Chapter 1

Introduction

1.1 Introduction

Understanding the nature at its fundamental level is, without any doubt, one of the most ambitious tasks. Historically, the speculations and investigations started from celestial objects since gravity was the first known force. With the passage of time, as we learn about the nature at microscopic level, a new trend to understand fundamental particles in nature and different forces in nature also sets in. A huge amount of efforts have already been made in an attempt to understand how the nature behaves at its fundamental scale. The question lying at the heart is, how fundamental particles interact with each other. With time it was discovered that the long known gravitational interaction is not the only possible interaction. There are, so far, three more kinds of interactions, hence three more kinds of forces, namely Electromagnetic, Weak and Strong interactions [1]. Each interaction has its (their) own mediating particle(s). Since Gravitational interactions have negligible effects for the current energies in the experiments, their effects are usually not considered while attempting to understand fundamental particles and their interactions, specially for low energies. From the theoretical side, so far the accepted theory of nature, the Standard Model [2], contains Electromagnetic, Weak and Strong interactions.

For the gravitational interactions, one of the worst problem is that inclusion of gravitational interaction renders the perturbative picture of the Standard Model non-renormalizable. Hence negligible contribution and the problem of renormalization kept the Standard Model from smoothly including gravitational interaction in it.

It was realized few decades ago that, just like combining electricity and magnetism, Electromagnetic and Weak interactions can also be combined together to form *Electroweak sector*. The predicted particles, W and Z bosons, were soon discovered. It also revived the question whether it is possible to combine all the 4 forces together to form a single theory. Several *so called* Grand Unified Theories [3] have been proposed which combine all but Gravitational force, they await experimental confirmation. For the case of the Standard Model, as time goes by, experimental results keep confirming validity of the Standard Model as a trustable theory

for fundamental interactions.

Beside combining the forces, there exists an interesting idea that every fundamental particle has its *so called* super partner with a different *kind* of spin. For example, every lepton (such as Electron) has a super partner which is a boson. A theory with this idea is called a Supersymmetry theory [4]. So far, there exists no claim of experimental finding of Supersymmetry in nature [5, 6]. Hence the Standard Model still remains as the the only trustable candidate to describe fundamental particles and their interactions, as observed in accelerators.

Beyond the observations in the results by accelerators, there exist a number of observations which have no explanation in the Standard Model. Baryogenesis, dark energy and dark matter are some of the examples. However, these are more in the common domain of particle Physics and Cosmology, and their role in the observations inside accelerators are not as significant as in the data for Astroparticle Physics.

There also exist theories which are speculated to be working at around Plank scale energy, Superstrings is an example. However, the obvious problem is the unavailability of data at such high energy values.

Hence it becomes clear that so far the Standard Model is the only known reliable theory to describe nature at its fundamental level.

One of the main tests of the Standard Model was to find a way to explain the experimental results involving massive particles in such a way that the theory remains renormalizable. In the sense of perturbative calculations, it means that the theory remains renormalizable to every order of perturbative calculations. From the theoretical side a mechanism, known as Higgs mechanism, seems very convincing. It demands existence of a scalar particle in the Standard Model, known as Higgs, which triggered decades long experimental searches for Higgs. Finally in 2012 these searches have paid off in the form a discovery [7, 8] at the LHC, CERN. At the moment, further results (statistics) confirm, at least, existence of a Higgs (like) particle [1]. This historic discovery has further increased our confidence in the Standard Model.

If we briefly look at our scientific progress chronically, the Standard Model was historically taken as a perturbative explanation of the fundamental particles for many problems. As the time passes by, perturbative calculations turned out to be in great agreement with experimental results with remarkable accuracy, and hence the perturbative picture for many problems is justified. However, there are a number of problems for which perturbative picture of fundamental interactions have proved to be either irrelevant or of a little use. Low energy QCD, phase transition, confinement and bound states are among examples of them [2]. For these problems, either perturbative calculations do not give satisfactory results or it becomes irrelevant in the

---

[1]The 2013 noble prize in Physics have already been given to Francois Englert and Peter W. Higgs for their contribution in theoretical Physics in this area.

[2]Confinement and Bound states are focused on during in this thesis.

sense that perturbative picture does not fit for the problem.

For the case of Higgs particle, irrespective of the outcome of experiments, the perturbative picture demands that the Higgs *mass* must be less than around 750 GeV. The reason for this restriction is that for heavier Higgs, the coupling constant becomes large hence rendering perturbative calculations useless [3] (trivially because this is a perturbation theory). Fortunately Higgs *mass* turns out to be around 126 GeV. Finding of the Higgs with this *mass* not only supports the perturbative picture of the Standard Model, but also encourages the idea of a perturbative picture of Supersymmetry, and hence existence of Supersymmetric particles. However, let us note here that the nature could have chosen *any* value of mass for Higgs which makes it very obvious that it is only a pleasant surprise that perturbative picture of nature works well, where it works, just because of nature's own selection.

Bound states are, in the author's opinion, the most interesting area where perturbative description looses usefulness. As it is already known that in perturbative picture interacting particles come from very large distance from the point of interaction, where they are essentially free particles and are not aware of existence of other particle(s), and after interacting with each other the resultant particles go (infinitely) far from the interaction point that they are in oblivion of existence of other particles. In bound states, this may not happen which means that perturbative picture becomes irrelevant. The situation becomes even more interesting for the case of low energy Quantum Electrodynamics which is in remarkable agreement with experimental results. It is already known that existence of atoms and molecules, and most of the world around us, is mostly due to the Electromagnetic interaction at low energies. The presence of bound states in the energy regime where QED works remarkably well is a manifestation of how difficult it is to avoid non-perturbative aspects for phenomenology as well as complete understanding of a theory.

Another interesting example is the problem of confinement [9], which is a non-perturbative problem. For the Yang-Mills-Higgs theory, there is a specific realization of confinement which will be used in chapter 3.

Even for the situations when perturbative calculations work well, it remains to be investigated how much role non-perturbative contributions play in the perturbative picture. These investigations are also important for the development and improvement of non-perturbative techniques themselves.

Hence both from the point of view of complete theoretical understanding and phenomenology, for an accepted theory for phenomenology (currently the Standard Model) it is crucial to investigate the non-perturbative aspects of the theory.

When it comes to non-perturbative calculations, serious challenges arise. Three among a number of methods for non-perturbative calculations are Dyson-Schwinger equations (DSE)

calculations [10], functional renormalization group (FRG) method [11] and lattice calculations [12]. Each of them comes with its own limitations and challenges. For example, for the case of DSE calculations, finding solutions to the full DSEs is, to say the least, a very hard problem. Different assumptions for unknown correlation functions in the equations and truncations are made in order to find solutions. As a result, if there exist a solution, it will be the one depending upon assumptions and truncation. For the case of lattice calculations, the results are usually effected by finite volume as well as descritization effects [13].

Given the challenges posed by non-perturbative calculations, the most reasonable starting point of such investigations is to consider only one part of the whole Standard Model with the hope that later on further parts of the Standard Model will be added once the part at hand is understood well and the challenges of non-perturbative techniques are also met. Already extensive efforts have been made to non-perturbatively explore Yang-Mills (**YM**) theory [14], which is also a part of the Standard Model. Hence, the obvious choice is to glue YM theory with another part of the Standard Model. Higgs field [12] in fundamental SU(2) is added to the YM theory, hence the result is Yang-Mills-Higgs (**YMH**) theory [13].

Since the resulting theory is important in the sense that the fields in the theory, and hence in the Lagrangian, interact with each other, investigation of YMH theory should start with computation of propagators and continue to vertices in the theory [13] and even higher correlation functions. Computation of such quantities will also allow us to compare the results with YM theory to understand how the quantities are effected by introduction of another field. For completion, knowing all the correlation functions in a theory can, in principle, be used to understand the whole theory.

From the point of view of phenomenology, YMH theory offers us a chance to study spectrum of energy states in the theory and possible transitions [15] among them. For this purpose, gauge invariant correlation functions are used, details are given in chapter 2. Though in principle any gauge theory can have such spectrum, study of YMH theory has more importance since it is a part of the Standard Model.

In order to explore areas such as confinement and Spectroscopy in the theory, calculation of both gauge dependent and gauge invariant correlation functions are performed. For the case of gauge dependent correlation functions, the chosen gauge is Minimal Landau gauge [16]. Beside understanding the interaction vertices, they can also be used to calculate gauge invariant quantities. A good example is the method of DSEs in which known correlation functions act as input for calculations.

It has already been mentioned before that YMH is a part of the Standard Model. Hence, not considering the complete Standard Model effects the quantities calculated, specially observables. Hence, for any phenomenology, calculation of observables is made with the assumption that adding other parts of the Standard Model will not introduce considerable deviation from

the results. However, this assumption can only be checked after taking into account the remaining parts of Standard Model.

The thesis is arranged as follows: The current chapter is mostly focusing on the relevant aspects of Yang-Mills-Higgs theory which will be used in the coming chapters. The second chapter is on the gauge invariant quantities along with their aspects, which will be used to study the spectrum in the theory while almost always ignoring all the channels except 0^+ singlet and 1^- triplet. In the third chapter, gauge dependent quantities, propagators, three point vertices and running coupling are considered in detail. In the end conclusion is given.

1.2 Yang-Mills-Higgs Theory

Yang-Mills theory [3] is a non-abelian gauge theory, and a part of the Standard Model. Being a non-abelian gauge theory, it is a richer theory compared with Quantum Electrodynamics, which is an abelian gauge theory. It has only one field, i.e., gauge field, introduction of the ghost field depends upon the gauge used. The Lagrangian of the YM theory (L_{YM}), while neglecting the Lagrangian part of ghost fields, is given by

$$L_{YM} = -\frac{1}{4} F_{\mu\nu}^a F_a^{\mu\nu} \tag{1.1}$$

where

$$F_{\mu\nu}^a = \partial_\mu W_\nu^a - \partial_\nu W_\mu^a - g f^{abc} W_\mu^b W_\nu^c \tag{1.2}$$

In above $F_{\mu\nu}^a$ is the field strength tensor while W_μ^a is the gauge field of the theory, g and f^{abc} are the gauge coupling constant and structure constant of the corresponding Lie algebra [3], respectively, and ∂_μ denotes partial derivative with respect to Lorentz index μ. In the YM theory, the Lagrangian contains terms with three and four gauge fields which represent the vertices of the theory.

For the scalar field [3] the Lagrangian (L_s) is

$$L_s = (\partial_\mu h_k)^\dagger (\partial^\mu h^k) - \frac{1}{2} m^2 h^{i\dagger} h^i - \lambda (h^{a\dagger} h^a)(h^{b\dagger} h^b) \tag{1.3}$$

where h_k is the scalar field of the Lagrangian while m is the tree level mass of the scalar field and λ is the quartic coupling constant. In order to write a gauge theory Lagrangian, it is necessary to make changes in the L_s. Thus changing the partial derivatives into the covariant derivatives,

$$\partial_\mu \phi_i \to D_\mu^{ik} \phi_k = \delta^{ik} \partial_\mu \phi_k - ig W_\mu^s t_s^{ik} \phi_k \tag{1.4}$$

renders the theory status of a gauge theory. In above equations W_μ^s has the same meaning as in the L_{YM}, D_μ^{ik} are covariant derivatives, and t_s^{ik} are elements of Pauli matrices for the theory.

---

[3]The scalar field in the theory is also the Higgs field. Hence, the words scalar and Higgs will be used interchangeably throughout the thesis.

Gluing both Lagrangians gives us the final Lagrangian L_{YMH} in continuum for YMH theory[4].

$$L_{YMH} = -\frac{1}{4}F^a_{\mu\nu}F^{\mu\nu}_a + (D^{ik}_\mu \phi_k)^\dagger (D^{il}_\mu \phi_l) - \frac{1}{2}m^2 \phi^{i\dagger}\phi^i - \lambda(\phi^{a\dagger}\phi^a)(\phi^{b\dagger}\phi^b) \qquad (1.5)$$

In YMH theory there are two fields, i.e., gauge field and scalar field, while ghost field is introduce for gauge fixing if required. Since the theory is a part of the Standard Model, the theory has SU(2) gauge group and fundamental scalar with SU(2) flavor symmetry. It means that scalar field in the theory is a complex doublet and contains four real scalar degrees of freedom which is scalar field's flavor symmetry. For the case of scalar field, which is also the Higgs field in the theory, the flavor symmetry is also known as custodial symmetry breaking in literature. There are three parameters in the theory; g, λ, and m. It means that when lattice simulations are conducted, the results will depend upon the chosen set of parameters. As it will be explained later on, this issue becomes highly non-trivial when close examinations are made for different sets of parameters.

For the purpose of completion and consistency, there are two (main) standard schemes to take a scalar product in differential geometry. In one scheme, one vector is covariant vector and the other one is contravariant vector, while in the other scheme both vectors can be covariant or contravariant but they also involve the metric tensor or some associated metric tensor. Here for us, the coordinates are orthogonal and the metric tensor components are constant (equal to 1, to be precise). It means that writing both vectors as covariant or contravariant vectors can be done without any explicit mention of the metric tensor. Hence, for our situation alittle bit of sloppiness makes no difference as long as the indices are balanced in equations. Furthermore, Einstein summation convention is used as in standard texts [17, 18].

1.3   Lattice Calculation Method

In comparison with Dyson Schwinger equations and Functional Renormalization Group methods, lattice calculation method is an ab initio technique for calculations [12] in the sense that all the configurations are numerically computed directly from the action. In this method a whole numerical computation is performed to calculate fields, or components, in the theory which can be used to calculate the quantities of interest. The simulation procedure will be given in section 1.5. Lattice method was used for all the computations in the following.

As the name itself implies, lattice calculation method is the one in which the spacetime coordinates are reduced from continuum into pre-decided number of points along each dimension and nothing is defined in between. Thus the fields defined in such an environment are also not continuous functions of space time and exist only on the lattice points. The number of points along each dimension defines the dimension of the lattice along that dimension, hence the volume of the lattice is trivially just the multiple of the number of the points in all dimensions. Similarly the derivatives turn into differences and integrals turn into summations. The

---

[4]The ghost field is not shown in the Lagrangian L_{YMH} since they are implemented after gauge fixing.

action is a dimensionless quantity on lattice which means that there has to be one particular variable which could take care of dimensions of each quantity in the action and Lagrangian. Mathematically,

$$x_\mu \to n_\mu a \tag{1.6}$$

$$\phi(x) \to \phi(na) \tag{1.7}$$

$$\int d^4x \to a^4 \sum_n \tag{1.8}$$

$$\partial_\mu \phi \to \frac{\phi((n+1)a) - \phi(na)}{a} \tag{1.9}$$

$$D\phi \to \Pi d\phi(na) \tag{1.10}$$

where a is the parameter which is used to make the action dimensionless. x, n and ϕ are the points in continuum, the point in lattice space and field of the Lagrangian, respectively.

Using above equations, the lattice version of action (volume integrated form of Lagrangian in equation 1.5) S is given by [13],

$$S = \beta \sum_x (1 - \frac{1}{2} \sum_{\mu<\nu} R(tr(U_{\mu\nu}(x))) + \phi^\dagger(x)\phi(x) + \lambda(\phi^\dagger(x)\phi(x) - 1)^2$$

$$-\kappa \sum_\mu (\phi^\dagger(x)U_\mu(x)\phi(x+e_\mu) + \phi(x+e_\mu)^\dagger U_\mu(x)^\dagger \phi(x))) \tag{1.11}$$

$$U_{\mu\nu}(x) = U_\mu(x)U_\nu(x+e_\mu)U_\mu(x+e_\nu)^\dagger U_\nu(x)^\dagger \tag{1.12}$$

$$W_\mu(x) = \frac{1}{2agi}(U_\mu(x) - U_\mu(x)^\dagger) + \bigcirc(a^2) \tag{1.13}$$

$$\beta = \frac{4}{g^2} \tag{1.14}$$

$$a^2 m^2 = \frac{(1-2\lambda)}{\kappa} - 8 \tag{1.15}$$

$$\lambda = \kappa^2 \gamma \tag{1.16}$$

where R and tr means real part and trace, respectively, in the usual sense. S, U_μ, W_μ and m are action, link, gauge field, and bare mass values. Other variables have the same meaning as in the Lagrangian in continuum for YMH theory.

In lattice calculations path integral approach is used for simulations [12]. In path integral approach, the integrand contains a complex quantity on exponential which fluctuates in positive and negative values. This function acts like a weight functions in the meaning of Statistics, hence it is the place of trouble on the ground of Statistics. The solution is to change the coordinates system from Lorentzian, with signature (-1,1,1,1) or (1,-1,-1,-1), to Euclidean coordinates system with signature (1,1,1,1). This is achieved [12] by redefining time as an imaginary

quantity $(t \to it)$. Hence the partition function becomes

$$Z = \int \prod_l d\phi_l e^{-S[\phi]} \tag{1.17}$$

and, as an example, correlation function $< \phi_i^\dagger \phi_i >$ becomes

$$< \phi_i^\dagger \phi_i > = \frac{\int \prod_l (\phi_i^\dagger \phi_i) d\phi_l e^{-S[\phi]}}{\int \prod_l d\phi_l e^{-S[\phi]}} \tag{1.18}$$

As the left hand side of the above equation implies, knowing the values of fields on each point of the lattice provides us a way to calculate the correlation function directly from the fields.

As is the case for perturbation theory, DSEs and FRG methods, lattice calculations also come with some disadvantages which are important to always consider.

Perhaps the most obvious disadvantage is that for the same computing facility as the volume (size) of the lattice is increased it takes more time to calculate the same quantities. As every point in space time is independent of all other points, calculation of the same quantities may also demand more statistics, and hence more data. A good example is vertices in YMH theory [13] which will be discussed in chapter 3. It means that practically there may always exist a point where the available resources may exhaust.

Every lattice calculation is performed on a finite size of lattice, hence finite size of space time coordinates can effect calculated quantities for the same statistics. Hence their study becomes important to see how these effects behave while the lattice size increases [13]. A completely different type of effect is due to the fineness of lattice, known as descritization effect. The variable a is the corresponding parameter which has already been discussed in this section. It actually implies how fine a lattice is in the units of inverse of energy. The goal is to choose the smallest possible value for this parameter. However, determination of a is not possible in advance because each value of a comes from simulation(s) done with pre-selected values of the parameters in the theory. Another obstacle is to remain on the same line of constant Physics, which is discussed in 1.6. Such fineness and coarseness of lattice also effect quantities calculated on lattice [13].

In lattice calculations, only numerical results can be obtained. For analytical results the numerical results can be fitted by a function which can be studied or used for other purpose like input functions for DSEs [10]. However, it does not truly guarantee that nothing happens between the points at which computed quantities are determined by lattice calculations. Furthermore, even if the results are assumed to be reliable, there is no guarantee what happens beyond these points. For this case, vertices at infrared end of momentum is a good example [13].

It is observed in YMH theory, for all the other factors and specifications fixed, as the correlation functions contain more number of fields, they become more noisy and demand

more statistics [13]. As it is already explained, YMH theory is just a part of the Standard Model. Inclusion of other parts of the Standard Model will involve fermions in the resulting theory. Presence of fermions may worsen the overall situation from the perspective of numerical computation [19].

1.4 Triviality for YMH Theory

One of the important questions about a theory, which could describe nature, is its non-triviality. Consider a field ϕ on lattice with N points along each dimension. Since lattice calculation method contains finite number of points, it has an upper limit of momentum value which can be easily seen by taking a fourier transformation of the ϕ field in momentum space $(\phi'(p))$ as

$$\phi'(p) = \sum_x a^4 e^{-ipx} \phi(x) \tag{1.19}$$

with a as the constant which provides dimensions in the theory, p and x are momentum and lattice points, respectively. Structure of the above equation implies periodic condition

$$p_\mu \equiv p_\mu + \frac{2\pi}{a} \tag{1.20}$$

defining a Brillouin zone

$$\frac{-\pi}{a} < p_\mu \leq \frac{\pi}{a} \tag{1.21}$$

It gives us the upper cutoff in momentum given as

$$\mid p_\mu \mid \leq \frac{\pi}{a} \tag{1.22}$$

In the continuum, when a quantity (lets say a propagator) is calculated beyond tree level in momentum space, a cutoff is introduced for regularization purpose. Later on, once the cut off is removed to infinity, the quantity being calculated remains finite if the theory is renormalizable, which is the case for the Standard Model [20] with perturbative calculations. However, for the case of lattice method as there are finite number of momentum values and a non-zero value of the a variable, triviality [21] can not be easily checked. From each set of lattice parameters, a specific value of a is calculated, which means that, in principle, it is possible to go to smaller and smaller values of a in an attempt to push the upper value of momentum to infinity [12]. If a theory is non-trivial, it is, in principle, possible to keep finding lower values of a and at the same time at least one vertex in the theory will be non-zero for each determined value of a.

There is another way a trivial theory can reveal itself. It is also possible that irrespective of whether any interaction vertex remains non-zero, the lattice spacing can not be reduced more than a certain value and hence it is not possible to go to continuum in the first place. Figure 1.1 shows schematically how the second type of triviality behaves.

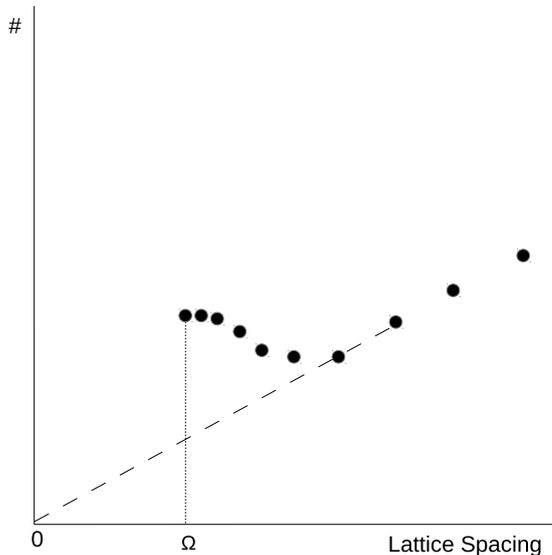For the case of YMH theory, so far it is unclear whether the theory is non-trivial or not [21].

Figure 1.1: Schematic diagram for a trivial theory, in which the lattice spacings can not be found beyond Ω. 0 represents the point for zero lattice spacing while the dotted line meeting the 0 point is the expected continuation of trend of the points. # represents other quantity (quantities) such as parameters of the theory.

Throughout the studies, it is assumed that triviality has no impact on the results.

1.5 Simulation Details

For the simulations for lattice calculations, there are two central ideas. First, and the most important, is to choose configurations which are, in ideal case, statistically independent. A configuration is history of fields, and/or links, which is numerically the arrays of field variables at each point and for each of its quantum number. For the scalar field it is the field arrays at each point in Euclidean coordinates and for each internal symmetry index, while Lorentz indices are also added for the case of gauge fields. As far as the ghost fields are considered, they do not play any role in our simulations. Hence, mathematical quantities, propagators and three point vertices for our case, involving these fields are calculated by Faddeev Popov operator [22], see section 3.2. The reason of independent configurations is the demand of statistical treatment and since the whole lattice computation comes on the same footing as statistics' calculations, a statistical treatment in simulation becomes of utmost importance [12]. In fact, it is the requirement of any Monte Carlo simulation.

The second idea is to choose the most interesting data during simulations. Considering configurations with all the statistically possible weights is surely not very efficient approach. However, keeping statistics with a fixed weight is also not desired because it destroys the statis-

tical fluctuations which are on the similar footing as quantum fluctuations during simulations. In Euclidean coordinates, the weight of the functions is exponentially decaying function [12] and it is possible that for many configurations the probability, and hence the contribution to the quantities to be calculated later on, is negligible. Hence, it becomes important that a criterion is set for acceptance of a configuration.

It brings us to the matter how to find acceptable configurations which are to be statistically found. The starting point is a configuration which can also be generated by an algorithm for random number generation. There are a number of techniques (algorithms) to find a new configuration [19], i.e., an update of configuration (also called a Monte Carlo step). Two key algorithms are used to make a complete update, (1) Heat bath algorithm and (2) overrelaxation algorithm. The function of heat bath algorithm is to choose links U_μ according to a local probability distribution [19] defined by the surrounding staples of the link under consideration. Overrelaxation algorithm is based on the idea that if a candidate link gives the same probability weight, it is automatically accepted [19].

The generation of configurations [23] is performed using a combination of one heat bath [19] and five overrelaxation sweeps for the gauge fields according to [24]. In between each of these are 6 sweeps of the gauge fields and one Metropolis sweep for the Higgs field using a Gaussian proposal. The width of the proposal is set to achieve a 50% acceptance probability. The updates are performed in lexicographical fashion. This whole set of 12 different types of updates constitute 1 complete update of field configuration.

In Monte Carlo simulations, there is always a chance that observables calculated from these simulations are correlated. Auto-correlation time is one of the parameters which are representatives of how much they are correlated [19]. If this time is small, it means that the calculated quantities are not correlated. The auto-correlation time of the plaquette is of the order of 1 or less such update. Thus N updates lie between measurement of a gauge-invariant observable, which reduces the auto-correlation time. For thermalization, 2(10N+300) such updates have been performed.

All errors are calculated using bootstrap with 1000 re-samplings and give a possibly asymmetric 67.5% (1σ) interval. The validity of code is established by comparing to other reliable codes which were already checked by comparing to the results in [25, 26].

All the calculations are performed using many independent runs, which is statistically more helpful and reduces correlations between quantities during simulation runs.

1.6   Lines of Constant Physics

Every lattice simulation is carried out with a choice of pre-selected values of parameter(s) in the theory. The data from simulation(s) are also used to calculate the descritization parame-

ter *a* which is used to render the calculated quantities (and fields in the Lagrangian) physical dimensions. Since in nature there is no such descritization (zero lattice spacing), one has to attempt to reach down to lowest possible lattice spacing corresponding to the *a* value which is closest to the nature's choice, i.e., zero lattice spacing. Since the only way to get to finer and finer lattices is to choose another set of parameters, for each simulation an educated guess is made for selecting the parameters of the theory. However, it is important to be on the *constant Physics* because random selection of the set of parameters may take us close to the continuum but it may be a different Physics. Hence, it needs to be clearly understood exactly what it means by constant Physics.

As it is clear in the Lagrangian, YMH theory has 3 parameters. Hence if any quantity, which is an observable, is calculated using lattice approach, it will have a corresponding point in the 3 dimensional parameter space. However, since this is just one quantity and it is calculated from the selection of 3 parameters, there is no guarantee of a one-to-one correspondence. If there are three such quantities which are calculated using these 3 parameters, they will have a one to one correspondence with the 3 dimensional parameter space of YMH theory. Now we can select some function of these three quantities. For our case, the first function is the ratio of the lowest state in 0^+ channel to that in 1^- channel. The second one is the fixing of the lowest state of 1^- channel, which is also used for scaling and calculation of descritization (in chapter 2). Thus two functions can be calculated and fixed. In an ideal situation, 3 quantities would work well. However, since for the theory at hand, only 2 suitable experimentally measured quantities are known, for YMH theory the problem still remains that at least one more experimentally known quantity needs to be calculated, which persists till the end of all the projects to be included here. For theoretical understanding, a third observable in chapter 2 is used which is not and experimentally measured quantity yet.

Hence, for the YMH theory once 3 quantities are known it is easy to calculate 3 functions and fix them as a convention. And for all the sets of parameter values, as long as these functions are fixed we will be on the same line of constant Physics. One way to form these functions is to take ratios, which is the adopted method and explained in detail in chapter 2.

Chapter 2

Gauge Invariant Correlation Functions

2.1 Introduction

The gauge invariant correlation functions (**GICF**) have the merit, as the name implies, of being independent of gauge choice. As it will be seen in section 2.2.1, due to the reason that they can be related to masses (or energies) of the states in the theory, from the point of view of experiments these correlation functions are much more interesting in comparison to gauge dependent quantities which can not be directly accessed. The only condition is that the theory should describe the nature, which is the case for the YMH theory. Since it is a part of the full Standard Model, anything we calculate in this theory will have possible contributions from other parts of the Standard Model, such as fermions and QED interactions. However, assuming that their contributions do not take the results far from those of YHM theory, it is still a very potent theory to explore from phenomenological as well as theoretical point of view. If the spectrum from gauge invariant quantities in YMH exist in nature, beside opening a whole new door to Spectroscopy for exploration [27], it will also be very helpful during new Physics searches in the sense that as the exploration continues for spectrum in YMH theory, the knowledge of the already-known states in the Standard Model will help us in identifying the experimental findings. Using these functions Physics related to transitions among different states in the theory can also be studied. Furthermore, there are theories, such as Supersymmetry [4], which have several scalar particles with different masses. The YMH theory can serve as a laboratory to see what happens in the non-abelian bosonic sector if the Higgs becomes heavy.

From a more theoretical point of view, considering that in YMH theory no phase transition is found so far [28], calculation of GICFs also gives us a way to *operationally* define different *phases*, which are in fact regions in the parameter space of the YMH theory with some interesting properties [13], in the theory which leads us to the Higgs like and QCD like regions [13]. It will play an important role in the gauge dependent quantities, which are discussed in the chapter 3. Some of these correlation functions also provide us a chance to see similarities

between elementary particle states and bound states for the YMH theory. Duality between these two states will also be included in the following [27].

The chapter starts with the discussion of operators. It is followed by techniques to improve the results. They are followed by detailed results and discussion of GICFs and the duality between elementary particle states and bound states. The order of the sections in the chapters are in accordance with the work flow during investigation of GICFs. The chapter also includes the analysis of results in a broader sense, i.e., different volumes and parameters, and our findings related to the Spectroscopy of YMH theory.

2.2 Calculation Tools

2.2.1 Operators

A note on terminologies in the construction of the gauge invariant correlation functions: Every field has quantum number(s). The central ingredient of a GICF is *Operator* which contains the quantum number(s) of interest and each *Operator* is composed of field(s). It means that selection of operators will be dictated by the quantum number(s) for the observable, and hence the *channel*. A channel can (and does) have more than one operator with the same quantum number(s).

Calculation of full correlation functions is usually the first step before the connected part of the correlation functions are computed from the full correlation functions. The relation between these two correlation functions is given by [28],

$$< O(t_i)O(t_j) >_F = < O(t_i)O(t_j) > + < O(t_i) >< O(t_j) > \tag{2.1}$$

where $< O(t_i) >$ is in fact the one point function of the operator $O(t_i)$ (not field), $< O(t_i)O(t_j) >$ is the connected GICF and $< O(t_i)O(t_j) >_F$ is the full GICF. However, there is a way to avoid calculating the full GICF and then taking the connected part out of the full GICF,

$$< O(t_i)O(t_j) > = < O(t_i)O(t_j) >_F - < O(t_i) >< O(t_j) > \tag{2.2}$$

Above equation can also be written as [28]

$$< O(t_i)O(t_j) > = < (O(t_i) - < O(t_i) >)(O(t_j) - < O(t_j) >) > \tag{2.3}$$

The GICF are related with the energies of different energy levels by [19]

$$< O(t_f)O(t_i) > = \sum_n c_n e^{-(t_f - t_i)E_n} \tag{2.4}$$

Above equation implies that the GICF can be written in terms of the contributions from

different energy levels weighed by coefficients c_n. However, this equation also implies that for a *good* selection of operators it is possible to have the dominant contributions (in terms of coefficients c_n) from relatively fewer number of energy levels, hence the result is a relatively *cleaner* GICF in the sense that contributions from the rest of the energy levels is not significant. In ideal situation if only one c_i is non-zero, (effective) masses can be calculated using

$$m_{eff} = ln \left(\frac{e^{-(t_f - t_i)E_n}}{e^{-(t_f - t_i + 1)E_n}} \right) \tag{2.5}$$

which also emphasizes that the operator being used does not have contribution from any state but one. So far there is no such operator in the knowledge for YMH theory which means that using solely this approach may not pay off in the form of masses directly calculated from operators [1].

In terms of Statistics, more bosonic fields in the correlation function demand larger collection of the required statistics for the same size of statistical error. Just to give an idea for the statistical errors for the YMH theory, for the same amount of statistics if the statistical error for 8^4 lattice size is less than 1 percent, it is found to be larger than 50 percent for the case of 24^4 lattice size. Another way to look at this same point is to see at what statistics two point functions, and what statistics three point functions have results statistically good enough to make a statement [13]. It necessitates use of various techniques to improve the data and get rid of some part of fluctuations in the data. Smearing is one of these techniques [19].

2.2.2 Smearing

The motive behind this technique is to extract information without avoiding the situation when all the important information is lost. In this technique, one attempts to improve the data by reducing the local fluctuations of the fields. However, let us note here that there must be a trade between reducing the local fluctuations and averaging out all the fluctuations, because if the process of smearing is continued one will eventually average out even the long distance fluctuations, hence loosing all the interesting information in the data. There are a number of smearing techniques [19]. However, the trick in almost each of them is to replace the link variables by some averages around them.

Here in our case, APE smearing [19] has been used. In this technique, the link variables U_μ at each point are replaced by the original link and the perpendicular staples connecting the end points of the considered link. Thus in case of 4 dimensional space, which is the focus throughout our investigation, there are 6 such staples for each link, given by [29]:

$$U_\mu(x)^n = \frac{1}{\sqrt{det R_\mu(x)^n}} R_\mu(x)^n$$

---

[1]Hence, in general, taking these masses as effective masses is reasonable.

$$R_\mu^n = \alpha U_\mu(x)^{n-1} + \frac{1-\alpha}{2(d-1)}\{\sum_{\nu\neq\mu}(U_\nu^{n-1}(x+e_\mu)U_\mu^{(n-1)\dagger}(x+e_\nu)U_\nu^{(n-1)\dagger}(x)$$

$$+U_\nu^{(n-1)\dagger}(x+e_\mu-e_\nu)U_\mu^{(n-1)\dagger}(x-e_\nu)U_\nu^{(n-1)}(x-e_\nu))\}$$

and for the case of the scalar field

$$\phi^{(n)} = \frac{1}{1+2(d-1)}(\phi^{(n-1)}+$$

$$\sum_\mu\{U_\mu^{(n-1)}(x)\phi^{(n-1)}(x+e_\mu)+U_\mu^{(n-1)}(x-e_\mu)U_\mu^{(n-1)}(x-e_\mu)\phi^{(n-1)}(x-e_\mu)\})$$

with $\alpha = 0.55$, d=4 and n is the number of iteration levels. During our exploration, up to four level of iterations, hence four levels of smearing, have been used.

2.2.3   Time Averaging

It is easy to notice that in equation 2.4 translational invariance in time holds true. This can be used to further reduce the fluctuations from the correlation functions by using the so-called *time averaging* [28]. In this technique, the correlation functions $< O(t_i)O(t_f) >$ with $t_f = t_i + \delta t$ can be used to construct quantities which are functions of only δt using the following equation.

$$f(\delta t) = \frac{1}{N}\sum_t < O(t)O(t+\delta t) >$$

where N is the number of values of the allowed time values while in lattice calculations δt has values from 0 to the highest value of the lattice size along the time direction. On lattice these quantities are periodic which is also taken care of during the calculations.

2.2.4   Variational Analysis

After the use of smearing technique and time averaging, the GICFs (or f(δt)) are with relatively smaller statistical fluctuations. However as it is clear from the equation (2.1), for each GICF there are contributions from all the energy levels in the theory. It means that for any Spectroscopy all the energy levels should be known which is practically not possible. Hence, a mathematical trick is needed which could change the coefficients c_n in equation (2.4) to a situation when as few as possible number of c_n are non-zero. This technique is called Variational Analysis [19].

In this technique, the idea is to construct a matrix from the operators of GICFs and solve it at each time for eigenvalues and eigenvectors [19]. It can be understood by an example. For the case of two operators $O_1(t_i)$ and $O_2(t_f)$, four f(δt) functions can be constructed using the given operators, $< O_1(t_i)O_1(t_f) >$, $< O_1(t_i)O_2(t_f) >$, $< O_2(t_i)O_1(t_f) >$ and $< O_2(t_i)O_2(t_f) >$. The functions f(δt) from the correlation functions mentioned above serve as the matrix elements for the eigenvalue (and eigenvector) calculations. Once eigenvalues for the matrix at each value of

time are calculated, their behavior over time can be used to calculate the energy values in the spectrum. The same procedure can be extended for more than two operators. In short, the whole procedure can be represented in following two equations:

$$\begin{pmatrix} a_{11} & a_{12} & \cdots & a_{1n} \\ a_{21} & a_{22} & \cdots & a_{2n} \\ \vdots & \vdots & \ddots & \vdots \\ a_{m1} & a_{m2} & \cdots & a_{mn} \end{pmatrix} \begin{pmatrix} v_1 \\ v_2 \\ \vdots \\ v_n \end{pmatrix} = \lambda \begin{pmatrix} v_1 \\ v_2 \\ \vdots \\ v_n \end{pmatrix}$$

and

$$E_n(t) = ln\left(\frac{\lambda_n(t)}{\lambda_n(t+1)}\right) \tag{2.6}$$

where $\lambda_n(t)$, $v_n(t)$ and $E_n(t)$ are nth eigenvalue at time t, nth eigenvector component at time t and nth energy value at time t, respectively. In the matrices above, all the $a_{ij}s$ represent the correlation functions used and $v_i s$ are the elements of the eigenvectors [19].

At this point the question arises; What information can be extracted from eigenvectors? Though, eigenvectors do not not provide any direct Physics information, their behavior over time may serve as an indicator how good the energy levels are clean, in the sense of contributions from other energy levels. For example, consider that there are two eigenvectors, V_1 and V_2, for the case of two operators for variational analysis. In ideal situation when both of the two energy levels are clean, the eigenvectors will be as follows;

$$V_1 = \begin{pmatrix} 1 \\ 0 \end{pmatrix}, V_2 = \begin{pmatrix} 0 \\ 1 \end{pmatrix}$$

Since there is an uncertainty (or statistical error) in the operators, it is important to include the corresponding uncertainty in the results. Assuming that there is a matrix M(t) at time t with statistical error $\delta M^{\pm}(t)$, for the calculation of eigenvalues and eigenvectors three matrices can be used, i.e., M(t), $M(t)+\delta M^+(t)$ and $M(t)-\delta M^-(t)$. It will give us three eigenvalues $\lambda(t)$, $\lambda^+(t)$ and $\lambda^-(t)$ which defines a window of values against time for the results. Same approach is taken for the computation of eigenvectors. Once the three sets of points are defined, the positive and negative errors can be easily calculated using the following equations.

$$\delta\lambda^+(t) = \left|\lambda^+(t) - \lambda(t)\right| \tag{2.7}$$

$$\delta\lambda^-(t) = \left|\lambda(t) - \lambda^-(t)\right| \tag{2.8}$$

2.2.5   Preconditioning

Once the information from the GICFs calculated is converted into an input matrix for Eigenvalue problem, preconditioning can be used to *partly* improve the results [19]. For this technique, the idea is to use a *constant* matrix and use it on the matrix at hand for the Eigenvalue problem. Hence for a matrix A with ν as its eigenvectors an λ as its eigenvalues, the equation

for Eigenvalue problem is given by;

$$A\nu = \lambda\nu \qquad (2.9)$$

A *suitable* matrix P can be used as follows;

$$PA\nu = P\lambda\nu = \lambda P\nu \qquad (2.10)$$

$$(PAP^{-1})(P\nu) = \lambda(P\nu) \qquad (2.11)$$

It can already be noted from above equations that (i) the eigenvalues are not changed by application of the P matrix, and (ii) the P matrix *must* be an invertible matrix. Now the only remaining question is, how can this P matrix be selected? In general, there is no strict mathematical constraint on the P matrix. However, on the grounds of numerics, a reasonable choice is to select a matrix which is similar to the input matrix, i.e., A matrix in the above equations. Selecting an invertible matrix which is similar to the matrix at hand, speeds up convergence in order to reach solutions, which is numerically very advantageous [19].

Lets note that for our case the A matrix is a time dependent matrix because the matrix elements, which are correlation functions, are time dependent quantities, hence one matrix for each time value. It trivially means that, in general, the eigenvalues and eigenvectors (their components in the space of eigenvectors) are also time dependent quantities. In our case here, the P matrix is chosen to be one of the A matrices at some time t_0.

2.3 Calculations

At this point it is already clear why GICFs are important in YMH theory, and the tools for calculations and improving the results have also been described. Details of calculations, which are relevant to our investigations, are given in this section along with intermediate results in order to clarify the arguments. For now, it is already assumed that the parameters of the theory have already been selected. Choosing these parameters is a non-trivial business in YMH theory both from the point of view of theoretical understanding as well as understanding the Physics, this matter will be discussed in some detail in this chapter, though mostly the intention is to see what role selection of different parameters plays for observables. The whole investigation is conducted in 0^+ and 1^- channels, except in section 2.5. The following studies begin with selecting operators with the quantum numbers in 0^+ and 1^- channels. Let us recall here that the operators can always be expanded as a combination of contributions from energy levels in the Spectrum of YMH theory with the only restriction of correct quantum numbers. Hence, it is likely that the operators selected will contain contribution from the ground state of the respective channel in YMH theory. The following operators are used for the studies of gauge invariant quantities.

$$\bigcirc_H^{0^+}(x) = \phi_i^\dagger(x)\phi_i(x) \qquad (2.12)$$

$$\bigcirc_w(x) = Tr\left(U_\mu(x)U_\nu(x+e_\mu)U_\mu(x+e_\nu)^\dagger U_\nu(x)^\dagger\right) \qquad (2.13)$$

$$\bigcirc_{ww}(x) = \bigcirc_w(x)^\dagger \, \bigcirc_w(x) \tag{2.14}$$

$$^2\bigcirc_{a\mu}^{1-}(x)_\varepsilon = \varepsilon Tr\left(\tau_a \varphi^\dagger(x) exp(i\tau_b W_\mu^b)\varphi(x+e_\mu)\right) \tag{2.15}$$

$$\bigcirc_{HH}^{0+}(x) = \bigcirc_H^\dagger(x) \, \bigcirc_H(x) \tag{2.16}$$

$$\bigcirc^{0+}(x)_\varepsilon = (\bigcirc_{a\mu}^{1-}(x)_\varepsilon)^\dagger \, \bigcirc_{a\mu}^{1-}(x)_\varepsilon \tag{2.17}$$

In above the ϕ_i, τ_a, W_μ^b, $U_\mu(x)$ and Tr are the scalar fields with i internal quantum number, the ath Pauli matrix, the gauge fields, link variable and trace of matrix, respectively. In parenthesis,H, HH, ω and $\omega\omega$ are merely for remembering the structure of operators for convenience. In above, φ are the SU(2) representation of the matrix comprising the $\phi^i(x)$ fields. The matrix is given by [13]

$$\varphi(x) = \begin{pmatrix} \phi^1(x) & -\phi^{*2}(x) \\ \phi^2(x) & \phi^{*1}(x) \end{pmatrix}$$

In principle, in above equation there must be an inverse of determinant as a constant multiple since it is an SU(2) representation and $\phi^i(x)$ fields are not normalized. However, as the quantum numbers do not depend upon choice of this multiple, different choices of the multiple will result in different operators of same quantum numbers. Hence, in order to have three operators, the chosen values of the constant multiple ε are $\frac{1}{det(\varphi)}$, $\frac{1}{\sqrt{det(\varphi)}}$ and $\frac{1}{(det(\varphi))^2}$.

At this point, let us note that all the operators from 2.12 to 2.17 are locally gauge invariant. $\bigcirc_H^{0+}(x)$, $\bigcirc_w(x)$, $\bigcirc_{ww}(x)$, $\bigcirc_{HH}^{0+}(x)$ and $\bigcirc^{0+}(x)_\varepsilon$ are the operators selected for 0^+ channel, while $\bigcirc_{a\mu}^{1-}(x)_\varepsilon$ are the ones (for each ε) selected for 1^- channel. Under global transformation, these operators are singlets and triplets, respectively.

The first step is to study the effects of smearing. It can be observed already from the correlation functions or the effective masses calculated from them. In figures 2.1-2.3, effective masses in both 0^+ and 1^- channels are plotted for different levels of smearing. The immediate observation is that for higher levels of smearing, the error is significantly reduced which is very useful for us particularly because these correlation functions serve as input for variational analysis, which executes non-linear calculations. Thus more reduction of errors, the better it will be.

The second step is to investigate the finite volume effects. This can be done in two ways. Either the observables are considered for different volumes, or the operators (or effective masses from them) for different volumes are observed. Since extracting masses needs good statistics, the effective masses calculated after variational analysis are used for this purpose. In figures 2.4-2.5 are shown the effective masses for different volumes. For different volumes, variations in effective mass plots are observed though they are not drastic for the operators used. It suggests that the role of higher lattice sizes is important here since the quantities may get effected because of volumes depending on the parameters used.

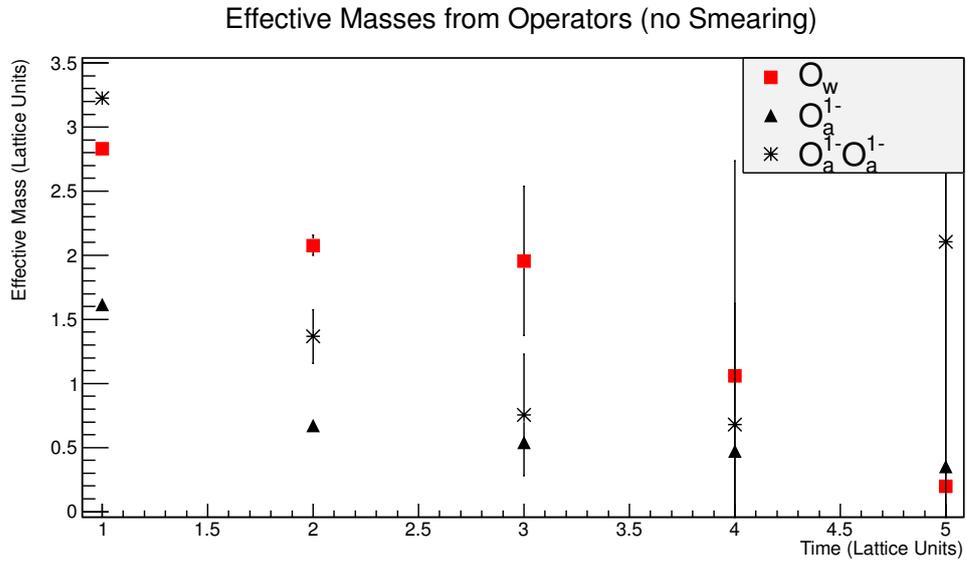[2]The current form of this operator will be useful in section 2.9.

Figure 2.1: Effective masses are plotted with no smearing performed, in both 0^+ and 1^- channels. The parameters used are $\beta = 2.3881$, $\kappa = 0.3214$, and $\lambda = 0.9974$, the simulation is performed on 12^4 lattice.
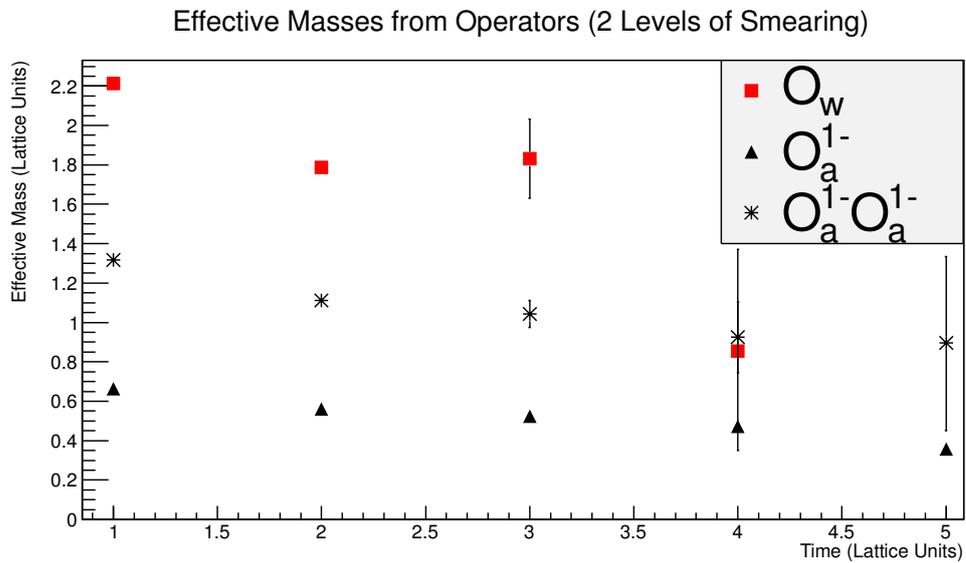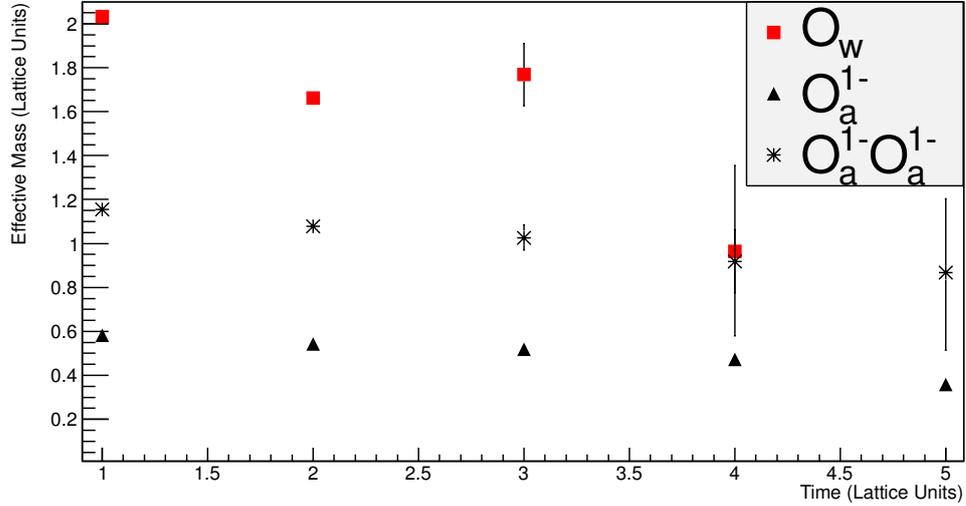

Figure 2.2: Effective masses are plotted with two levels of smearing performed, in both 0^+ and 1^- channels. The parameters used are $\beta = 2.3881$, $\kappa = 0.3214$, and $\lambda = 0.9974$, the simulation is performed on 12^4 lattice.

Figure 2.3: Effective masses are plotted with four levels of smearing performed, in both 0^+ and 1^- channels. The parameters used are $\beta = 2.3881$, $\kappa = 0.3214$, and $\lambda = 0.9974$, the simulation is performed on 12^4 lattice.

Figure 2.4: Effective masses are plotted for different lattice sizes in 0^+ channel. The parameters used are $\beta = 2.3881$, $\kappa = 0.3214$, and $\lambda = 0.9974$. Different colors represent effective masses for different energy levels while symbols with different styles represent different lattice sizes.

21
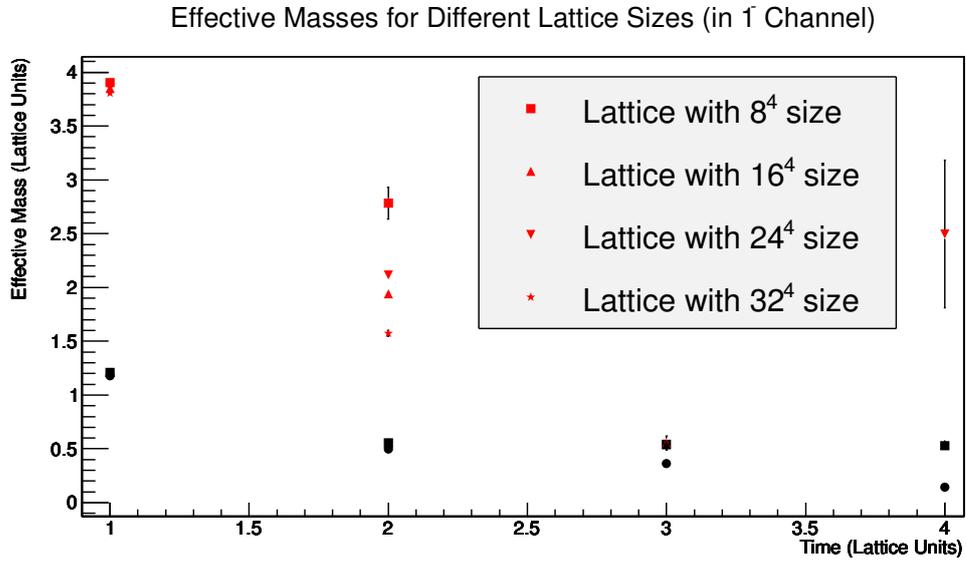
Figure 2.5: Effective masses are plotted for different lattice sizes in 1^- channel. The parameters used are $\beta = 2.3881$, $\kappa = 0.3214$, and $\lambda = 0.9974$. Different colors represent effective masses for different energy levels while symbols with different styles represent different lattice sizes.
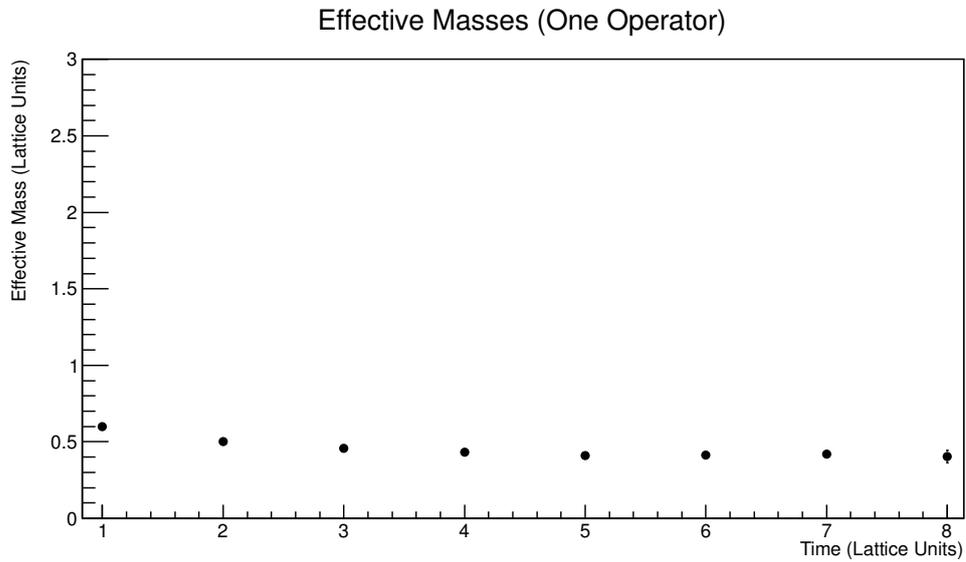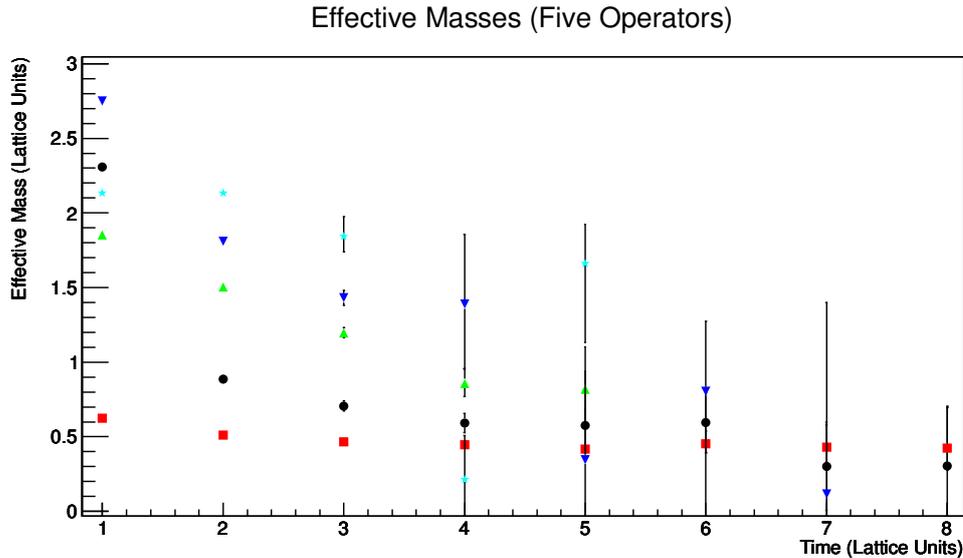

Figure 2.6: Effective masses are plotted using one operator in 0^+ channel, for parameters $\beta = 2.4728, \kappa = 0.2939$, and $\lambda = 1.036$, with lattice of 24^4 points.
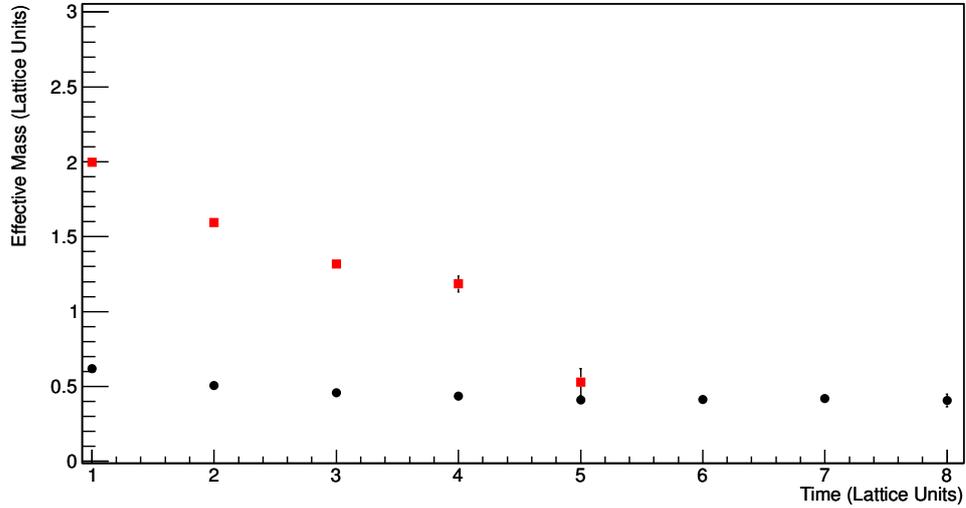
Figure 2.7: Effective masses are plotted using two operators 0^+ channel, for parameters $\beta = 2.4728$, $\kappa = 0.2939$, and $\lambda = 1.036$, with lattice of 24^4 points. Symbols of different colors and styles represent different effective masses.
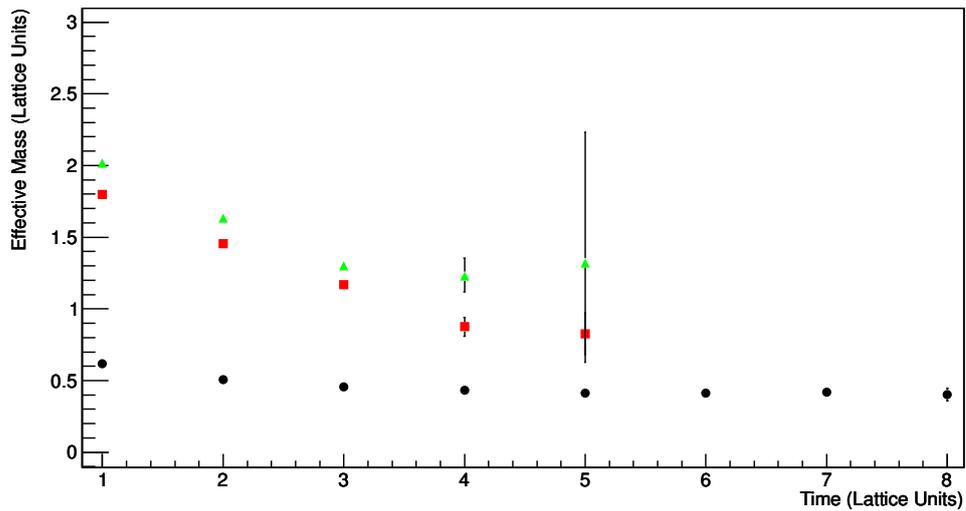
Figure 2.8: Effective masses are plotted using three operators 0^+ channel, for parameters $\beta = 2.4728$, $\kappa = 0.2939$, and $\lambda = 1.036$, with lattice of 24^4 points. Symbols of different colors and styles represent differnt effective masses.

Figure 2.9: Effective masses are plotted using five operators 0^+ channel, for parameters $\beta = 2.4728$, $\kappa = 0.2939$, and $\lambda = 1.036$, with lattice of 24^4 points. Symbols of different colors and styles represent differnt effective masses.

Another observation at this point is increasing of the statistical errors size as time increases. It can be understood easily. After variational analysis the eigenvalues obtained are overall monotonically decreasing functions of time. However, as their values grow smaller with time, the relative size of value becomes smaller compared to its error, which appears on the diagrams as large values of errors compared to the value of the mass in the end. However the level of severity is different for different sets of parameters, i.e., some parameters are more noisy and require more statistics compared with other values of parameters.

Let us note here that since the computation of eigenvalues and eigenvectors is highly non-linear, greater the size of the matrices used, greater the non-linear contributions in the results and noisier the result will become. It means that for a given statistics, there is always an upper bound on the number of operators before the results loose credibility. It implies that choosing the number of operators is also an important matter for these calculations. In figures 2.6-2.9, effective masses are shown for different number of operators. It is clear from the figures that increasing the operators for a given statistics causes larger fluctuations in the results. It also makes it difficult to find a good fit to extract masses (for determination of energy levels).

For the case of smaller lattice sizes, it is easy to raise statistics and suppress the fluctuations in masses. However, since the procedure of fitting involves 2 parameters for each contribution of energy level, finding a fit might still remain a problem to be considered specially if the lattice size is very small. Furthermore, smaller lattices may also introduce finite volume effects.
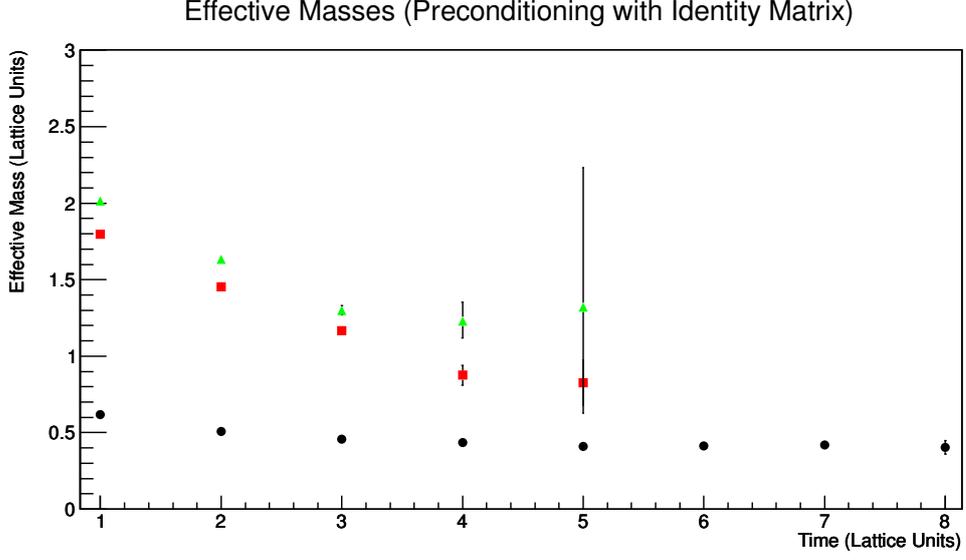
Figure 2.10: Effective masses are plotted with Identity matrix used as a preconditioning, which also means no preconditioning. The parameters used are $\beta = 2.4728$, $\kappa = 0.2939$, and $\lambda = 1.036$, with lattice of 24^4 points. Symbols with different styles and colors represent different effective masses in 0^+ channel.

Since lattice calculation is the method at hand, the quantities will have positive symmetry [12] on lattice because of periodicity. Hence, the weighed exponentials take the form of weighed *Cosh* functions. For the case of single exponential fittings

$$E(t) = ln\left(\frac{Cosh(mt)}{Cosh(m(t+1))}\right) = ln\left(\frac{\frac{e^{mt}+e^{-mt}}{2}}{\frac{e^{m(t+1)}+e^{-m(t+1)}}{2}}\right) \quad (2.18)$$

or

$$E(t) = ln\left(\frac{e^{mt}+e^{-mt}}{e^{m(t+1)}+e^{-m(t+1)}}\right) \quad (2.19)$$

and for the case of double exponential fitting, the following equation is used.

$$E(t) = ln\left(\frac{c_1 * Cosh(mt) + c_2 * Cosh(m't)}{c_1 * Cosh(m(t+1) + c_2 * Cosh(m'(t+1))}\right) \quad (2.20)$$

Since the general structure of these expressions is $ln(\frac{f(t)}{f(t+1)})$ with f(t) as a function of time, both the positive and negative errors can be calculated by

$$\delta E(t) = \sqrt{\left(\frac{\delta f(t)}{f(t)}\right)^2 + \left(\frac{\delta f(t+1)}{f(t+1)}\right)^2} \quad (2.21)$$

When it comes to preconditioning, it proved to be less helpful than expected for our investigation. For the case of matrices M(t) at time t some matrix M(τ) is used at some particular value of time τ. In figures 2.10-2.13 masses are calculated with different preconditioning matrices. It is clear from the figures that as we select higher value of time for preconditioning
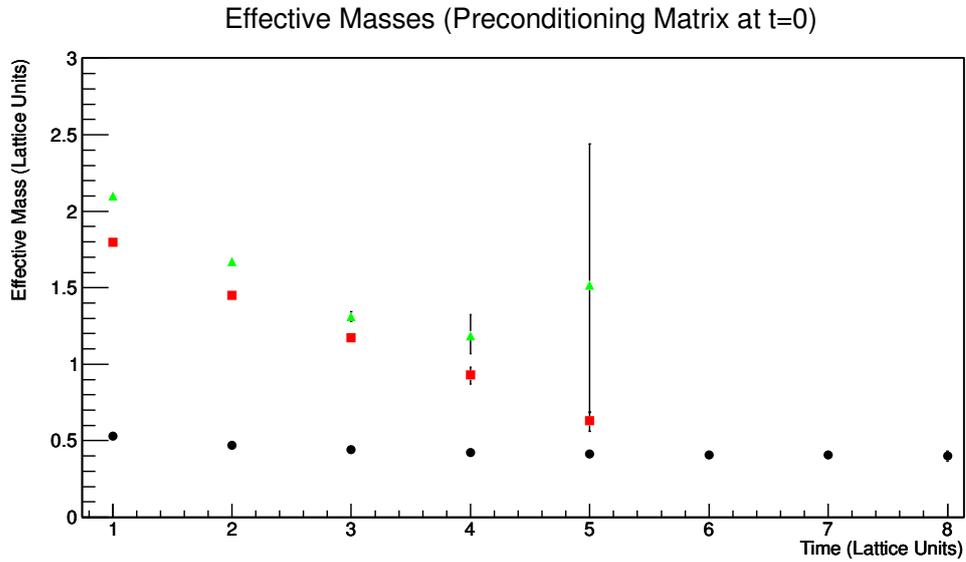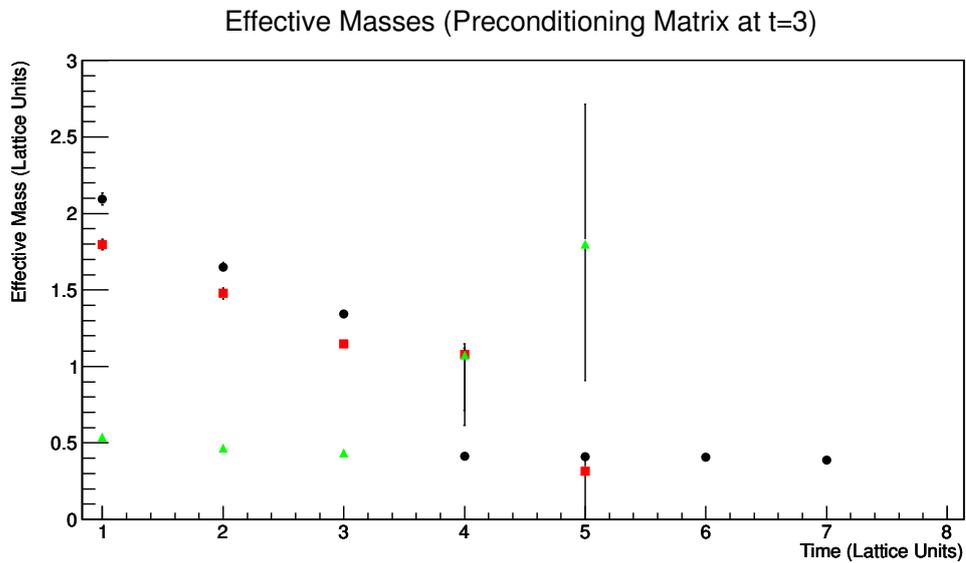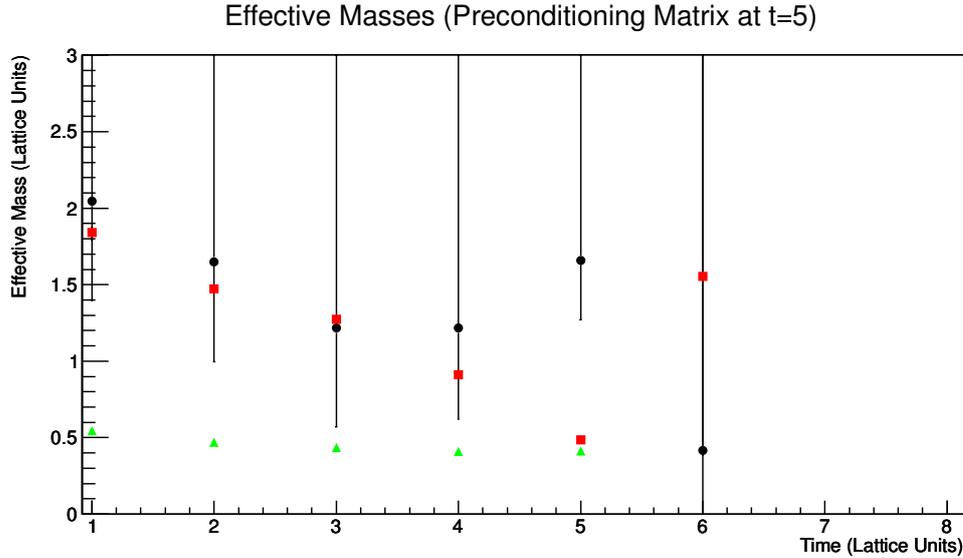
Figure 2.11: Effective masses are plotted with matrix at t=0 used as preconditioning matrix. The parameters used are $\beta = 2.4728$, $\kappa = 0.2939$, and $\lambda = 1.036$, with lattice of 24^4 points. Symbols with different styles and colors represent different effective masses in 0^+ channel.

Figure 2.12: Effective masses are plotted with matrix at t=3 used as preconditioning matrix. The parameters used are $\beta = 2.4728$, $\kappa = 0.2939$, and $\lambda = 1.036$, with lattice of 24^4 points. Symbols with different styles and colors represent different effective masses in 0^+ channel.

Figure 2.13: Effective masses are plotted with matrix at t=5 used as preconditioning matrix. The parameters used are $\beta = 2.4728$, $\kappa = 0.2939$, and $\lambda = 1.036$, with lattice of 24^4 points. Symbols with different styles and colors represent different effective masses in 0^+ channel.

matrix, the quantities become more noisy in terms of statistical error. Hence, for our case it is concluded that lower the value of time, the better the results in terms of statistical error in the quantities. This is the reason that throughout the investigation, either identity matrix or matrix at the lowest value of time was chosen.

Based upon the observations discussed above, 4 levels of smearing is used for our investigation, and the number of operators as well as the maximum time for these time dependent quantities are chosen such that they make sense. Beyond that, quantities do not make much sense and hence that part is always omitted. For preconditioning, the matrix at the lowest value of time is chosen or, trivially, the identity matrix is used which means no preconditioning.

Once the results in lattice units are obtained, it is easy to turn the masses into physical masses by giving them physical units. Since the mass of W gauge boson has already been measured to a good precision [30], the scheme here is to use this mass for the ground state in the channel 1^- to set the descritization parameter and using this parameter all other masses are given physical units. In nature, Z boson also exists and measurements have been made to a good precision [30]. However, the masses of W and Z bosons are degenerate in the absence of QED and hence in our electroweak sector we only have a triple degenerate W boson. Mathematically, physical and lattice masses are related by,

$$M_{physical} = \Omega M_{lattice} \tag{2.22}$$

where Ω is the quantity to be determined, while $M_{physical}$ and $M_{lattice}$ are the physical and lattice masses, respectively. Thus for our scheme, the following equation gives us the parameter
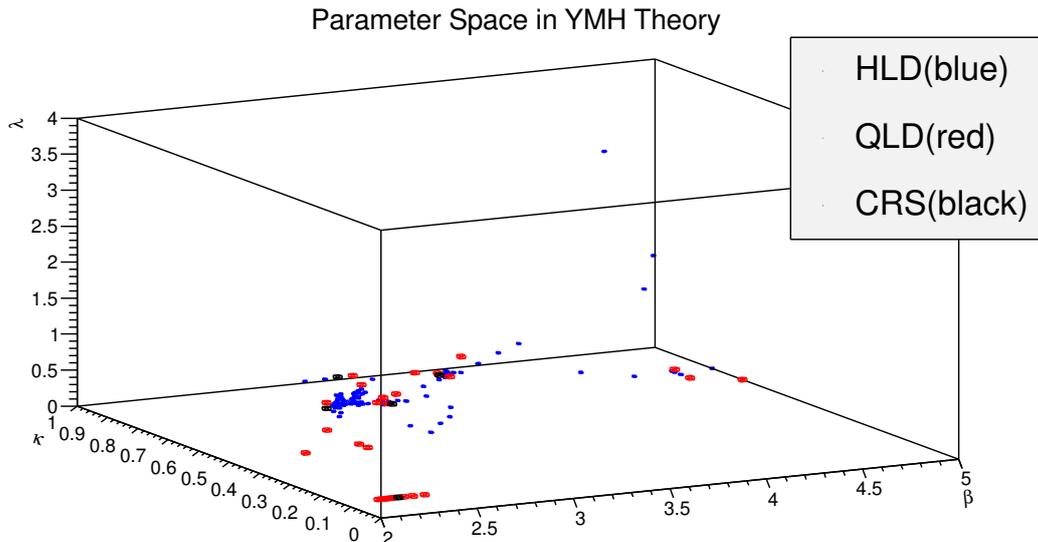
27

Figure 2.14: Parameter space in YMH Theory. Blue, red and black points represent HLD ($r < 1$), QLD ($r > 1$) and COR ($r \approx 1$) in the parameter space.

needed for giving the other masses physical units.

$$\Omega = \frac{M_{w(physical)}}{M_{1^-(lattice)}} \tag{2.23}$$

Hence, with the Ω calculated, it is always possible to change the units of masses from lattice units to physical units, which will be done in section 2.6.

2.4 Sensitivity of Parameters in YMH Theory

So far the lattice parameters were kept fixed since the main focus was on the behavior of quantities in different circumstances, e.g., changing volumes, changing number of operators, etc. However, in order to understanding the theory it is important to relax the condition of fixed parameters, which leads us to whole lot of choices of parameters. For every selected set of values for parameters, masses were computed in different channels. Since the focus is mostly on the masses in 0^+ and 1^- channels, a ratio $r = \frac{m_{1^-}}{m_{0^+}}$ for ground state masses m_{1^-} in 1^- channel and m_{0^+} in 0^+ channel can be defined. This ratio can be used to catalogue the points into two situations when the ground mass in m_{1^-} channel is heavier than m_{0^+} or vice versa, or these masses are the same within statistical error. In figure 2.14, points for different sets of explored parameters have been shown, while the color of the points are representative of value of the ratio. The immediate observation is that there exist sets of parameters in YMH theory when m_{1^-} is lighter than m_{0^+} ($r < 1$) and there are sets of parameters when m_{1^-} is heavier than m_{0^+} ($r > 1$), while there also exists a cross over when these masses are almost the same ($r \approx 1$). As will be explained in chapter 3, existence of these different regions in parameter space is very useful and interesting.
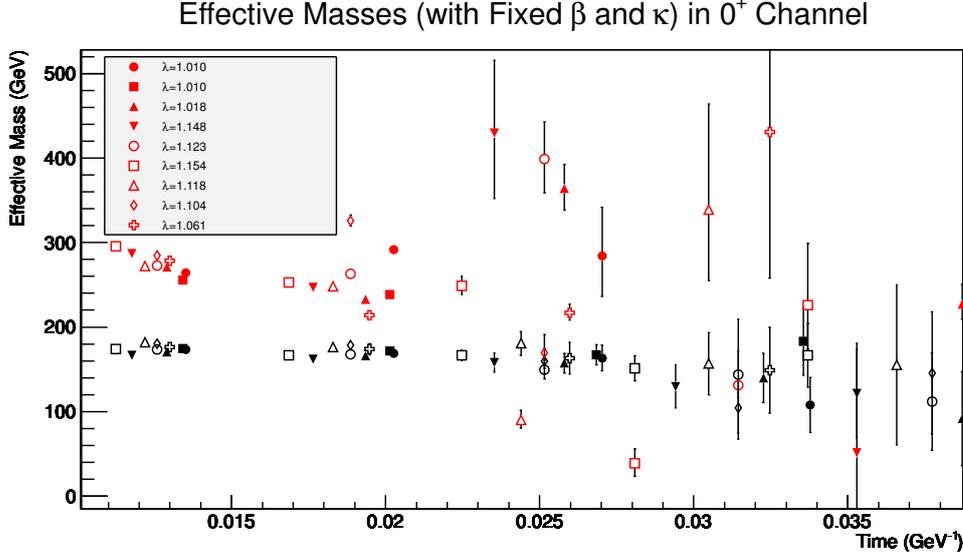
Figure 2.15: Effective masses of two energy levels are plotted from eigenvalues for $2.35 < \beta < 2.38$ and $0.30 < \kappa < 0.33$ for lattice of size 24^4 in 0^+ channel. Black colored points represent the first energy level and red colored points represent the second energy level. Different symbol styles represent effective masses for different values of λ.

One of the very important aspects of a theory is sensitivity to its parameters, 3 parameters for the case of YMH theory. One possibility is to keep two of the parameters fixed and let the third parameter vary. Since the whole investigation was conducted with lattice calculation method, only finite number of values of the third parameters can be used to vary it. One can also define a convention for how to define a *fixed* parameter since it is also not easy to find many situations with some parameter(s) held fixed. Here the convention is that the *held fixed* parameters have lesser variation than the third parameter which is allowed to vary. In figures 2.15-2.20 such situations are shown for 0^+ channel while in figures 2.21-2.26 such situations are shown for 1^- channel.

A general observation is that effective masses of the lowest states are less sensitive compared to those of higher states, though it is clear that there does exist dependency specially in figure 2.17.

Considering only ground state, for situation with β and κ *held fixed*, the deviation in the effective masses is less than 30% in figures 2.15, 2.16, 2.21, and 2.22. For the third similar situation in figures 2.17 and 2.23, it is hard to make comparison but the dependency is on λ is clear. For the situation when β and λ are held fixed, the sensitivity is relatively considerably smaller than the previous situation, as in figures 2.18, 2.19, 2.24, and 2.25. Similar situation arises when κ and λ are held fixed as in figures 2.20 and 2.26, though the deviation is alittle larger than the previous case.
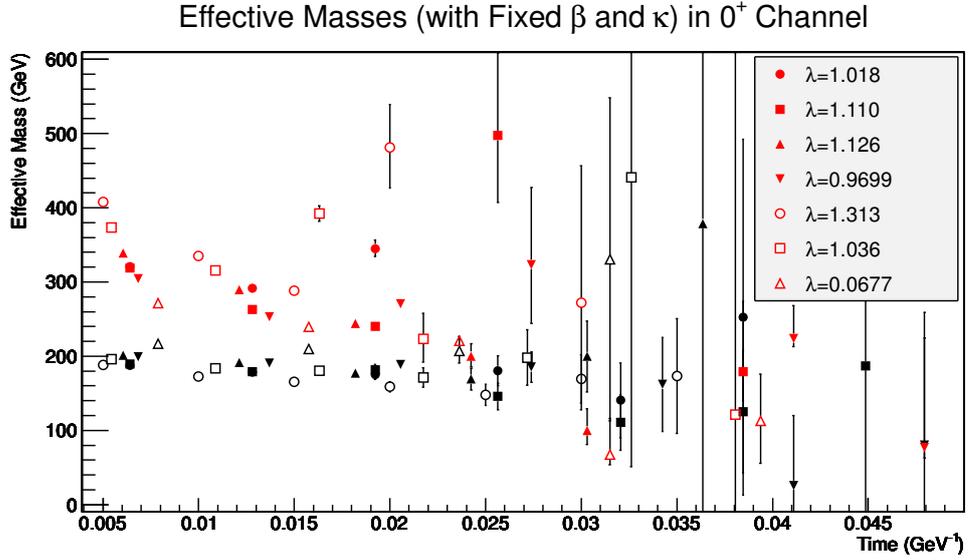
Figure 2.16: Effective masses of two energy levels are plotted from eigenvalues for $2.43 < \beta < 2.48$ and $0.30 < \kappa < 0.34$ for lattice of size 24^4 in 0^+ channel. Black colored points represent the first energy level and red colored points represent the second energy level. Different symbol styles represent effective masses for different values of λ.
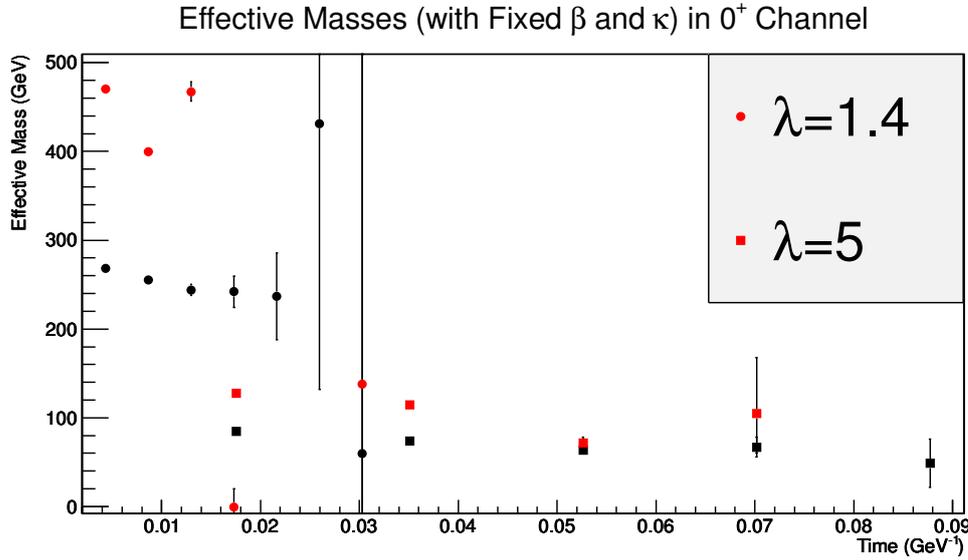

Figure 2.17: Effective masses of two energy levels are plotted from eigenvalues for $\beta = 3.0$ and $\kappa = 0.315$ for lattice of size 24^4 in 0^+ channel. Black colored points represent the first energy level and red colored points represent the second energy level. Different symbol styles represent effective masses for different values of λ.
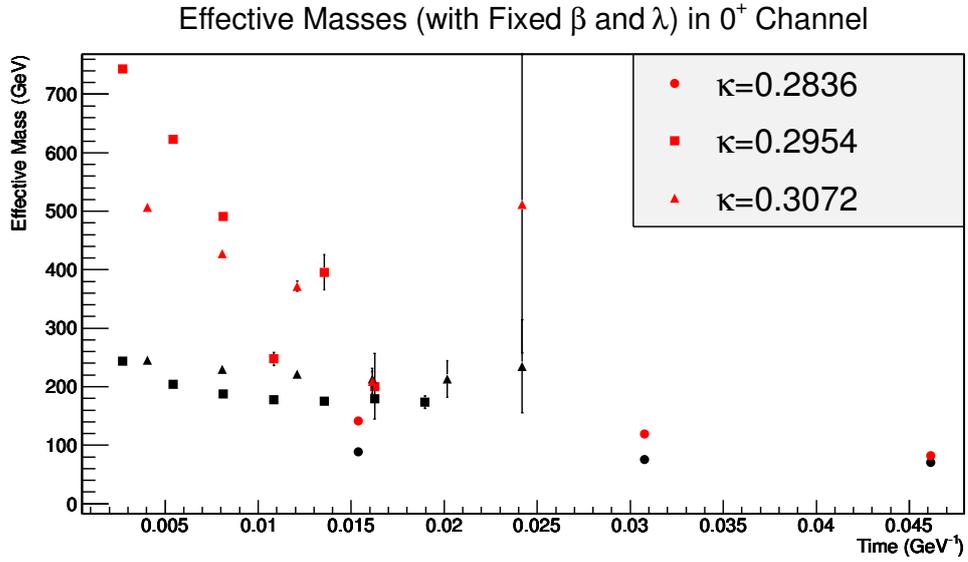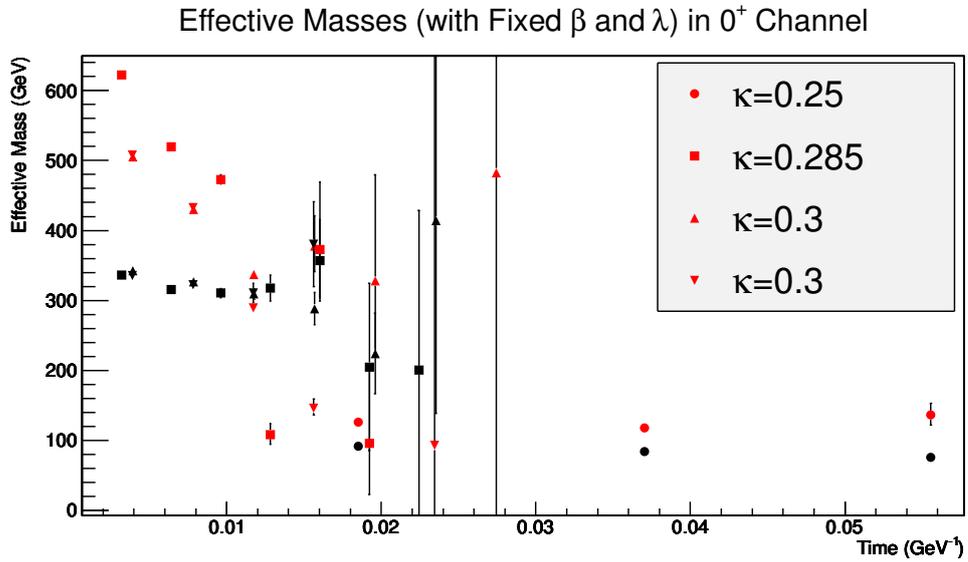
Figure 2.18: Effective masses of two energy levels are plotted from eigenvalues for $\beta = 3.0$ and $\lambda = 1.317$ for lattice of size 24^4 in 0^+ channel. Black colored points represent the first energy level and red colored points represent the second energy level. Different symbol styles represent effective masses for different values of κ.

Figure 2.19: Effective masses of two energy levels are plotted from eigenvalues for $\beta = 4.0$ and $\lambda = [1.0, 1.05]$ for lattice of size 24^4 in 0^+ channel. Black colored points represent the first energy level and red colored points represent the second energy level. Different symbol styles represent effective masses for different values of κ.
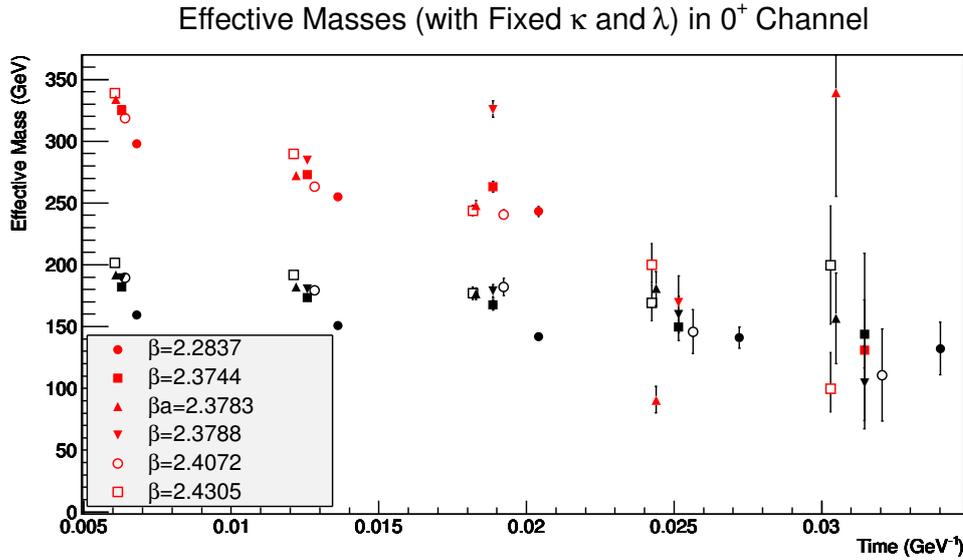
Figure 2.20: Effective masses of two energy levels are plotted from eigenvalues for $0.320 < \kappa < 0.329$ and $1.10 < \lambda = 1.13$ for lattice of size 24^4 in 0^+ channel. Black colored points represent the first energy level and red colored points represent the second energy level. Different symbol styles represent effective masses for different values of β.

For the case of higher states the situation is slightly different. The parameters seem to effect the effective masses without any considerable distinction, which implies that the YMH theory is effected by all 3 parameters in more or less the same way, particularly for higher states. However, for a definite answer a dedicated investigation in the parameter space is still required, and masses from fitting of Cosh function(s) is to be extracted which even now require alot more statistics for a number of sets of parameters.

2.5   LCPs in YMH Theory

It is already explained in chapter 1 that in the YMH theory 3 quantities are needed to set the parameters, so that investigations are carried out as the lattice becomes finer. However, for YMH theory only two relevant quantities are experimentally known, i.e., masses of W and Higgs bosons. W boson's mass is used to set the scale as already explained in section 2.3, and Higgs boson's mass is used to calculate the ratio $\frac{m_{1-}}{m_{0+}}$ in this chapter. It necessitates considering the third quantity from purely theoretical side in order to define a line of constant Physics. The third quantity chosen for such investigation is the lowest state in the 1^- singlet channel [3]. For this purpose the following operator is used to extract the ground state's mass in 1^- singlet channel [31].

$$\bigcirc_\mu^{1-}(x)_\varepsilon = \varepsilon Tr \left(\varphi^\dagger(x) exp(i\tau_b W_\mu^b)\varphi(x + e_\mu) \right) \qquad (2.24)$$

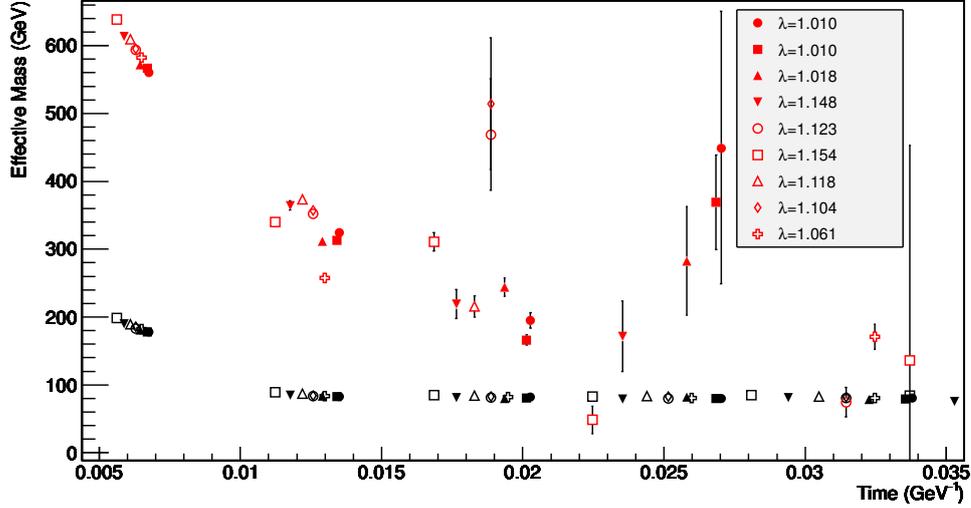[3]It is the only place where 1^- singlet channel is considered.

Figure 2.21: Effective masses of two energy levels are plotted from eigenvalues for $2.35 < \beta < 2.38$ and $0.30 < \kappa < 0.33$ for lattice of size 24^4 in 1^- channel. Black colored points represent the first energy level and red colored points represent the second energy level. Different symbol styles represent effective masses for different values of λ.
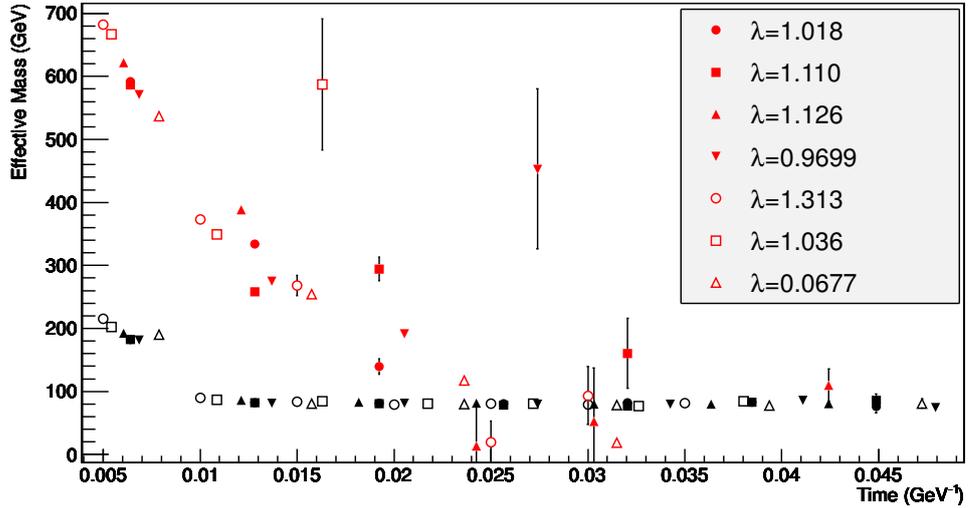

Figure 2.22: Effective masses of two energy levels are plotted from eigenvalues for $2.43 < \beta < 2.48$ and $0.30 < \kappa < 0.34$ for lattice of size 24^4 in 1^- channel. Black colored points represent the first energy level and red colored points represent the second energy level. Different symbol styles represent effective masses for different values of λ.
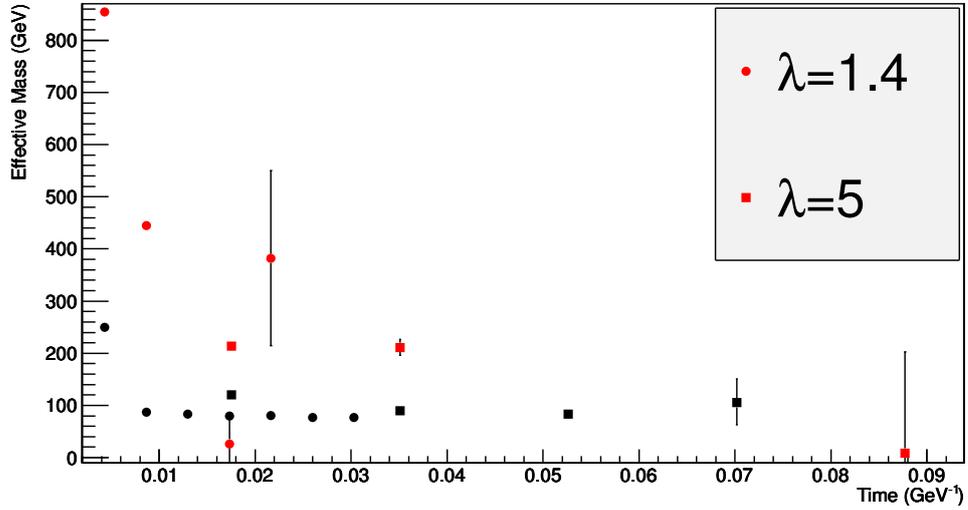
Figure 2.23: Effective masses of two energy levels are plotted from eigenvalues for $\beta = 3.0$ and $\kappa = 0.315$ for lattice of size 24^4 in 1^- channel. Black colored points represent the first energy level and red colored points represent the second energy level. Different symbol styles represent effective masses for different values of λ.
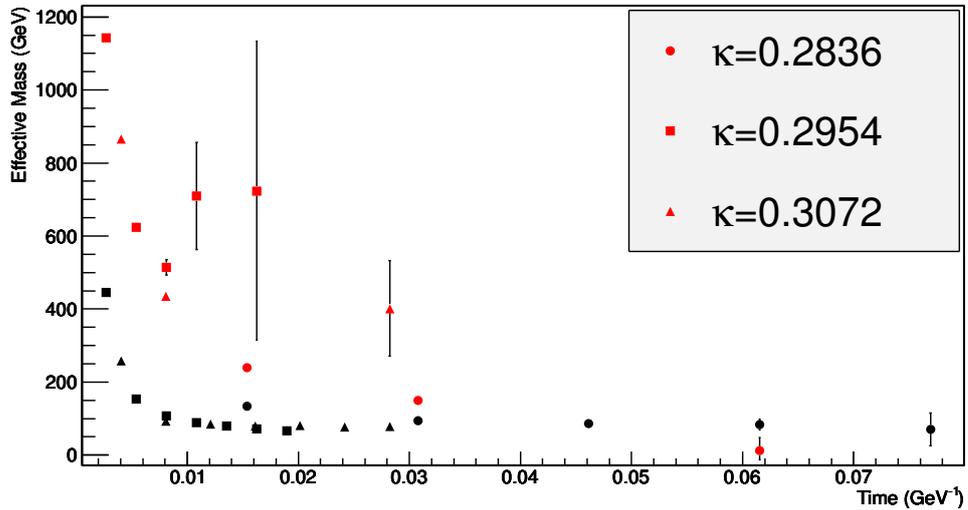

Figure 2.24: Effective masses of two energy levels are plotted from eigenvalues for $\beta = 3.0$ and $\lambda = 1.317$ for lattice of size 24^4 in 1^- channel. Black colored points represent the first energy level and red colored points represent the second energy level. Different symbol styles represent effective masses for different values of κ.
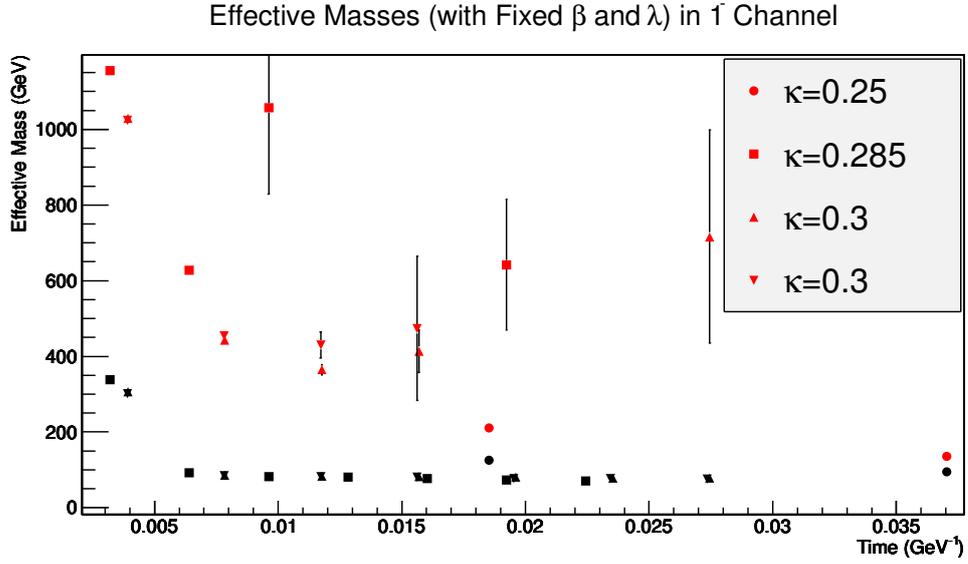
Figure 2.25: Effective masses of two energy levels are plotted from eigenvalues for $\beta = 4.0$ and $\lambda = [1.0, 1.05]$ for lattice of size 24^4 in 1^- channel. Black colored points represent the first energy level and red colored points represent the second energy level. Different symbol styles represent effective masses for different values of κ.
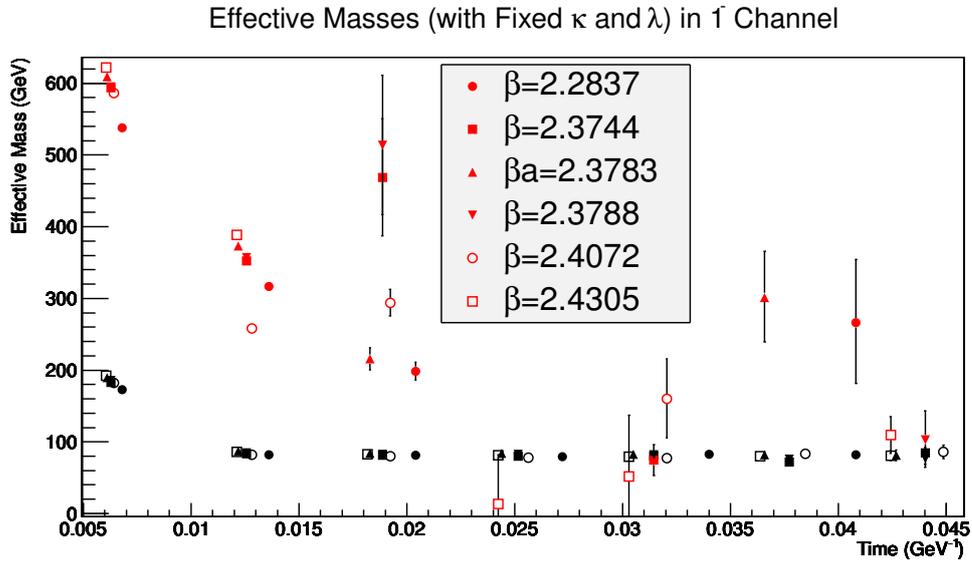

Figure 2.26: Effective masses of two energy levels are plotted from eigenvalues for $0.320 < \kappa < 0.329$ and $1.10 < \lambda = 1.13$ for lattice of size 24^4 in 1^- channel. Black colored points represent the first energy level and red colored points represent the second energy level. Different symbol styles represent effective masses for different values of β.

Figure 2.27: Masses in 0^+ channel for different LCPs are show in the figure. For these LCPs, $0.52 < R_1 < 0.56$ and $R_2 \approx 0.5$. Black points represent the ground state and red points represent first first excited state. The parameter a is lattice spacing.

Figure 2.28: Masses in 0^+ channel for different LCPs are show in the figure. For these LCPs, $2.12 < R_1 < 2.15$ and $R_2 \approx 1.63$. Black points represent the ground state and red points represent first first excited state. The parameter a is lattice spacing.

Figure 2.29: Masses in 0^+ channel for different LCPs are show in the figure. For these LCPs, $1.51 < R_1 < 1.54$ and $R_2 \approx 1.63$. Black points represent the ground state and red points represent first first excited state. The parameter a is lattice spacing.
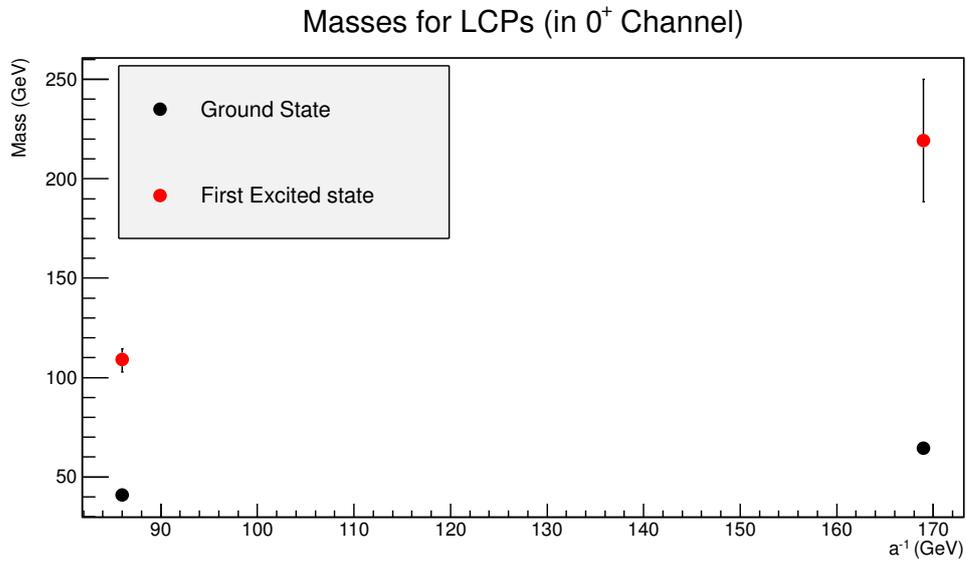

Figure 2.30: Masses in 1^- channel for different LCPs are show in the figure. For these LCPs, $0.52 < R_1 < 0.56$ and $R_2 \approx 0.5$. Black points represent the ground state and red points represent first first excited state. The parameter a is lattice spacing.

Figure 2.31: Masses in 1^- channel for different LCPs are show in the figure. For these LCPs, $1.51 < R_1 < 1.54$ and $R_2 \approx 1.63$. Black points represent the ground state and red points represent first first excited state. The parameter a is lattice spacing.
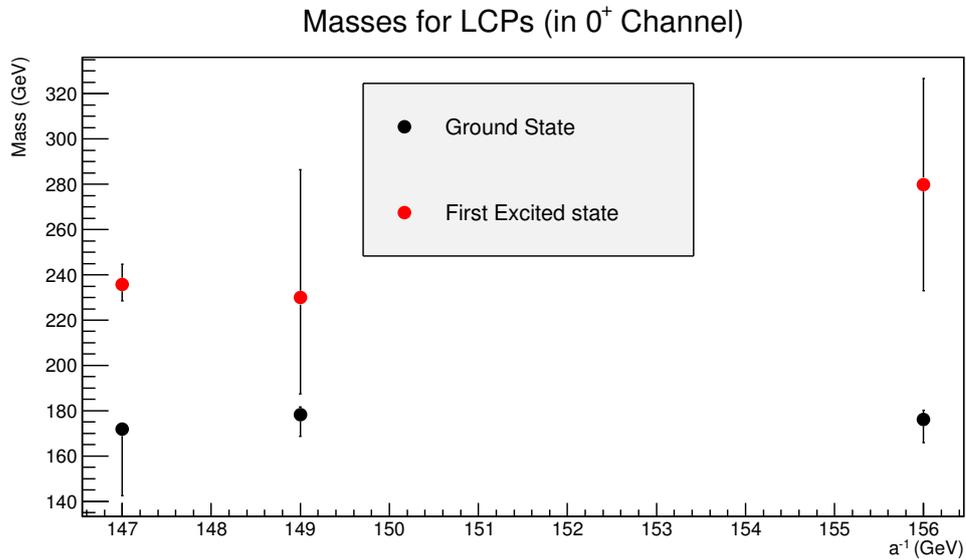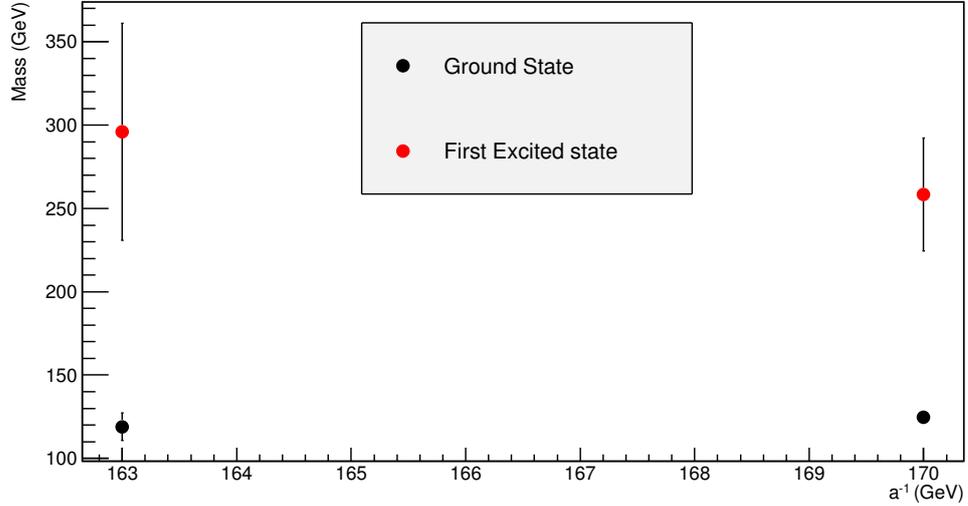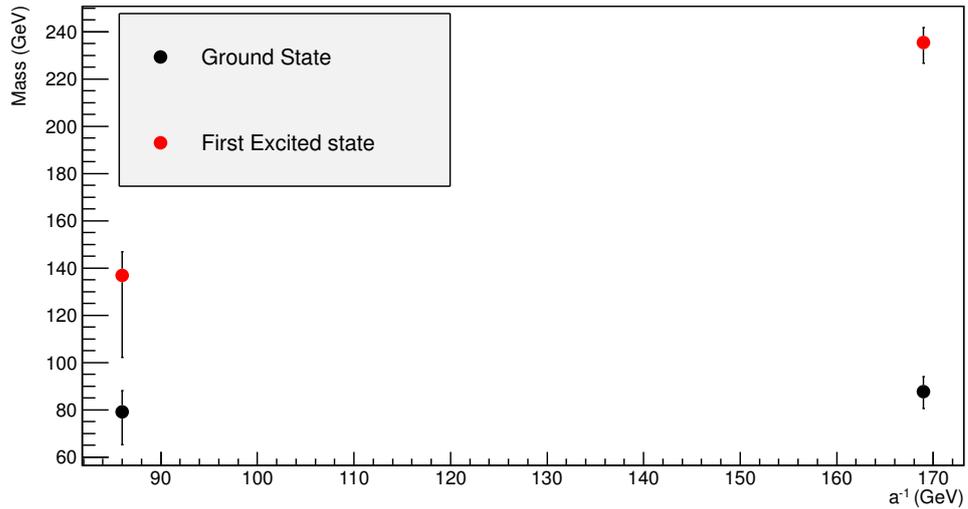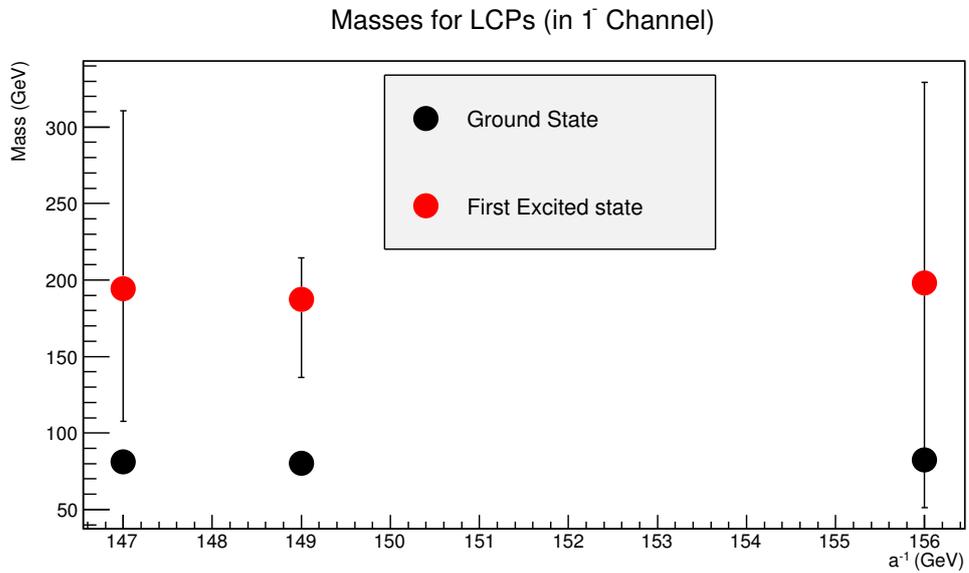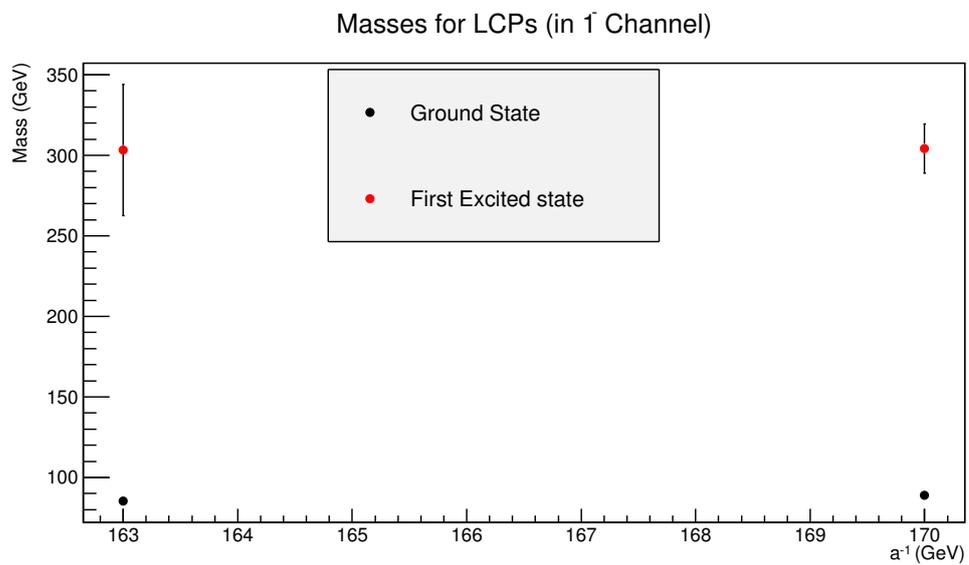

Figure 2.32: Masses in 1^- channel for different LCPs are show in the figure. For these LCPs, $1.51 < R_1 < 1.54$ and $R_2 \approx 1.63$. Black points represent the ground state and red points represent first first excited state. The parameter a is lattice spacing.
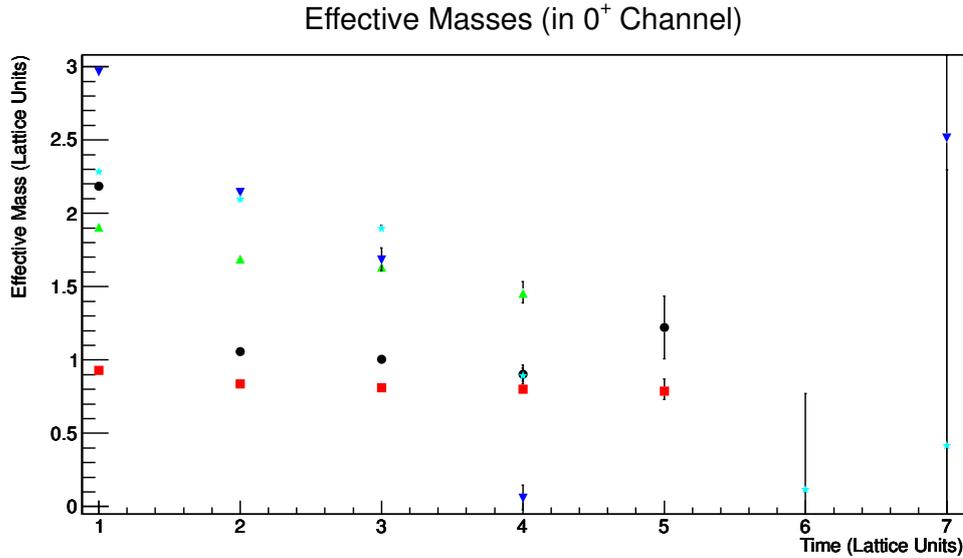
Figure 2.33: Effective masses in 0^+ channel are plotted using 5 operators on the lattice of size 24^4. The parameters are $\beta = 2.2945$, $\kappa = 0.3191$, and $\lambda = 1.143$. Symbols with different styles and colors represent different effective masses.

With the help of the three masses, two ratios $R_1 = \frac{m_{0^+}}{m_{1^-}}$ and $R_2 = \frac{m_{0^+}}{m_{1_s^-}}$ are considered along with the lowest state in 1^- triplet channel which is used to set the scale and hence serves as the third quantity. The effect of lattice discretization is investigated in both 0^+ and 1^- triplet channels. The results are shown in figures 2.27-2.32 for three different cases, mentioned on the caption of the figures.

As the masses are already not known in advance, based upon the available information [31] ranges of values for ratios are set for same LCPs instead of fixed values. Overall the observation is that within statistical errors, the masses in both 0^+ and 1^- triplet channels are in agreement for different chosen values of lattice spacings. There is an exception for the case in figure 2.30. Though, currently there are not many LCPs available for selected ratios, it gives at least a preliminary idea that it might be possible that for the chosen range of lattice spacings there is no considerable dependence of masses on lattice spacing. The most convenient situation would be that masses do not depend upon any lattice spacing, and hence the descritization effects would not play any role in the masses. However, more LCPs are required to reach any conclusion for YMH theory.

2.6   Phenomenology in YMH Theory

It is already mentioned that YMH theory is a part of the SM, it means that the predictions of this theory will not contain any contribution from other parts of the SM. However, it is very interesting to see how close its predictions are with its current status from the point of view of phenomenology. This investigation will give us a chance to compare our results with naive
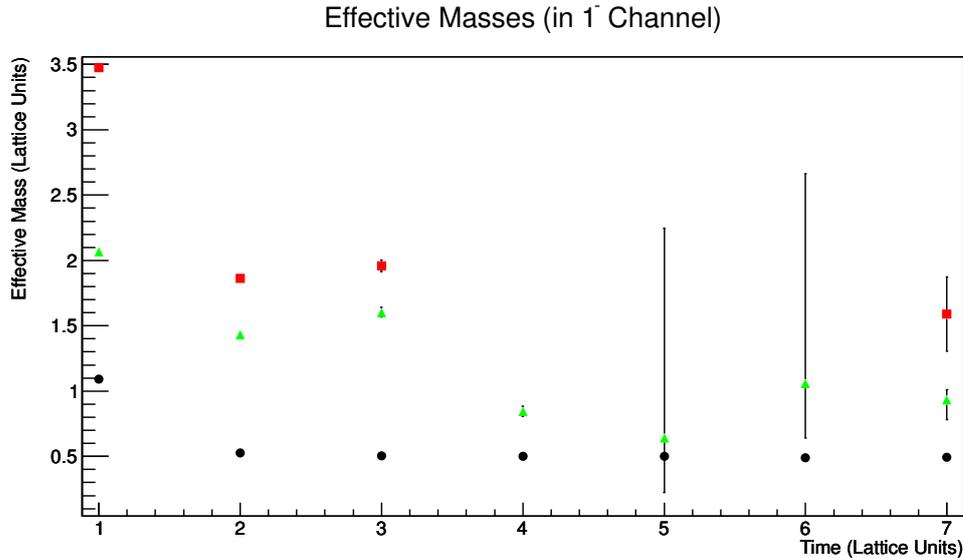
Figure 2.34: Effective masses in 1^- channel are plotted using 3 operators on the lattice of size 24^4. The parameters are $\beta = 2.2945$, $\kappa = 0.3191$, and $\lambda = 1.143$. Symbols with different styles and colors represent different effective masses.

expectations for a weakly interacting theory. Based on the current status of the results for Higgs searches, the key to such investigation is to choose (or find) a set of parameters for which the ground state in the spectrum of 1^- and 0^+ channels is in 1^-, and then investigating the spectrum in these channels. However, from more theoretical point of view, it is interesting to study the spectra for the cases when the ground state in the spectrum lies in 0^+ channel, and when the ground state is 1^- channel but the lowest state in 0^+ is heavier than around 126 GeV. For the first situation, the relevant Physics is also important from the point of view of QCD. This matter will be considered in chapter 3, though for gauge dependent quantities. For the second situation, since nature could have chosen any mass for experimentally found Higgs, it is very interesting to see how the spectrum would look like with a state in 0^+ which is heavier than currently known Higgs. For all the cases, the calculated spectra are compared with naively expected spectra.

In figures 2.33 and 2.34, effective masses in 0^+ singlet and 1^- triplet are shown for different energy levels for the nature of parameter values mentioned above. Their respective eigenvalues, as a function of time, are fitted by the Cosh function(s) described in detail in section 2.3. The masses are converted from lattice units into physical units using the prescription described before, such that the lowest state in 1^- triplet channel for our chosen parameters is 80.375 GeV. Note that in figure 2.34, the masses for higher than ground energy level do not show any particular pattern which is already suggestive that fitting such a behavior by *Cosh* function(s) will not be easy. It is the reason that the spectrum, which is shown schematically in figure 2.35 does not even contain as many masses of energy levels as the number of operators. A similar situation with the parameters, which provide us the lowest state in 0^+ channel around

40

Figure 2.35: Spectrum for YMH theory is shown in the figure in HLD. The dotted lines represent the naively expected energy levels in each of 0^+ and 1^- channel. Red and blue boxes, with their average value of masses, represent our findings for the parameters $\beta = 2.2945$, $\kappa = 0.3191$, and $\lambda = 1.143$, using 24^4 lattice. The width of the boxes represents uncertainty in the values of masses. The details about shown the naively expected energy levels, represented by dotted lines, is as follows: The lowest line in 1^- channel is used to give physical dimensions to masses of energy levels. The lowest line in 0^+ channel corresponds to the Higgs found in LHC. The first higher line in 0^+ channel is double of the lowest state in 1^-, the second is twice of lowest LHC Higgs state, the third line in 0^+ channel is combination of the two lowest lines in 0^+. The first higher line in 1^- channel is combination of the lowest line in 0^+ channel and the lowest line 1^- channel. The second higher line in 1^- channel is three times the lowest line in 1^- channel.
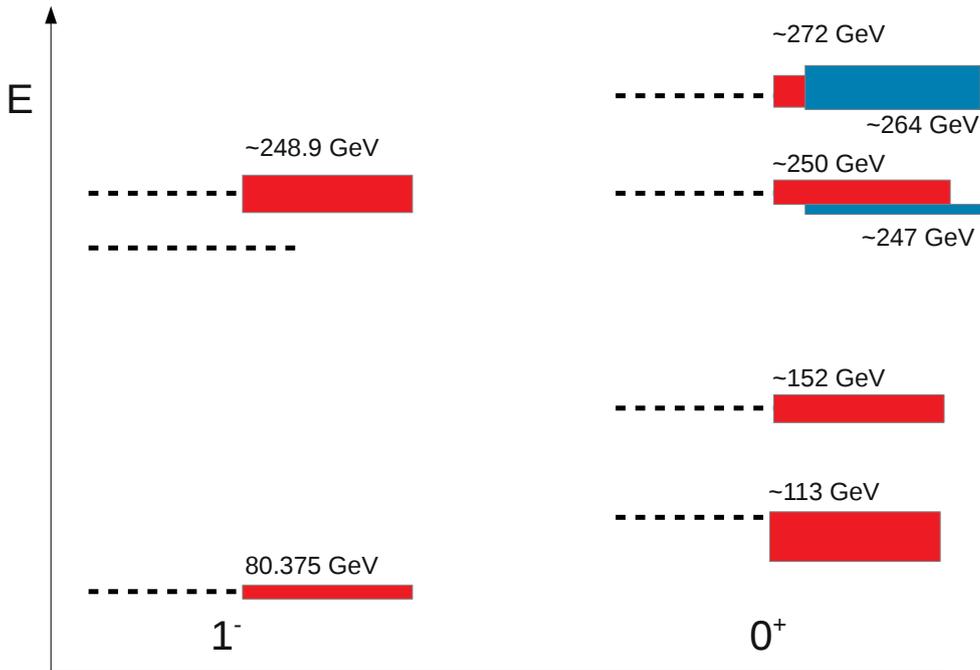
Figure 2.36: Spectrum for YMH theory is shown in the figure in HLD. The dotted lines represent the naively expected energy levels in each of 0^+ and 1^- channel. Red boxes, with their average value of masses, represent our findings for the parameters $\beta = 2.8303$, $\kappa = 0.2954$, and $\lambda = 1.317$, using 24^4 lattice. The width of the boxes represents uncertainty in the values of masses. The details about the shown naively expected energy levels, represented by dotted lines, is as follows: The lowest line in 1^- channel is used to give physical dimensions to masses of energy levels. The lowest line in 0^+ channel corresponds to the Higgs found in LHC. The first higher line in 0^+ channel is twice of the lowest line in 1^- channel. The second higher line in 0^+ channel is twice of the lowest line in 0^+ channel. The third higher line in 0^+ channel is twice the first higher line in 0^+ channel. The fourth higher line in 0^+ channel is combination of the third higher line and ground state in 0^+ channel. The first higher line in 1^- channel is combination of the lowest states in 0^+ and $1-$ channels. The second higher line in 1^- is thrice the lowest state in 1^- channel. The third higher line in 1^- channel is combination of the second higher line in 0^+ channel and the lowest state in 1^- channel. The fourth higher line in 1^- channel is 5 times heavier than the lowest state in 1^- channel.
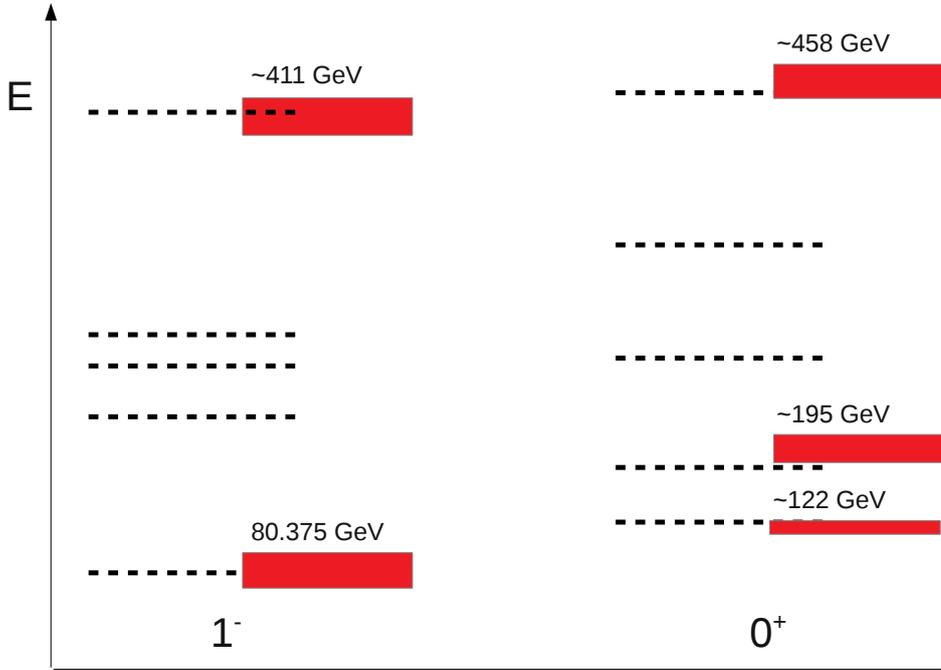
Figure 2.37: Spectrum for YMH theory is shown in the figure in QLD. The dotted lines represent the naively expected energy levels in each of 0^+ and 1^- channel. Red boxes, with their average value of masses, represent our findings for the parameters $\beta = 2.4492$, $\kappa = 0.2939$, and $\lambda = 1.036$, using 24^4 lattice. The width of the boxes represents uncertainty in the values of masses. The details about the shown naively expected energy levels, represented by dotted lines, is as follows: The lowest line in 1^- channel is used to give physical dimensions to masses of energy levels, despite that now it not the ground state of the whole spectrum. The lowest state in 0^+ channel is found from simulations, hence it trivially coincides with the found lowest level in 0^+ channel. The first higher line in 0^+ channel is 4 times heavier than the lowest state in 0^+ channel. The second higher line in 0^+ channel is the double of first higher line in 0^+ channel. The third higher line in '0^+ channel is the combination of second and first higher lines in 0^+ channel.The fourth higher line in 0^+ channel is twice the second higher line in 0^+ channel. In 1^- channel, the first higher line is the combination of the ground and first higher line in 0^+ and the lowest state in 1^- channels. The second higher line in 1^- channel is a combination of 5 times heavier than lowest state in 1^- channel and the lowest state in 0^+ channel.
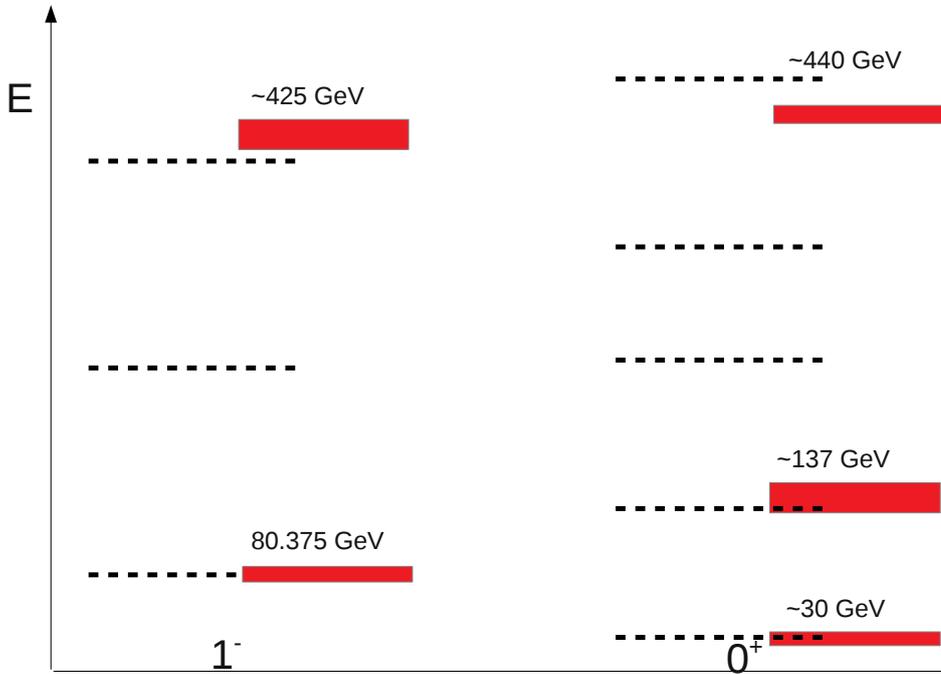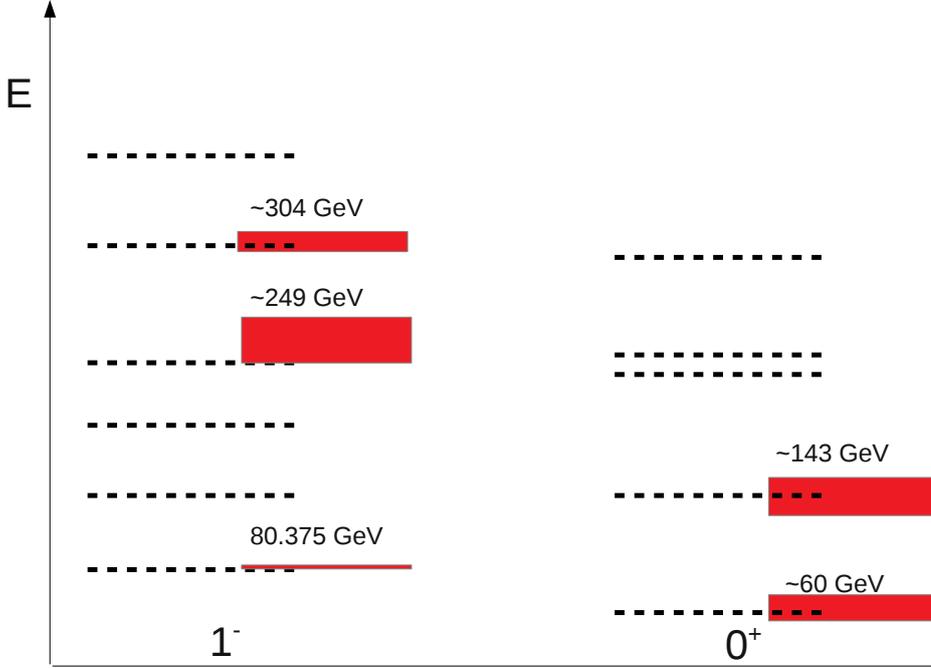
Figure 2.38: Spectrum for YMH theory is shown in the figure in QLD. The dotted lines represent the naively expected energy levels in each of 0^+ and 1^- channel. Red boxes, with their average value of masses, represent our findings for the parameters $\beta = 2.4728$, $\kappa = 0.2939$, and $\lambda = 1.088$, using 24^4 lattice. The width of the boxes represents uncertainty in the values of masses. The details about the shown naively expected energy levels, represented by dotted lines, is as follows: The lowest line in 1^- channel is used to give physical dimensions to masses of energy levels, despite that now it not the ground state of the whole spectrum. The lowest state in 0^+ channel is found from simulations, hence it trivially coincides with the found lowest level in 0^+ channel. The first higher line in 0^+ channel is twice the lowest state in 1^- channel. The second higher line in 0^+ channel is the combination of the two lowest lines in 0^+ channel. The third higher line in 0^+ channel is 4 times heavier than the lowest line in 0^+ channel. The fourth higher line in 0^+ channel is twice the first higher line in 0^+ channel. The third higher line in 0^+ channel is the twice of the first higher line in 0^+ channel. The first higher line in 1^- channel is the combination of the lowest states in 0^+ and 1^- channels. The second higher line in 1^- channel is the combination of the first higher line in 1^- and the lowest line in 0^+ channel. The third higher line in 1^- channel is thrice of the lowest line in 1^- channel. The fourth higher line in 1^- channel is the combination of the lowest line in 1^- channel and the second higher line in 0^+ channel. The fifth higher line in 1^- channel, which is the highest shown line on the figure in this channel, is 5 times heavier than the lowest line in 1^- channel.
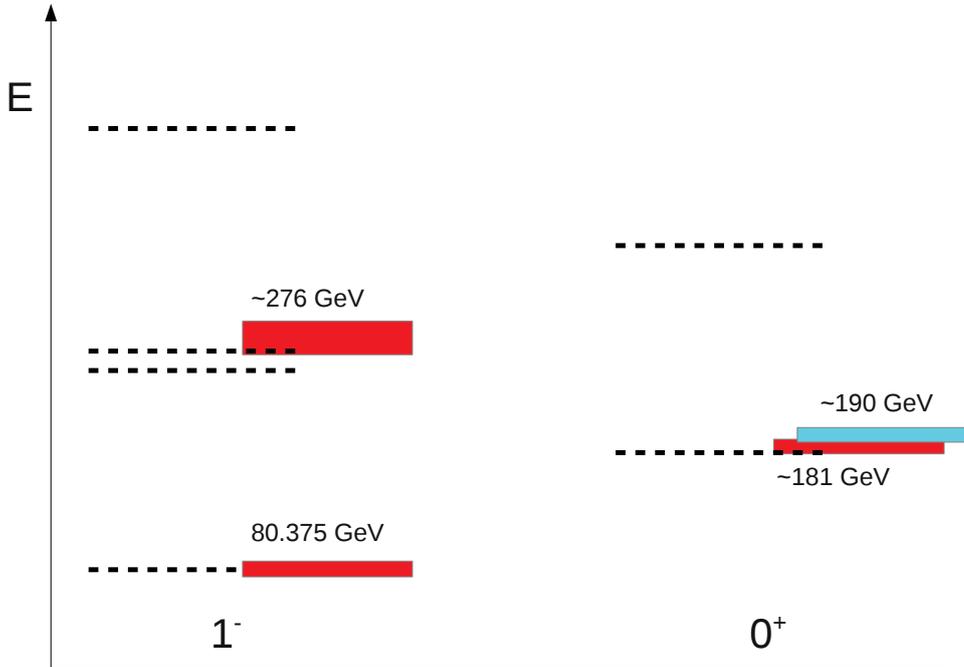
Figure 2.39: Spectrum for YMH theory is shown in the figure in HLD with heavy state in 0^+ channel. The dotted lines represent the naively expected energy levels in each of 0^+ and 1^- channel. Red and blue boxes, with their average value of masses, represent our findings for the parameters $\beta = 2.4072$, $\kappa = 0.3228$, and $\lambda = 1.110$, using 24^4 lattice. The width of the boxes represents uncertainty in the values of masses. The details about shown the naively expected energy levels, represented by dotted lines, is as follows: The lowest line in 1^- channel is used to give physical dimensions to masses of energy levels. The lowest line in 0^+ channel corresponds to the situation when this state is heavier than the Higgs mass found at LHC. The first higher line in 0^+ channel is twice the lowest line in 0^+ channel. The first higher line in 1^- channel is thrice the lowest line in 1^- channel. The second higher line in 1^- channel is the combination of the first higher line in 0^+ channel and the lowest line in 1^- channel. The third higher line in 1^- channel is 5 times heavier than the lowest line in 1^- channel.

the experimentally found Higgs, is also shown in figure 2.36.

It is clear from figures 2.35 and 2.36 that our finding is similar to what is expected naively in a weakly interacting theory. There are couple of more masses we found but still with the present status it is hard to conclude whether they are really some other energy levels or they will disappear when higher statistics is considered. Due to their vague status, if they are not given status of a different state than the ones with which they are statistically in agreement, at least for the selected values of parameters the YMH theory behaves like a weakly interacting theory. If this is really the case for the YMH theory, the expectation is that nothing out of the ordinary will be found before the TeV scale when the theory is speculated to become strongly interacting anyway.

In figures 2.37 and 2.38, the spectra are shown for the situation when the ground state of the spectrum lies in 0^+ channel. During the whole investigation, the scale is set for the lowest state in 1^- channel. Despite that there are afew levels which do not exactly coincide with naive expectations, they still agree within 3σ.

In figure 2.39 is shown the spectrum for the situation when the lowest state in 0^+ singlet channel is heavier than twice the lowest state in 1^- triplet channel. For this situation, despite only a few available energy levels in the theory, the agreement with naive expectation for spectrum is evident. It supports that the YMH theory might be indeed a weakly interacting theory till the point when non-perturbative Physics takes over. Furthermore, 2.39 also encourages us to consider a situation when transitions among different channels take place, which is the subject of discussion in the next two sections.

2.7 Lüscher Method

As importance of YMH theory has already been established, study of spectroscopy takes the utmost importance from the point of view of phenomenology. As it is already explained how gauge invariant states can be used to calculate masses of the energy levels in the theory, experimentally what is observed is not energy levels but the transitions between these levels. The only requirements are conservation of the four momentum (momentum in four dimensions) and quantum numbers. When it comes to calculating quantities, such as decay width and phase shift, in continuum there exist formulas in the literature. For the case of lattice, there exist Lüscher method [15] which can be used to relate information from the situation of a particle in a box, to continuum. Since there exist energy levels in YMH theory, it can also be employed in YMH theory.

However, there are limitations on this method. Every field comes with a (or set of) quantum number(s). Set of energy levels with the same quantum number(s) forms a *channel*. Hence it trivially also means that a transition can take place between one channel or more than one channels. For Lüscher method to work, there has to be only one type of decay among the

channels in YMH theory. Such decays or scatterings are called *elastic scattering*. Since the method itself can already be found in [15, 32], here only those mathematical expressions are mentioned which are used during investigation of YMH theory.

In the following, the transition considered is from 0^+ (parent) channel to 1^- (daughter). In terms of energy levels, one energy level with quantum numbers 0^+ decays into two energy levels in 1^- channel. Since there are two daughters, and the whole computation is in the center of mass coordinate system, each daughter takes the same value of energy which can be calculated by

$$m_p = 2\sqrt{m_d^2 + k_d^2} \tag{2.25}$$

where m_p is the mass (energy) of the parent energy level, and m_d and k_d are mass and momentum of each daughter. The masses are calculated using the gauge invariant correlation functions, which means that k_d can be calculated from above equation. With this information, a variable q can be calculated using [15]

$$q = \frac{k_d L}{2\pi} \tag{2.26}$$

where L is the length of lattice along one direction. It can be used to calculate the zeta function $Z_{00}(1;q)$ using the following equation [33] [4]

$$Z_{00}^d(1:q^2) = \gamma \int_0^1 dt e^{tq^2} \sum_{\mathbf{u}\epsilon Z^3, u\neq 0} (-1)^{u.d} y_{00}^*(\frac{-\pi \overrightarrow{\gamma}.\overrightarrow{u}}{t})(\frac{\pi}{t})^{\frac{3}{2}} e^{\frac{-|\pi \overrightarrow{\gamma}.\overrightarrow{u}|^2}{t}}$$

$$+\gamma \int_0^1 dt (e^{tq^2} - 1)\frac{1}{\sqrt{4\pi}}(\frac{\pi}{t})^{\frac{3}{2}} - \gamma\pi$$

$$+ \sum_{\frac{2\pi\mathbf{u}}{L}\epsilon P_d} \frac{y_{00}^*(\mathbf{n})}{|\mathbf{n}|^2 - q^2} e^{-(|\mathbf{n}|^2 - q^2)} \tag{2.27}$$

where, other than the traditionally used symbols, d, $\gamma, \overrightarrow{\gamma}$,y_{lm} and L are number of dimensions, relativistic factor, its vector form, spherical harmonics and lattice size along one direction, respectively. The bold letters are for the vector components in three dimensions. For our purpose $\frac{2\pi\mathbf{u}}{L}$ becomes a set of integers in 3 dimensions [33]. Once the zeta function $Z_{00}(1;q)$ is known, it is easy to calculate the angle $\phi(q)$ (phase shift) using [15]

$$\phi(q) = tan^{-1}(-\frac{\pi^{\frac{3}{2}} q}{Z_{00}(1;q^2)}) \tag{2.28}$$

2.8 Spectral Transitions in Yang-Mills-Higgs Theory

The spectra in YMH theory for 0^+ singlet and 1^- triplet channels have already been discussed for different regions in parameter space. It is always possible in these channels, and in principle

---

[4]An expression for $Z_{00}(1;q^2)$ is also found in [15]. However, it was not used because from this expression is divergent. The expression in [32] does not have this problem and hence it was used.
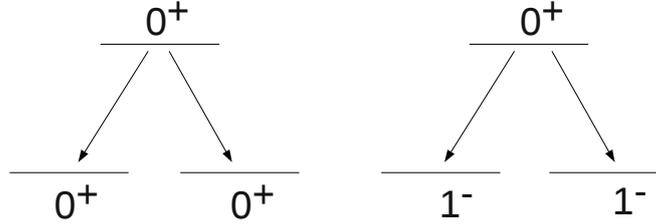
Figure 2.40: A pictorial display of two possible transitions from 0^+ channel into 0^+ channel and into 1^- channel. On left hand side, the 0^+ state is equal or more than twice of a state in 0^+ channel, which makes the transition possible. On the right hand side, a 0^+ is equal or heavier than twice of a state in 1^- channel, hence making the transition possible.

in other channels too, that the system can make a transition from one energy level to another energy level, provided that quantum numbers and the four momenta are conserved. These transitions can take place within as well as among different energy levels. Figure 2.40 shows two examples of such transitions pictorially. From the point of view of phenomenology, it is interesting to investigate these transitions for HLD so that the ground state of the theory is in 1^- channel. Transition from 0^+ singlet to 1^- triplet channel is discussed in this section [5].

In order to investigate these transitions, the first step is to check the nature of these excited states. For this purpose Lüscher's method can be used with the assumption that the transition from a level in 0^+ to the ground state in 1^- lies in the so-called elastic scattering window. The results for the parameters $\beta = 3.881, \kappa = 0.3214, \lambda = 0.9974$ in our theory fulfill the requirement for this task because there exists an state in 0^+ which is in the elastic region. Hence, results from different volumes can be used to calculate phase shift as a function of center of mass energy.

As in figure 2.41, there is a vague sign that the phase shift might not cross the 90 degrees. However, it is obvious from the figure that the error is still considerable for the present statistics. Hence right now no reliable conclusion can be drawn from the situation in order to truly see the trend of points in the figure. Since the whole calculation right from the variational analysis to phase shift calculation is highly non-linear, it is also very hard to say how much more statistics

---

[5]For the transition 0^+ to 0^+, the situation is still not very encouraging. The reason is that already some of the simplest operators have been used and as in the figures they turned out to be statistically very noisy. Even for the variational analysis most of these operators were never used since they spoil the numerical computations because of their statistical noise.
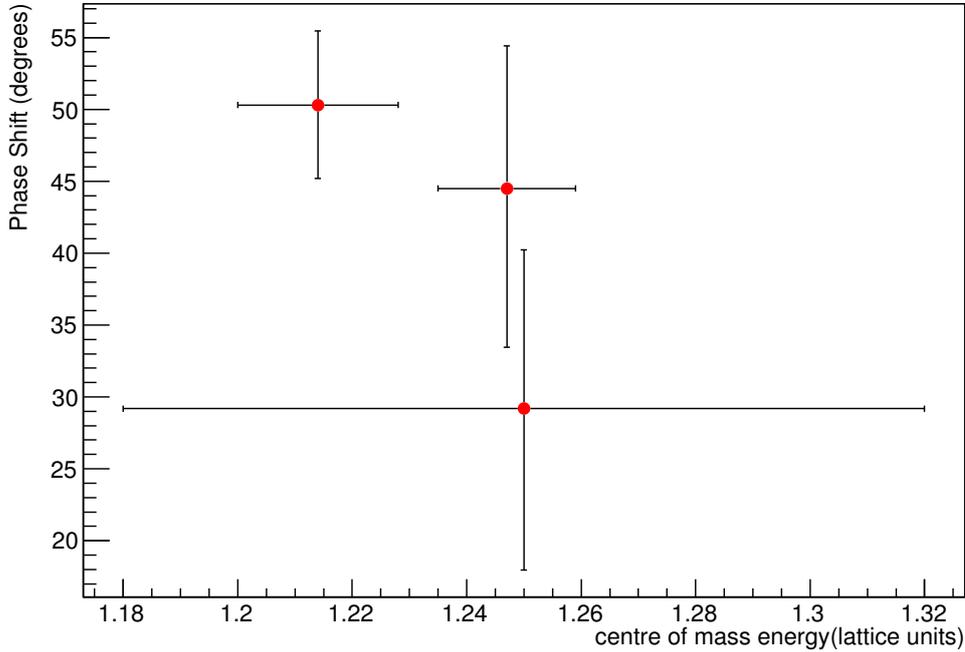
Figure 2.41: Phase shift plot from Lüscher's method, using the transition from 0^+ to 1^-, for the parameters $\beta = 3.881, \kappa = 0.3214, \lambda = 0.9974$.

is needed to suppress the error bars in the figure to the point that a reliable conclusion can be drawn. Moreover, since the lattice is rather coarse, such energy levels are also required to be investigated for relatively finer lattices. If for higher, and maybe also with finer lattices, the trend of points does pass through 90 degrees, it will be the indicative of a resonance for the set of parameters which will be theoretically very fascinating discovery from the point of view of Spectroscopy.

2.9 Duality between Elementary Particles and Bound States

The experimentally found Higgs turns out to be not too heavy to raise questions on the validity of perturbative calculations [3]. It means that the Higgs mass can be a pole in the tree level scalar propagator, while the perturbative corrections are not very significant for a Higgs with around 126 GeV mass. However, theoretically it is also possible to propose a gauge invariant state as a candidate for the experimentally found scalar state [27] with the experimentally found mass for Higgs. It raises the question whether an elementary particle in a gauge theory can mimic a gauge invariant state, such as a bound state, and in case it is true, if this is true irrespective of how heavy the bound state is.

For this purpose, lets first note that (i) the propagators are gauge dependent quantities, and (ii) the chosen gauge is a non-aligned gauge [27]. The four point function considered for

Figure 2.42: Effective masses from Schwinger function and ground state in 0^+ channel, with lowest mass around 113 GeV in the channel, are plotted for parameters $\beta = 2.4728, \kappa = 0.2939, \lambda = 1.036$. The lattice size is 24^4.

Figure 2.43: Effective masses from Schwinger function and ground state in 0^+ channel, with lowest mass around 171 GeV in the channel, are plotted for parameters $\beta = 3.881, \kappa = 0.3214, \lambda = 0.9974$. The lattice size is 24^4.

Figure 2.44: Effective masses from Schwinger function and ground state in 1^- channel, with lowest mass around 113 GeV in the channel, are plotted for parameters $\beta = 2.4728, \kappa = 0.2939, \lambda = 1.036$. The lattice size is 24^4.
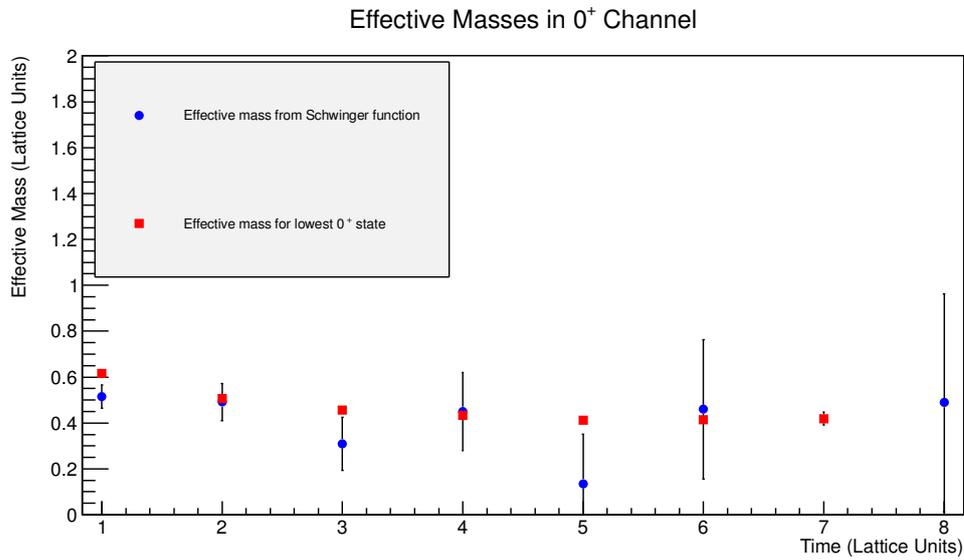

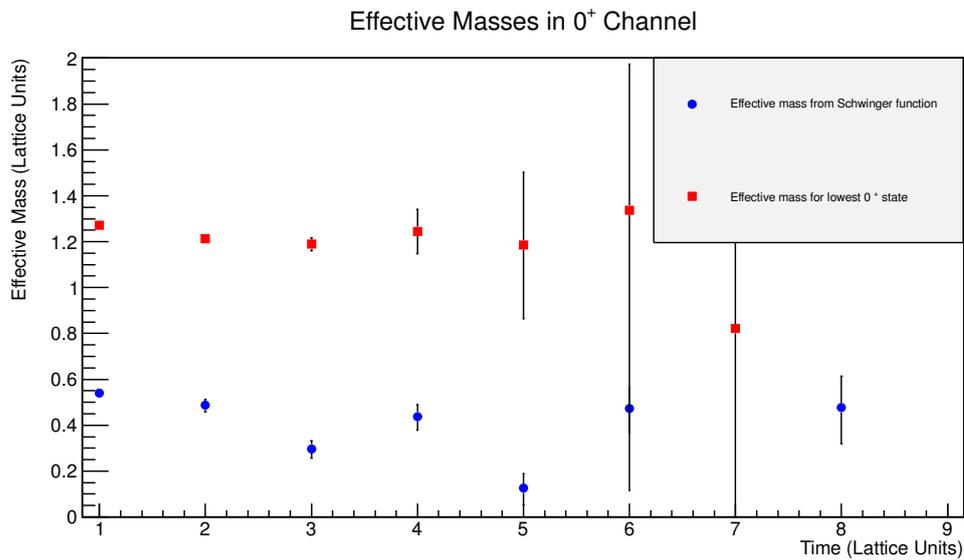Figure 2.45: Effective masses from Schwinger function and ground state in 1^- channel, with lowest mass around 171 GeV in the channel, are plotted for parameters $\beta = 3.881, \kappa = 0.3214, \lambda = 0.9974$. The lattice size is 24^4.
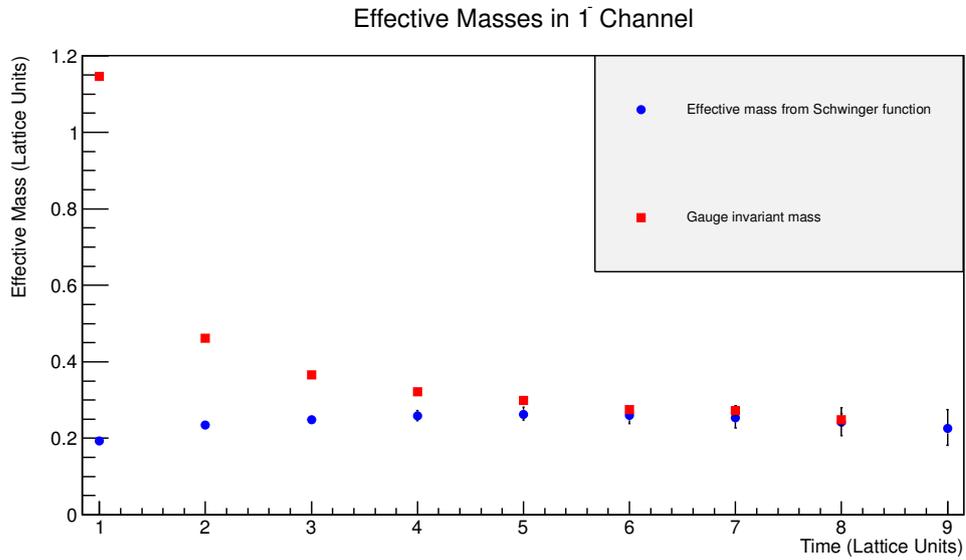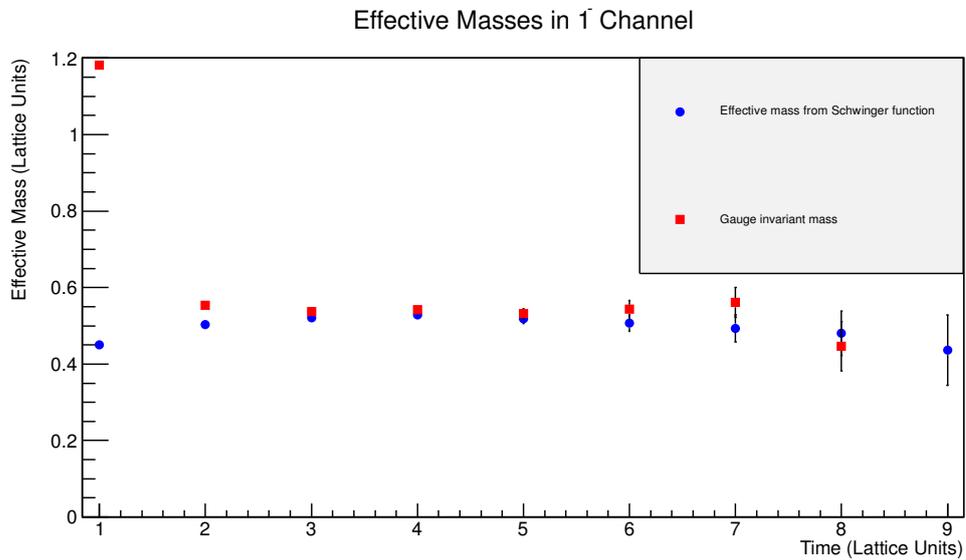
two Higgs states is given by $< h_i^\dagger(x)h_i(x)h_k^\dagger(y)h_k(y) >$. Here h is the scalar (Higgs) field, the Latin indices (i and k) are internal symmetry indices while x and y represent position in space time coordinates. Scalar field can be written as [27]

$$h_i(x) = vn_i(x) + \lambda_i(x) \tag{2.29}$$

with v as a constant and $n_i(x)$ is the component of the unit vector in the direction along i. $\lambda_i(x)$ is a fluctuating field in the space of internal symmetry indices. Expanding the scalar field using the above equation

$$< h_i^\dagger(x)h_i(x)h_k^\dagger(y)h_k(y) > = < (vn_i(x) + \lambda_i(x))^\dagger(vn_i(x) + \lambda_i(x))$$

$$(vn_i(y) + \lambda_i(y))^\dagger(vn_i(y) + \lambda_i(y)) > \tag{2.30}$$

Since $n_i(x)$ is a component of unit vector,

$$n_i^\dagger n_i = 1 \tag{2.31}$$

we can use this information and the zeroness of one point functions, and considering negligible quantum fluctuations, to achieve the equation [27],

$$< h_i^\dagger(x)h_i(x)h_k^\dagger(y)h_k(y) > \approx v^4 + v^2 < h_i^\dagger h_i > + c_0 + \bigcirc(\lambda) \tag{2.32}$$

where c_0 and $\bigcirc(\lambda)$ are irrelevant constants and negligible terms, respectively, which are not interesting at the moment.

Above equation implies that up to a multiplicative and an additive constant the two point function, which is the propagator, behaves like a four point function which is a gauge invariant quantity. If this is true, the mass calculated from the gauge invariant quantity should coincide with the pole of tree level scalar propagator. However, this is the case only when λ is negligible. If the quantum fluctuations are considerable, this duality may no longer exist. One of the possibilities to observe these two scenarios is to plot an *effective mass* from the Schwinger function of Higgs (Schwinger function will be discussed in chapter 3, for now it is sufficient to know that it is a propagator in space time coordinates) and mass from the GICF. This situation can be seen in the results given in figures 2.42 and 2.43.

In figure 2.42 the agreement between the two masses suggests that when the pole mass of bound state in 0^+ is low, due to the negligible quantum fluctuations the pole mass of Higgs, which came from Schwinger function, coincides with that of a gauge invariant mass in 0^+ channel. On the other hand, in figure 2.43 the disagreement is also evident before the statistical fluctuations become relatively stronger.

In the same way, it is also possible to investigate the existence of duality for the gauge field

in YMH theory [27]. It is done choosing the operator in equation 2.15 which is in 1^- channel. However, for simplicity and direct relevance it is already considered that (1) the expectation value of the Higgs field is zero, which is true for non-aligned gauges, and (2) the expectation value of gauge field is zero, this point is explained in section 3.3.1. For simplicity, the operator in equation 2.15 can be rewritten as follows;

$$\bigcirc_{a\mu}^{1^-}(x) \approx Tr\left(\tau_a \varphi^\dagger(x)(1 - i\tau_b W_\mu^b + \bigcirc(W_\mu^c))\varphi(x + e_\mu)\right) \tag{2.33}$$

where $\bigcirc(W_\mu^c)$ represents all the higher order terms, which are not very interesting for our purpose, and hence will be ignored. Assuming that the quantum fluctuations in scalar field is negligible, the (matrix of) fields $\varphi(x)$ can be taken as approximately constant in comparison with W_μ^b. For this situation, they can be treated as constants and with a little bit of algebra and properties of trace of matrix, the equation takes the following form;

$$\bigcirc_{a\mu}^{1^-}(x) \approx c_{a\mu} + W_\mu^b(x)d_{ab} \tag{2.34}$$

where $c_{a\mu}$ and d_{ab} are not interesting terms for our purpose. Using equation 2.34 for expanding the gauge invariant correlation function gives us the following expression.

$$< \left(\bigcirc_{a\mu}^{1^-}(x)\right)^\dagger \bigcirc_{a\mu}^{1^-}(y) > = k_{lb} < W_\mu^b W_\mu^l > + constant \tag{2.35}$$

where k_{bl} is also an irrelevant term, while higher order terms in W have already been neglected. With the most interesting parts explicit in above equation, it is clear that as long as the higher order corrections are small, duality also holds for the gauge field.

In figures 2.44 and 2.45, the effective masses from Schwinger functions of gauge fields, and masses from gauge invariant states are shown. For the situation when the lowest state in 0^+ channel is around the observed Higgs mass, when the quantum fluctuations are considered to be negligible, the agreement between the two masses for gauge field is very clear, which supports the existence of duality. However, despite the fact that there seems to be some agreement between the two masses for the case of heavy Higgs state, the matter is not completely resolved since it is unclear till what extent the agreement between the masses from the ground state in 1^- channel and that of gauge field propagator [13] will last for this particular set of parameters [27].

Chapter 3

Gauge Dependent Correlation Functions

3.1 Introduction

The contents of this chapter have already been published [13]. In contrast to GICFs, gauge dependent correlation functions can not be observables, trivially because anything that depends upon gauge can not be the choice of nature for an observable.

There are a number of reasons for such investigations. Both for the propagators and the vertices, knowledge of them can be used as input correlation functions for analytical methods, such as Dyson Schwinger Equations [10]. As it has already been pointed out in chapter 1, DSEs are mostly composed of coupling constants and correlation functions. It means that if DSE for a particular correlation function is to be solved, it will require knowledge of other correlation functions which are present in the DSE. Either an educated guess can be used for these input correlation functions, or the knowledge of already known correlation functions can be used.

Not only is it very helpful for the purpose of computation, but such investigations are also important for development of analytical techniques, finding solutions in DSEs is again an example. As it is already known that in DSEs, solutions are attained by different assumptions, such as truncation. Since these solutions are, in general, dependent upon ansatz and/or truncation used, they can be attained and studied to see if they make sense, and in the meantime computation techniques can also be developed and/or improved.

From phenomenology's point of view, YMH theory is very helpful in understanding confinement problem due to the reason that it has gauge field-scalar field vertices which can act as a gauge field-matter field vertices for some special sets of parameters which represent QCD like Physics [13]. This vertex can be helpful in understanding how the gauge field interacts with matter fields which can gives us insight into confinement. Knowledge of these vertices will also tell us different behaviors for different choices of parameters.

The propagators of fields (in spacetime coordinates) in YMH theory can also be used to study duality between the elementary particle state and bound state, which has already been discussed in 2.9.

Here only the two point functions, which are propagators of gauge, ghost and Higgs fields, and three point functions in the Lagrangian and the one by gauge and ghost fields, are studied. In principle, it is possible to calculate even higher correlation functions. However, even for Lagrangian vertices in YMH theory, calculating vertices has been a serious challenge due to high demand of statistics of the vertices. This is the reason that 4 point gauge field vertices are not computed while already 3 point vertices are statistically very noisy [13].

3.2   Gauge Fixing

Since the quantities in this chapter are gauge dependent correlation functions, non-aligned Minimal Landau gauge is chosen for gauge fixing [16]. The mathematical condition on gauge fields in Landau gauge is given by,

$$\partial_\mu W_\mu^i = 0 \tag{3.1}$$

It means that only the local part of the field is fixed for every index of internal symmetry of the gauge fields. Beyond perturbation theory, there exists no unique solution to the above equation [34]. Such independent solutions are called Gribov copies, and the ambiguity associated with them is called Gribov-Singer ambiguity [34, 35]. A further restriction on the Gribov copies is to demand that the Faddeev-Popov operator M defined as

$$M^{ij} = -\partial_\mu D_\mu^{ij} \tag{3.2}$$

has eigenvalues which are zero or positive, i.e., it is strictly positive semi-definite. The lattice version of Faddeev Popov operator is [22, 36]

$$M(y,x)^{ab}\omega_b = c\left(\sum_x \left(G^{ab}(x)\omega_b(x) + \sum_\mu A_\mu^{ab}(x)\omega_b(x+e_\mu) + B_\mu^{ab}(x)\omega_b(x-e_\mu)\right)\right) \tag{3.3}$$

where

$$G^{ab}(x) = \sum_\mu Tr\left(\{\tau^a, \tau^b\}\left(U_\mu(x) + U_\mu(x-e_\mu)\right)\right) \tag{3.4}$$

$$A_\mu^{ab}(x) = -2Tr\left(\tau^a\tau^b U_\mu(x)\right) \tag{3.5}$$

$$B_\mu^{ab}(x) = -2Tr\left(\tau^a\tau^b U_\mu^\dagger(x-e_\mu)\right) \tag{3.6}$$

and c is a normalization parameter, while ω_b is an arbitrary function acted upon by the Faddeev Popov operator. Set of such copies is collectively called first Gribov region [34]. The prescription, in which such a Gribov copy is selected randomly gives us gauge dependent quantities which are Gribov copy independent. Hence throughout the collection of statistics, there has

been no bias for Gribov copies, and in the end an average (arithmetic mean) is taken over the samples. This prescription is called minimal Landau gauge [22].

At the same time, since gauge fields and the action are calculated using only positive Polyakov loop [37], only the configurations with positive Polyakov loop have been considered. Hence overall, with the absence of any other bias on how to select a gauge copy, collecting such statistics and averaging over these quantities is equivalent to implementing the minimal Landau gauge [22, 38, 39]. A random global gauge transformation is performed after fixing the gauge. Hence the resulting quantity is the one calculated in non-aligned minimal Landau gauge [13, 16]. It is the non-alignness in the theory which eventually results vanishing of the expectation values with in statistical fluctuations of the scalar fields.

Since the procedure tends to show a longer auto-correlation time than the plaquette [40], at least 2(N+30) updates were performed between measurement of gauge-fixed quantities. The local part of gauge-fixing was performed by a self-tunning stochastic over-relaxation algorithm with a quality parameter $e_6 < 10^{12}$ [24].

3.3   Correlation Functions

3.3.1   Propagators

One point correlation function is the simplest correlation function. In YMH theory all the one point correlation functions are zero. For the case of scalar (Higgs) field, it is zero because during the simulations no specific direction is kept constant in global part of the field. Hence, the mean value of the field is zero within statistical fluctuation, which is the one point function of scalar field. It also establishes that the symmetry breaking is not present in our theory, though even in the case of a non-zero expectation value of Higgs field it is symmetry hiding than breaking. For the case of gauge field, it is a field with a Lorentz index. If a one point correlation function, which is the expectation value of the field, is non-zero, it will mean that there is a gauge field along some specific direction. Since for us there is no such specific direction, this correlation function has to be zero too. For the case of ghost field, since it is not a part of the theory for the selected gauge, there exists no one point function of the ghost field. It brings us to propagators, which are the next simplest correlation function.

Aside from knowing the propagators for understanding of theory, they also have advantage that they can be used to calculate connected and amputated part of higher correlation functions, whenever needed. Schwinger functions, which are space-time representation of propagators, are also very important. A good example is duality between elementary particle state and bound state, which has already been discussed in chapter 2. In comparison to what perturbation theory tells us, it is also very interesting to see how much the results from non-perturbative calculations differ from those of perturbative calculations. In principle, it is possible to calculate the propagators to any order of correction in perturbation theory, the biggest contribution is expected to come from the tree level. Hence it is reasonable to compare the results from

non-perturbative calculations with the tree level result of the propagators. Furthermore, as YM theory has already been investigated, it is also very important to understand how much the YM theory's propagators [22], of the fields which are also present in YM theory, differ from the corresponding YMH's propagators after the inclusion of scalar field.

For the case of scalar field, the tree level expression for propagator in minimal Landau gauge is given by

$$D(p) = \frac{1}{p^2 - m^2} \tag{3.7}$$

where D(p), p and m are the tree level scalar propagator, momentum and bare mass, respectively. In the absence of higher order corrections, there is no need to consider renormalization and hence bare mass in the above expression becomes the physical mass of scalar field.

For the scalar propagator to be non-perturbatively calculated on lattice, renormalization is more involved. Computation of unrenormalized Scalar propagator is straight forward business. The fields are already available from simulations, explained in chapter 1, hence the unrenormalized propagator is given by

$$D_{NR}^{ab}(p) = <\phi^{a\dagger}(p)\phi^b(p)> \tag{3.8}$$

where $\phi^b(p)$ is the scalar field with p momentum and Latin index as index of internal symmetry, and † implies complex conjugate in this case. $D_{NR}^{ab}(p)$ is the unrenormalized scalar propagator, with a and b indices of internal symmetry of scalar field, and p momentum, while NR in the subscript means that it is an unrenormalized scalar propagator. The renormalized propagator is calculated by

$$D^{ab}(p^2) = \frac{\delta^{ab}}{Z(p^2 + m^2) + \pi(p^2) + \delta m^2} \tag{3.9}$$

where $D^{ab}(p)$ has the usual meaning as $D_{NR}^{ab}(p)$ (with missing NR in parenthesis since the propagator is renormalized now), p is momentum, while Z and δm in above equation are normalization constant and mass correction term, respectively. $\pi(p)$ is calculated from

$$D_{NR}^{ab}(p) = \frac{\delta^{ab}}{p^2 + \pi(p^2)} \tag{3.10}$$

while the renormalization scheme is given by

$$D^{ab}(\mu^2) = \frac{\delta^{ab}}{\mu^2 + m_H^2} \tag{3.11}$$

$$\frac{\partial D^{ab}(\mu^2)}{\partial |p|} = \frac{-2\mu\delta^{ab}}{(\mu^2 + m_H^2)^2} \tag{3.12}$$

where μ is the renormalization point, the value of momentum at which renormalization takes places, and m is the bare mass value.

For the case of gauge field propagator, it is given by

$$D_{\mu\nu(NR)}^{ij}(p) = < W_\mu^i(p) W_\nu^j(p) > \qquad (3.13)$$

where $D_{\mu\nu}^{ij}(p)$ is gauge field propagator with p momentum and i, j color indices while μ and ν are Lorentz indices. $W_\nu^j(p)$ is gauge field at p momentum value with j color index and ν Lorentz index. Scheme of multiplicative renormalization is used, which means that with a renormalization constant c the renormalized gauge field propagator $D_{\mu\nu}^{ij}(p)$ is given by

$$D_{\mu\nu}^{ij}(p) = c D_{\mu\nu(NR)}^{ij}(p) \qquad (3.14)$$

where c is the renormalization constant. The multiplicative constant can be calculated from

$$c = \frac{1}{D_{\mu\nu(NR)}^{ii}(q)} \qquad (3.15)$$

where q is the normalization point and summation convention for the Latin index is not implied.

The ghost propagator is calculated from Faddeev Popov operator by the following equation [22].

$$D^{ab}(p) = < (-\partial_\mu D_\mu^{ab})^{-1}(p) > \qquad (3.16)$$

The renormalization scheme is the same as it is for the case of gauge field propagator. Hence, the overall picture is that propagators are computed from the fields (for the case of gauge and Higgs propagators) and the Faddeev Popov operator (for the case of ghost propagator), and renormalization of gauge and ghost propagators are multiplicatively renormalizable, while scalar propagator involves calculation of two quantities which are calculated from two renormalization conditions.

For the Schwinger functions $F_{sch}(t)$, they are obtained from the propagators $D(p^2)$ by

$$F_{sch}(t) = \frac{1}{a\pi N} \sum_{P_0=0}^{N_t-1} cos(\frac{2\pi t P_0}{N_t}) D(P_0^2) \qquad (3.17)$$

where a, P_0, t and N are lattice spacing, momentum values in lattice units, time values in lattice units, and number of points on the lattice along each axis, respectively.

3.3.2 Three Point Vertices

The next simplest correlation functions are the three point correlation functions, or three point vertices. Before explaining the involved quantities for lattice calculations, let us start with the Feynman rules for the three point vertices mentioned above [1].

$$\Delta_\mu^{ijk}(p,q,r) = g\tau_{ik}^j(r-p)_\mu \qquad (3.18)$$

---

[1]In the left hand side of the given expressions for Feynman rules, the expressions are used as only symbolic representation of the vertices. Hence, the place for indices on the symbols are chosen for convenience.

$$\Delta_{\mu\nu\eta}^{abc}(p,q,r) = gf^{abc}\left(\delta_{\mu\nu}(p-q)_\eta + \delta_{\nu\eta}(q-r)_\mu + \delta_{\eta\mu}(r-p)_\nu\right) \tag{3.19}$$

$$\Delta_\mu^{abc}(p,q,r) = -gf^{abc}q_\mu \tag{3.20}$$

In above $\Delta_\mu^{ijk}(p,q,r)$ is scalar-gauge field vertex with $\overline{\phi}^i(p)$, $W_\mu^j(q)$, and $\phi^k(r)$ are complex scalar, gauge, and scalar fields respectively with i,j,k and p,q,r as internal symmetry indices and momenta of fields, respectively. Similarly, $\Delta_{\mu\nu\eta}^{abc}(p,q,r)$ is 3 gauge field vertex with similar type of convention for indices, while $\Delta_\mu^{abc}(p,q,r)$ is gauge-ghost-anti ghost field vertex with a,b,c and p,q,r are respectively indices for anti ghost, gauge, and ghost fields and their momenta, respectively.

From lattice simulations, first the full correlation functions are calculated and then the amputated and connected part of the correlation functions are calculated [13]. In YMH theory, finding connected and amputated part of gauge-scalar fields vertices is not straight forward since if Lagrangian symmetries are not taken into account, the resulting vertex will be vanishing within statistical error.

For the case of scalar-gauge vertex in YMH theory, the corresponding terms in the Lagrangian are $\phi^\dagger(x+a)U_\mu^\dagger(x)\phi(x)$ and $\phi^\dagger(x)U_\mu(x)\phi(x+a)$. These terms can be used to calculate lattice corrections [12].

$$\phi^\dagger(x+a)U_\mu^\dagger(x)\phi(x) \simeq \phi^\dagger(x+a)(1+iW_\mu(x))\phi(x) \tag{3.21}$$

where $\phi(x)$, $U_\mu(x)$ and $W_\mu(x)$ are the scalar field, link variable and the gauge field, respectively. In above the second term is the relevant term since it forms a vertex. Hence,

$$S_1 = \phi^\dagger(x+a)W_\mu(x)\phi(x) \tag{3.22}$$

where S_1 is the relevant part for lattice corrections. The following equations are considered [12].

$$\phi(x+a) = \phi(x) + a\partial\phi(x) \tag{3.23}$$

$$\phi(x) = \Sigma e^{\frac{2\pi i x.p}{N}}\widetilde{\phi}(p) \tag{3.24}$$

$$W_\mu(x) = \Sigma e^{\frac{2\pi i x.p}{N}}\widetilde{W}_\mu(p) \tag{3.25}$$

where a is the minimum distance between two consecutive points on lattice lying on the same axis, while $\widetilde{\phi}(p)$ and $\widetilde{A}_\mu(p)$ are fourier transforms of $\phi(x)$ and $A_\mu(x)$, respectively. Note that in the equation 3.23, Lorentzian index is not explicitly mentioned. This is acceptable at this point since the lattice considered is symmetric, i.e., it has equal number of points along each of the 4 dimensions, hence it has the same value of a for each Lorentz index. There also is a constant of proportionality in the fourier transforms which has not been used because it does not play any role in finding the lattice corrections. Using these equations gives us the lattice corrections.

$$S_1 = \Sigma\widetilde{\phi}^\dagger(p)\widetilde{W}_\mu(q)\widetilde{\phi}(r)e^{\frac{2\pi i x.(-p+q+r)}{N}}\{e^{\frac{-2\pi i a.p}{N}}\} \tag{3.26}$$

where the term in the braces is the lattice correction term. Similarly for the second term, $\phi^\dagger(x)U_\mu(x)\phi(x+a)$, repeating the same procedure gives us

$$S_2 = \Sigma\widetilde{\phi}^\dagger(p)\widetilde{W}_\mu(q)\widetilde{\phi}(r)e^{\frac{2\pi ix.(-p+q+r)}{N}}\{e^{\frac{2\pi ia.r}{N}}\} \tag{3.27}$$

Thus the total lattice correction L_c for these two terms is given by,

$$L_{(c)\mu} = -2sin(\frac{\pi(r-p)_\mu}{N})cos(\frac{\pi(r+p)_\mu}{N}) - 2isin(\frac{\pi(r-p)_\mu}{N})sin(\frac{\pi(r+p)_\mu}{N}) \tag{3.28}$$

where r and p are the momenta (in lattice units) of the $\phi^\dagger$ and ϕ fields.

In momentum space there are three fields in the 3 point correlation functions, each with a momentum. Considering conservation of momentum, which is a constraint, renders two independent momenta. For the vertices with two independent momenta, two quantities are required for the purpose of forming projections in some function space. In Landau gauge, only the tensor component which is transverse in the W field momentum is accessible. Hence a dressing function is calculated whose behavior over momentum can give us information about deviation from the corresponding tree level structure. Furthermore, propagators are also included in order to take the amputated part out of the vertex [13].

$$< \phi^{a\dagger}(p)W_\mu^i(q)\phi^b(r) >= igVA\tau_{\acute{a}b}^{\acute{i}}D_{a\acute{a}}(p)D_{\mu\nu}^{i\acute{i}}(q)D_{b\acute{b}}(r)(r-p)_\nu \tag{3.29}$$

where g is the coupling constant, $\tau_{\acute{a}b}^{\acute{i}}$ are the components of the ith Pauli matrix, $D_{a\acute{a}}$ is the scalar propagators while $D_{\mu\nu}^{i\acute{i}}$ is the gauge field propagator. i is iota in its customary meaning and V is the volume. A peculiar advantage of this projection is that the right hand side of the above equation contains tree level expression for the vertex which means that computation of the function **A** in the expression can give information about how the non-perturbatively computed vertex behave compared with the tree level vertex expression. Hence the A function here is the dressing function which is, in fact, the most interesting quantity for us. Using the following property of Pauli matrices τ^i,

$$\tau_{ac}^i\tau_{cb}^j + \tau_{ak}^j\tau_{kb}^i = 2\delta^{ij}\delta_{ab} \tag{3.30}$$

the following expression for dressing function is arrived.

$$A = \frac{i}{gV}\frac{< \phi^{a\dagger}(p)W_{\acute{\mu}}^i(q)\phi^c(r) > (r-p)_{\acute{\mu}}\tau_{ca}^i}{D(p)D_{\mu\nu}(q)D(r)(r-p)_\mu(r-p)_\nu}$$

Since lattice method is used for computation, above equation needs to contain lattice corrections [12]. This is a straight forward procedure since the correction term L_c has already been calculated in above. Hence the final expression for the dressing function A is,

$$A = \frac{i}{gV}\frac{< \phi^{a\dagger}(p)W_{\acute{\mu}}^i(q)\phi^c(r) > (r-p)_{\acute{\mu}}\tau_{ca}^i}{D(p)D_{\mu\nu}(q)D(r)(r-p)_\mu(r-p)_\nu}$$

where for lattice calculations

$$(r - p)_{\acute{\mu}} \to L_{(c)\acute{\mu}} \tag{3.31}$$

The propagators without indices are (or similar to) color diagonal propagators. For this vertex, there is one additional subtlety. The vertex in the above equation is not a flavor invariant term. It means that since this symmetry is not broken in the YMH theory, the expectation value of this vertex will be zero (within statistical fluctuations) if the form of vertex given above is considered. The solution to this problem is to choose an expression which is flavor invariant. Hence in the above equation, the following modification is made:

$$< \phi^{a\dagger}(p) W_{\mu}^i(q) \phi^c(r) > \tau_{ca}^i \to < Tr\left(X(p)X^\dagger(r)W_{\mu}^i(q)\tau^i\right) > \tag{3.32}$$

with

$$X(p) = \begin{pmatrix} \phi_1(p) & -\phi_2^*(p) \\ \phi_2(p) & \phi_1^*(p) \end{pmatrix} \tag{3.33}$$

where Tr represents trace of the matrices. The reason for introducing the lattice correction [12] in above is that lattice calculations are performed on a discrete spacetime coordinate system. Since there nothing exists between the points, the derivatives in Lagrangian are particularly effected because they directly involve the space between two points. As soon as fourier transformation is performed to further continue in momentum space, terms with lattice spacings propagate throughout the calculation and modify almost everything, including the Feynman rules. Hence throughout the calculation of dressing function these modifications, or corrections, propagate till the end and modify the expression for our dressing function.

For the case of the three gauge field vertex, there is no problem similar to the flavor invariance of scalar field in the theory. Hence the only remaining work is to compare the non-perturbatively computed vertex with the tree level vertex of the three gauge fields. Hence with the dressing function A_{3w}, the full vertex is given by,

$$< W_\mu^a(p) W_\eta^b(q) W_\nu^c(r) >= A_{3w} g f^{\acute{a}\acute{b}\acute{c}} \left(\delta_{\acute{\mu}\acute{\nu}}(p-q)_{\acute{\eta}} + \delta_{\acute{\nu}\acute{\eta}}(q-r)_{\acute{\mu}} + \delta_{\acute{\eta}\acute{\mu}}(r-p)_{\acute{\nu}}\right)$$

$$\times D_{\mu\acute{\mu}}^{a\acute{a}}(p) D_{\nu\acute{\nu}}^{b\acute{b}}(q) D_{\eta\acute{\eta}}^{c\acute{c}}(r) \tag{3.34}$$

and after some algebra the final equations for the dressing function is given by (including lattice corrections),

$$A_{3w} = \frac{< W_\alpha^i(p) W_\beta^j(q) W_\gamma^k(r) > f^{ijk} \left(\delta_{\alpha\gamma}(p-q)_\beta cos\frac{1}{2}r_\beta + \delta_{\gamma\beta}(q-r)_\alpha cos\frac{1}{2}p_\gamma + \delta_{\beta\alpha}(r-p)_\gamma cos\frac{1}{2}q_\alpha\right)}{f^{abc} f^{\acute{a}\acute{b}\acute{c}} D_{\mu\acute{\mu}}^{a\acute{a}}(p) D_{\nu\acute{\nu}}^{b\acute{b}}(q) D_{\eta\acute{\eta}}^{c\acute{c}}(r) \left(\delta_{\mu\nu}(p-q)_\eta cos\frac{1}{2}r_\eta + \delta_{\nu\eta}(q-r)_\mu cos\frac{1}{2}p_\nu + \delta_{\eta\mu}(r-p)_\nu cos\frac{1}{2}q_\mu\right)}$$

$$\times \left(\frac{1}{\left(\delta_{\acute{\mu}\acute{\nu}}(p-q)_{\acute{\eta}} cos\frac{1}{2}r_{\acute{\eta}} + \delta_{\acute{\nu}\acute{\eta}}(q-r)_{\acute{\mu}} cos\frac{1}{2}p_{\acute{\nu}} + \delta_{\acute{\eta}\acute{\mu}}(r-p)_{\acute{\nu}} cos\frac{1}{2}q_{\acute{\mu}}\right)}\right) \tag{3.35}$$

For the case of ghost-gauge field three point vertex, the vertex can be written as

$$< \bar{u}^b(q)W_\mu^a(p)u^c(r) >= A_{w\bar{u}u}gf^{\acute{a}\acute{b}\acute{c}}q_{\acute{\mu}}D_{\mu\acute{\mu}}^{a\acute{a}}(p)D^{b\acute{b}}(q)D^{c\acute{c}}(r)$$

and after some algebra the dressing function A_{ggw} can be written as (including lattice corrections),

$$A_{w\bar{u}u} = \frac{< \bar{u}^j(q)W_\alpha^i(p)u^k(r) > q_\alpha(cos\frac{1}{2}q_\alpha)f^{ijk}}{D_{\mu\acute{\mu}}^{a\acute{a}}(p)D^{i\acute{i}}(q)D^{k\acute{k}}(r)q_\mu(cos\frac{1}{2}q_\mu)q_{\acute{\mu}}(cos\frac{1}{2}q_{\acute{\mu}})f^{aik}f^{\acute{a}\acute{i}\acute{k}}}$$

Note that all the dressing functions have same structure with the three propagators in the same place in the equations to get the amputated part and the same places for tree level structures. Hence, the structure of the dressing functions appears as

$$A = \frac{\Gamma^{tree}\Gamma}{\Gamma^{tree}\Gamma^{tree}DDD}$$

with Γ^{tree} is the tree level structure, Γ as the full vertex and D's are propagators.

Once the dressing functions are obtained, the next step is to renormalize them. They need only multiplicative renormalization which means that all the multiplicative constants are not very important for a renormalized vertex, while the renormalization point can be chosen which is suitable for the Physics to be understood [13].

Next simplest gauge dependent correlation function is 4 gauge field vertex, which has not been explored due to its immense statistical fluctuations.

3.4   QCD and Higgs like Physics

Once the details of the quantities to be computed are understood, simulations can be carried out for data collection and study of the results. At the same time it is also clear that not all the sets of parameters can be explored since there are infinite choices for parameters' values. Hence the first step is to choose what values of parameters are interesting for simulations.

As it has already been mentioned, for YMH theory the phase diagram is continuously connected [41]. It means that one can start at any point and end up continuously on any other point in the phase diagram. Hence, there exists no clear boundary which completely separates different parts (or regions) in the phase diagram. However, in YMH theory it is possible to classify two regions of phase diagram based upon ordering in energy values of the ground states in the 0^+ and 1^- channels. For some set of parameters, the ground state in 0^+ singlet channel is heavier than that in 1^- triplet channel, while for the other sets of parameters it is vice versa. Quantitatively, for m_{0^+} and m_{1^-} as the ground state masses (energies) in 0^+ and 1^- channels, the ratio m_{1^-}/m_{0^+} is less than 1 in one phase (**HLD**) and greater than 1 in another phase (**QLD**), while there also exists a cross over region (**COR**) where the ratio is equal to 1 within statistical fluctuations. For the QLD region, a non-negligible intermediate distance string ten-

sion can exist, before string-breaking sets in [42, 43]. Thus, loosely speaking, there is a phase transition in a particular way in the phase diagram, but it ends at a critical end-point, and therefore it does not completely separate phases [28, 44, 45]. Figure 2.14 shows the different regions in the parameter space.

Let us recall here that absence of QED and fermions has already effected the reliability of the results, and it remains to be seen precisely how much of error this *narrowed down* theory has introduced in the calculated quantities. Hence, strictly speaking, the results are a lot more important from the theoretical point of view rather than phenomenological point of view at the moment. Since further lines of constant Physics can also be explored to have better understanding of YMH theory, situation with heavier Higgs, in which m_{0^+} is much heavier than m_{1^-}, is also explored for gauge dependent quantities. This LCP lies deep in HLD region of the theory.

In order to give quantities physical dimensions, scale setting needs to be done. In the HLD region, the ground state is in 1^- channel. To set the scale, the ground state is set equal to 80.375 GeV.

For the case of QCD Physics, the gauge bosons (gluons in this case) are massless. Hence any comparison between the results from YMH and QCD like Physics is not possible using the above prescription for setting the scale. Furthermore, using the same prescription makes it possible to also study the results in comparison with those for HLD cases. Hence, for both HLD and QLD, same prescription for scale setting is used.

In the following three sets of parameters are chosen for three situations. For the case of QCD like Physics, the parameters are $\beta = 2.221$, $\kappa = 0.125$, and $\lambda = 0$. Two cases in HLD are chosen. The situation when the lowest state in 0^+ channel is around the Higgs mass found in LHC (~ 124 GeV) and the situation when this quantity is heavier than the Higgs mass found in LHC (~ 198 GeV). For the first situation, , the parameters are $\beta = 2.3$, $\kappa = 0.31$, and $\lambda = 1.0$ and for the later case, the parameters are $\beta = 2.3827$, $\kappa = 0.3176$, and $\lambda = 1.018$. The lattice sizes used for simulations are 12^4, 18^4 and 24^4.

3.5   Propagators

3.5.1   Gauge Field Propagator

For the gauge field propagator, it is known that in Yang-Mills theory lattice artifacts are considerable [22], hence the lattice artifacts are considered first. Figure 3.1 shows the finite volume effects on gauge propagators. As can be seen in the figure 3.1, the propagators for different Physics are effected in a different way. For the case of QLD, the propagators are suppressed as the volume of the lattice used increases, while for the case of HLD the propagators have slightly increased values. For the heavy 0^+ case the propagators are observed to be less effected which is also evident on the figure 3.1. However, lets note at this point that the volume at zero momentum is not important. In comparison to YM theory, gauge propagators in QLD

63

show similar behavior which is an indication that, at least in Landau gauge, gauge sector in YMH theory may not be affected by the scalar (Higgs) sector. For the corresponding Schwinger functions, the deviations observed are typical for the those coming in for the large time values for finite volumes.

As it is already very difficult to stay on the same LCP, which has already been mentioned in chapter 2, and determination of masses becomes more difficult for heavier states since they need relatively considerably more statistics, finding different lattice spacings for the same m_{1^-}/m_{0^+} is a challenging task. Hence on figure 3.2, gauge propagators are shown with different lattice spacings for the same or approximately the same m_{1^-}/m_{0^+}, different gauge propagators are shown. Though there exist very small difference, it is hard to make any statement because of the unavailability of more values of lattice spacings for the same LCPs. In comparison with YM theory [22], there also exist no considerable deviations for gauge propagators in YM theory. At the moment an educated guess is that the same behavior should be expected for YMH theory.

However, relaxing the condition of a particular LCP gives a chance to calculate propagators freely, figure 3.3 shows these propagators. All the propagators on the figure seem to indicate the same (asymptotic) behavior in momentum space. This is expected since the mass scale generated by the Higgs effect should become irrelevant at large energies. However, this behavior is not that of a massless field. There are logarithmic corrections and partly renormalization effects in the propagator. Furthermore, the space-time correlation functions also show different behavior for different Physics. For the case of QLD, they have a zero crossing, which is also observed in Yang-Mills theory [22, 46] as well as QCD [47, 48].

3.5.2 Ghost Field Propagator

Numerically, the ghost propagator is one of the most easily calculated quantities and the one who does not contribute in our computation. Despite the fact that ghost fields are merely the mathematically constructed fields and that they do not have the status of Physically important fields [2], they have importance of their own. Relevant to the work discussed here, it is used to calculate running coupling which is calculated using miniMOM scheme [49]. The ghost propagator can also serve as an input for other non-perturbative methods, such as DSEs. Furthermore, other methods can be tested by calculating the ghost propagator and comparing to the ghost propagator calculated here.

Since in Yang-Mills theory the ghost propagator is also effected by lattice artifacts, it is essential to start with study of these effects. In figure 3.4 finite volume effects are shown for the ghost propagator. It is clear that for the lattice sizes considered for simulations, there is no prominent finite volume effects on the ghost propagator [50–52]. Ghost propagator in QLD region is also included in figure 3.4, hence in comparison of QLD to Yang-Mills theory there exist similarity in role of finite volume effects [22]. Perhaps the most obvious observation in

---

[2]in the sense that they are not gauge or matter fields, and they do not even follow the *correct* statistical distribution.
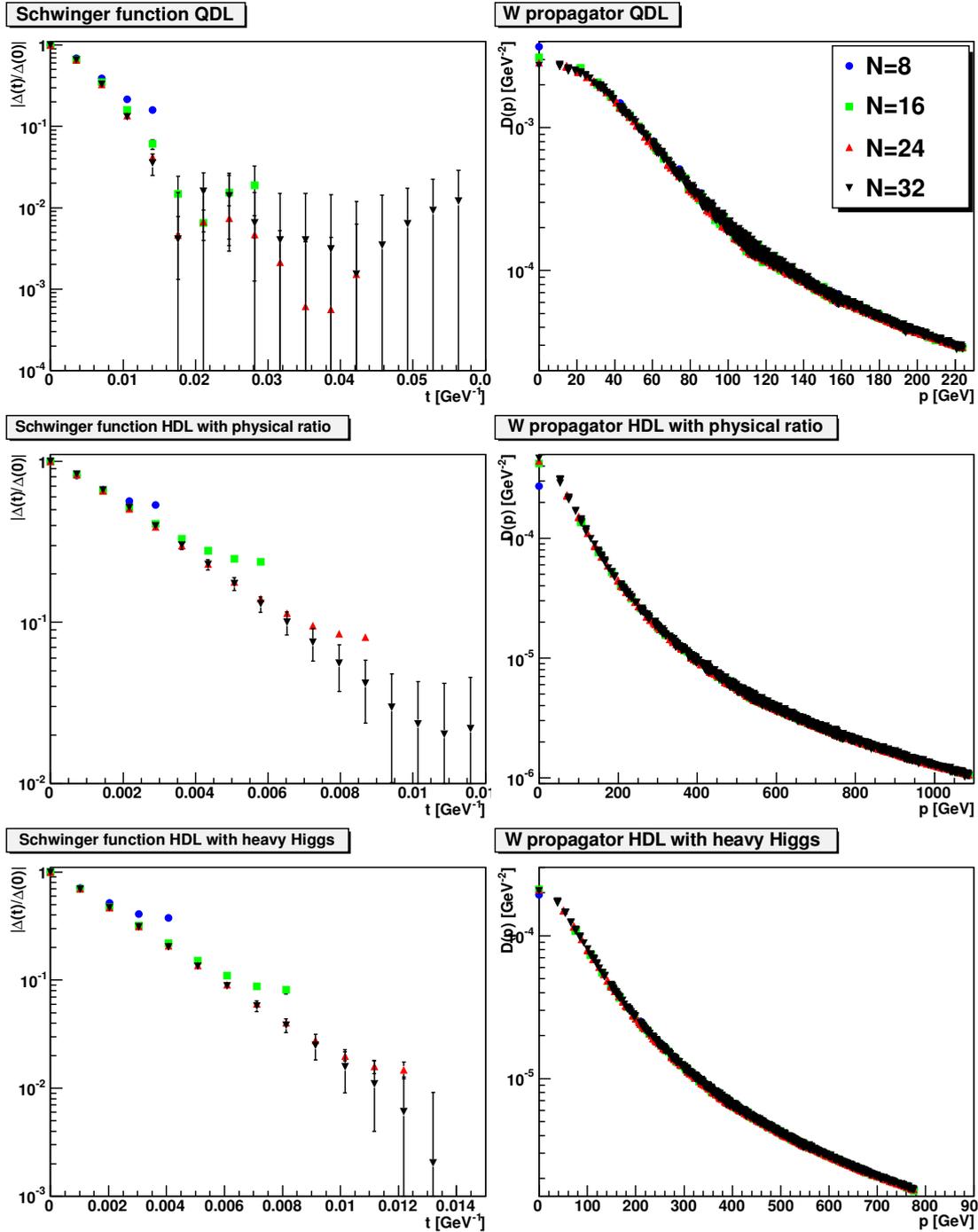
Figure 3.1: The gauge boson propagator in position space (left panel) and momentum space (right panel) for different volumes. The top panel is in the QLD with $m_{1^-}/m_{0^+} = 2.2$, the middle panel has the physical mass ratio $m_{1^-}/m_{0^+} = 0.72$, and the bottom panel is for a large Higgs mass $m_{1^-}/m_{0^+} = 0.31$, both in the HLD.
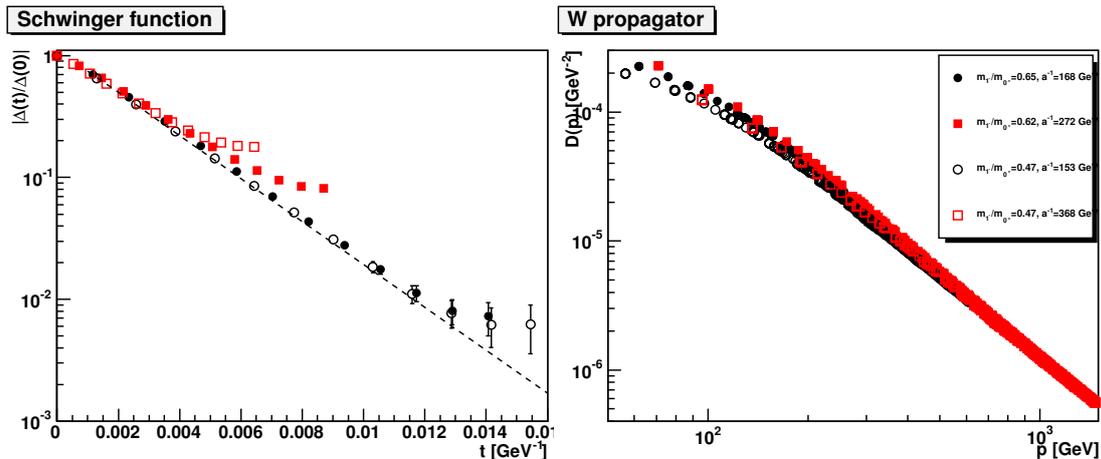
Figure 3.2: The gauge boson propagator in position space (left panel) and momentum space (right panel) for different mass ratios m_{1^-}/m_{0^+} on 24^4 lattices and for two different lattice spacings.

QLD is that the propagator is infrared finite in Landau gauge, see the figure 3.4. However, whether this is really the true statement remains to be seen for very small momentum values which are accessible on very large lattice volumes.

The situation is more interesting when it comes to the role of lattice spacing. In figure 3.5 ghost propagators with different lattice spacings for very close or the same ratio, m_{1^-}/m_{0^+} are shown. Qualitatively, the propagators behave similarly. However, they do show clear quantitative difference which implies dependence on the lattice spacings, though for the propagators this dependence does not influence very strongly and, as the dressing functions plotted in the figure 3.5 shows, quantitatively the two propagators for approximately the same (or the same) m_{1^-}/m_{0^+} do not differ by more a factor of 2. However more propagators with different lattice spacings and approximately the same (or the same) m_{1^-}/m_{0^+} are needed for a more detailed study of the effect of lattice spacings which is, in no doubt, a very difficult task since dependence of LCPs on these parameters is not known which makes it impossible to determine m_{1^-}/m_{0^+} in advance. The difference in figure 3.5 is not a mere multiplicative constant which could otherwise be removed by a multiplicative renormalization.

Lets relax the condition of having approximately the same, or the same, m_{1^-}/m_{0^+}. It will give us propagators with different m_{1^-}/m_{0^+} as well as lattice spacings. Figure 3.6 shows ghost propagators for both QLD and HLD. The first observation is that the ghost propagators in QLD and HLD behave drastically different from each other. For the QLD case, the propagators behave similar to the Yang-Mills theory [22]. Even with different lattice spacings, it is clear that the propagators are not infrared divergent, as in Yang-Mills theory. Though the dressing functions for QLD show that the difference between propagators is considerable but not more than a magnitude, it is still difficult to make a statement at this point since both m_{1^-}/m_{0^+} and lattice spacings vary for them. For the case of HLD, the ghost propagators do not differ a lot
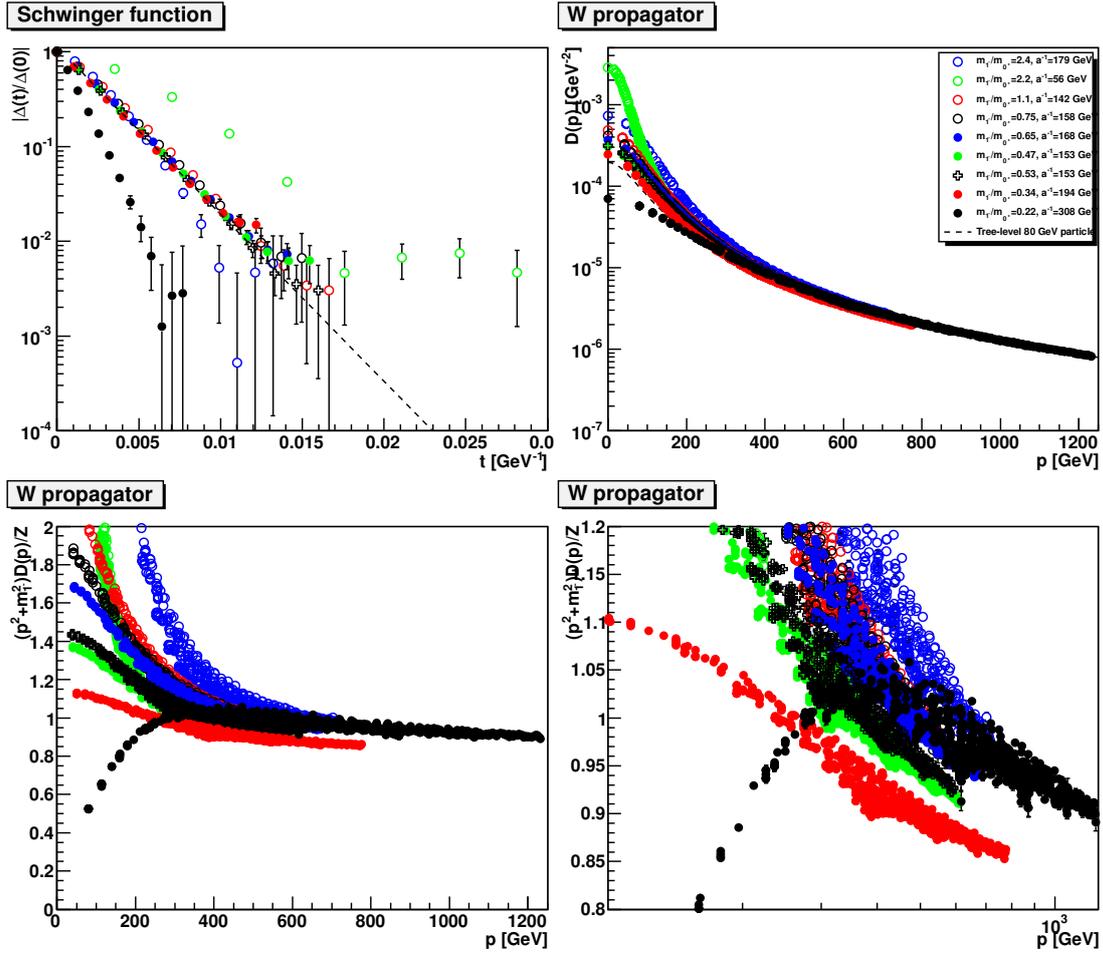
Figure 3.3: The top panels show the gauge boson propagator in position space (left panel) and momentum space (right panel) for different mass ratios m_{1^-}/m_{0^+} on 24^4 lattices. The tree-level result is for the infinite-volume case. The lower panels show the ratio to the expected dressing function, where $Z = 1.4$ is a wave-function renormalization constant. Note that the propagators are unrenormalized.
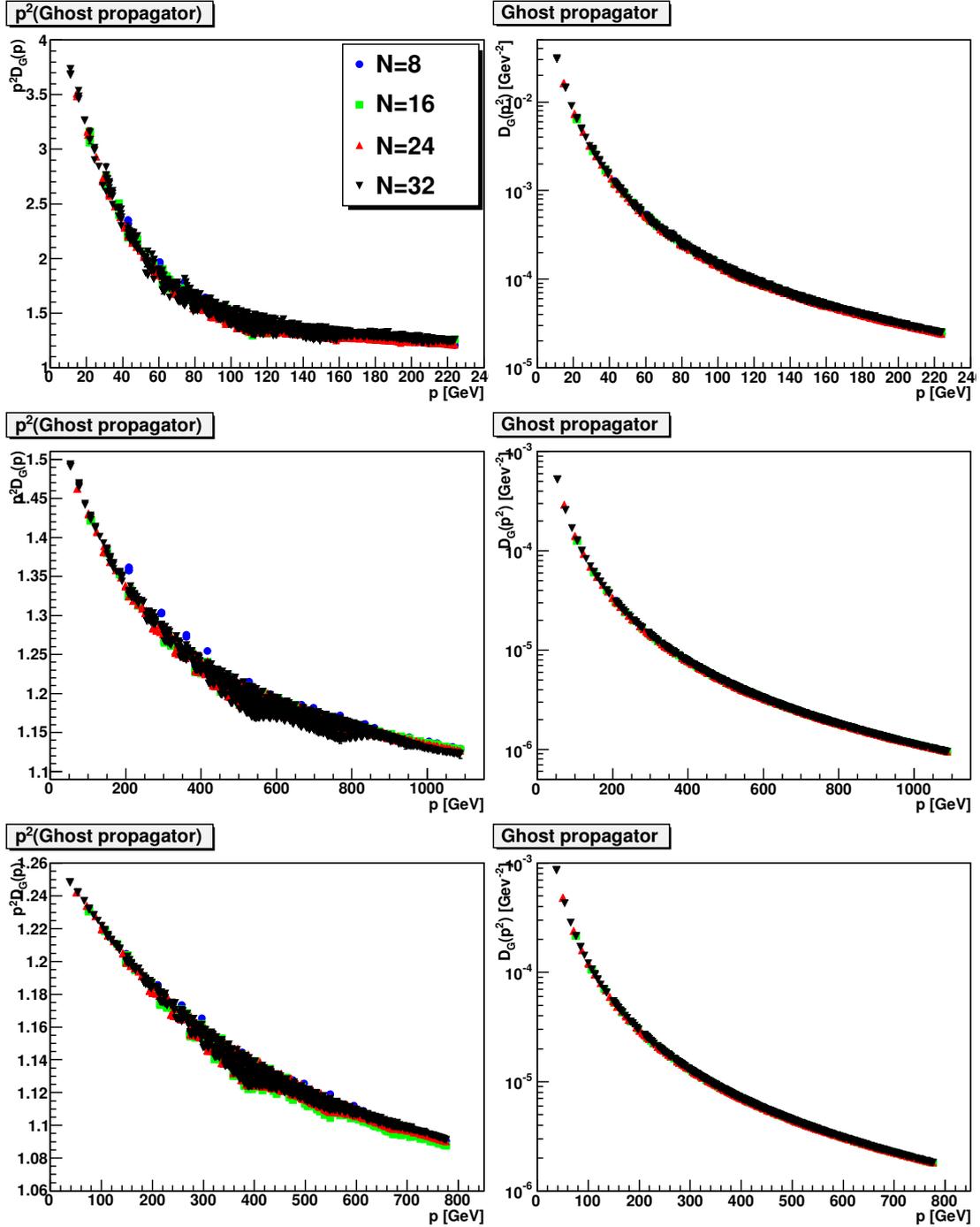
Figure 3.4: The ghost propagator (right panel) and dressing function (left panel) for different volumes. The top panel is in the QLD with $m_{1^-}/m_{0^+} = 2.2$, the middle panel has the physical mass ratio $m_{1^-}/m_{0^+} = 0.72$, and the bottom panel is for a large Higgs mass $m_{1^-}/m_{0^+} = 0.31$, both in the HLD.
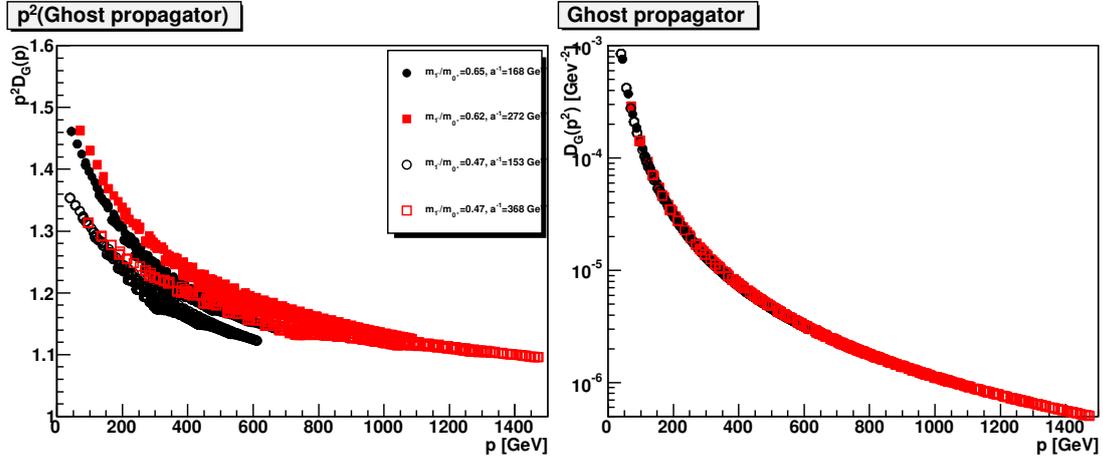
Figure 3.5: The ghost propagator (right panel) and dressing function (left panel) for different mass ratios m_{1^-}/m_{0^+} on 24^4 lattices and for two different lattice spacings.
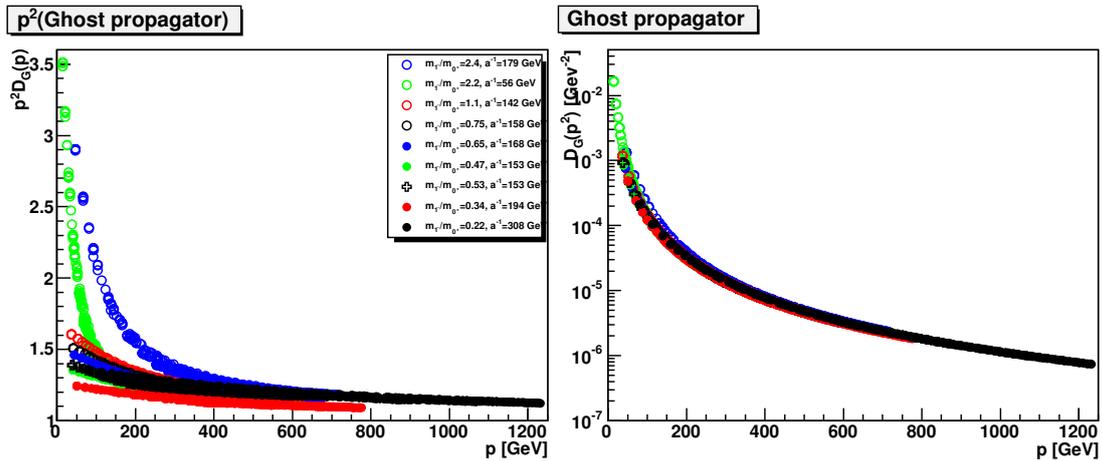

Figure 3.6: The ghost propagator (right panel) and dressing function (left panel) for different mass ratios m_{1^-}/m_{0^+} on 24^4 lattices. Note that the propagators are unrenormalized.

from each other, and the difference is also less than an order of magnitude. It supports the idea that maybe there is no drastic difference between the ghost propagators in HLD and they all behave similar to each other. Furthermore, there is not much difference from the behavior of a massless particle, as the construction of the dressing function shows, which is in agreement with perturbation theory in Landau gauge [3]. It is also compatible with earlier indirect evidence based on the spectrum of the Faddeev-Popov operator [53].

3.5.3 Higgs Field Propagator

Higgs Propagator also has its own merits for study. Since the discovered Standard Model Higgs is around 125 GeV, at least apparently it seems very encouraging to use perturbative approach whenever possible because the mass of Higgs is compatible with perturbative calculations [3]. However, it is clear that Higgs mass, which is perturbatively calculated as the pole in the propagator, is a renormalization dependent quantity and it is yet to be seen what happens when the same propagator is calculated non-perturbatively, and what happens if different values of parameters are chosen.

First comes the study of lattice artifacts for Higgs propagator. Figure 3.7 shows the finite volume effect for QLD, HLD and heavy HLD. It is clear from the figure that finite volume effects are negligible in both QLD and HLD. There is some deviations for Schwinger functions for different Physics but this deviation is not a surprise since they are fourier transforms of the propagators. For different lattice spacings, it is similar situation, see figure 3.8. For all the plotted propagators for different lattice spacings, there is no considerable difference between the propagators. The only key point for Higgs propagators is that since they have a more involved renormalization, the bare mass value needs to be fixed for all of them if agreement of propagators is being sought. Anyway, here the gist of study of lattice artifacts is that Higgs propagator is the least effected propagator among all the propagators in YMH theory.

The propagators for different spacings and different kinds of Physics are shown in figure 3.9. At higher momentum values, as the dressing functions in the figure 3.9 show, there is a clear disagreement between the propagators. Since they are renormalized propagators, it indicates that at least the effects of the mass, as a hard mass scale, pertain to the part of larger momentum values. Schwinger functions also show disagreement, though after a while they are overwhelmed by statistical noise.

3.6 Lagrangian Vertices

Vertices are formed by more than two fields. Since lattice calculation method is used during the whole investigation discussed here, in the absence of analytical results only a finite number of angles between the momenta of the involved fields are accessible. The first step is to choose these angles, and hence the momentum settings, to compute vertices.
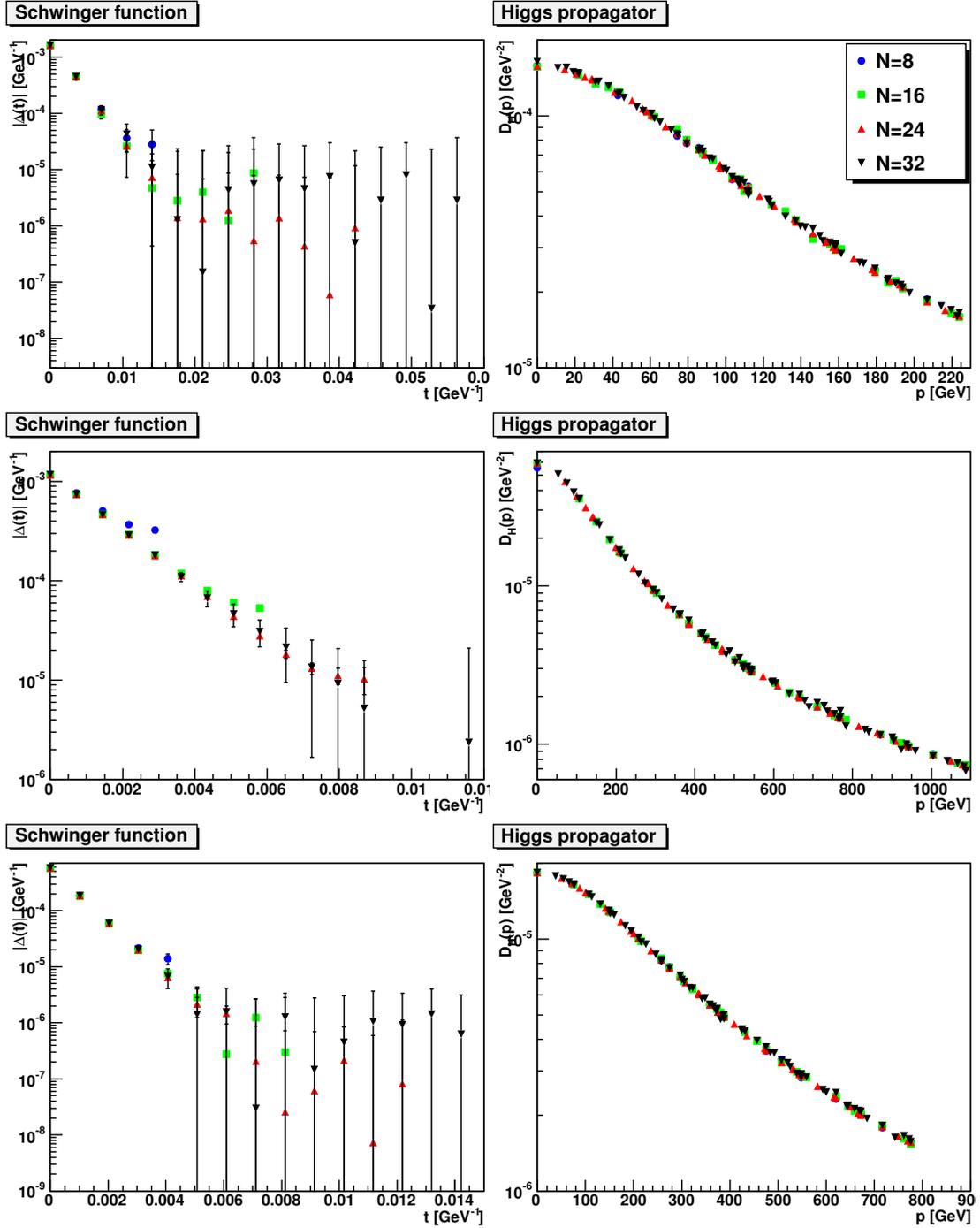
Figure 3.7: The Higgs propagator (right panel) and dressing function (left panel) for different volumes. The top panel is in the QLD with $m_{1^-}/m_{0^+} = 2.2$, the middle panel has the physical mass ratio $m_{1^-}/m_{0^+} = 0.72$, and the bottom panel is for a large Higgs mass $m_{1^-}/m_{0^+} = 0.31$, both in the HLD. Note that the renormalization has been performed for all volumes with the same renormalization constants.
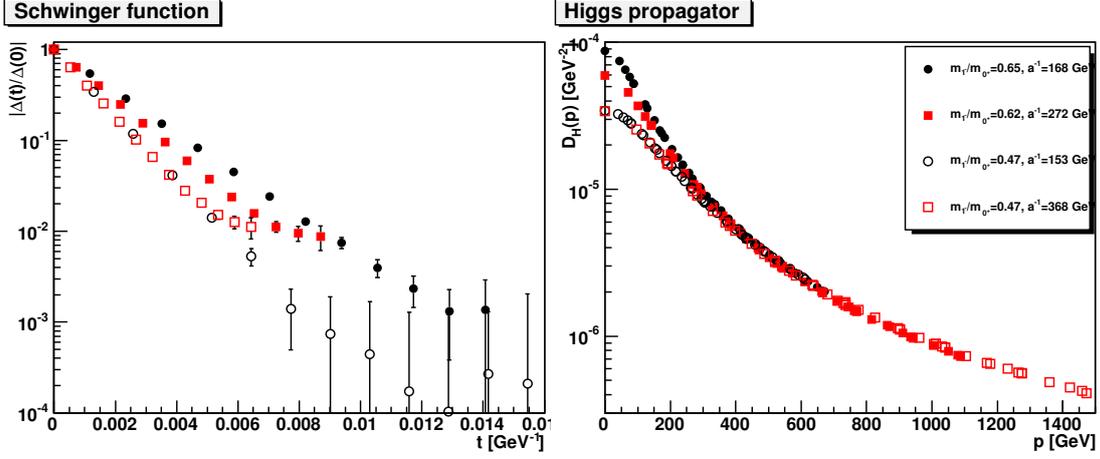
Figure 3.8: The Higgs propagator (right panel) and dressing function (left panel) for different mass ratios m_{1^-}/m_{0^+} on 24^4 lattices and for two different lattice spacings.
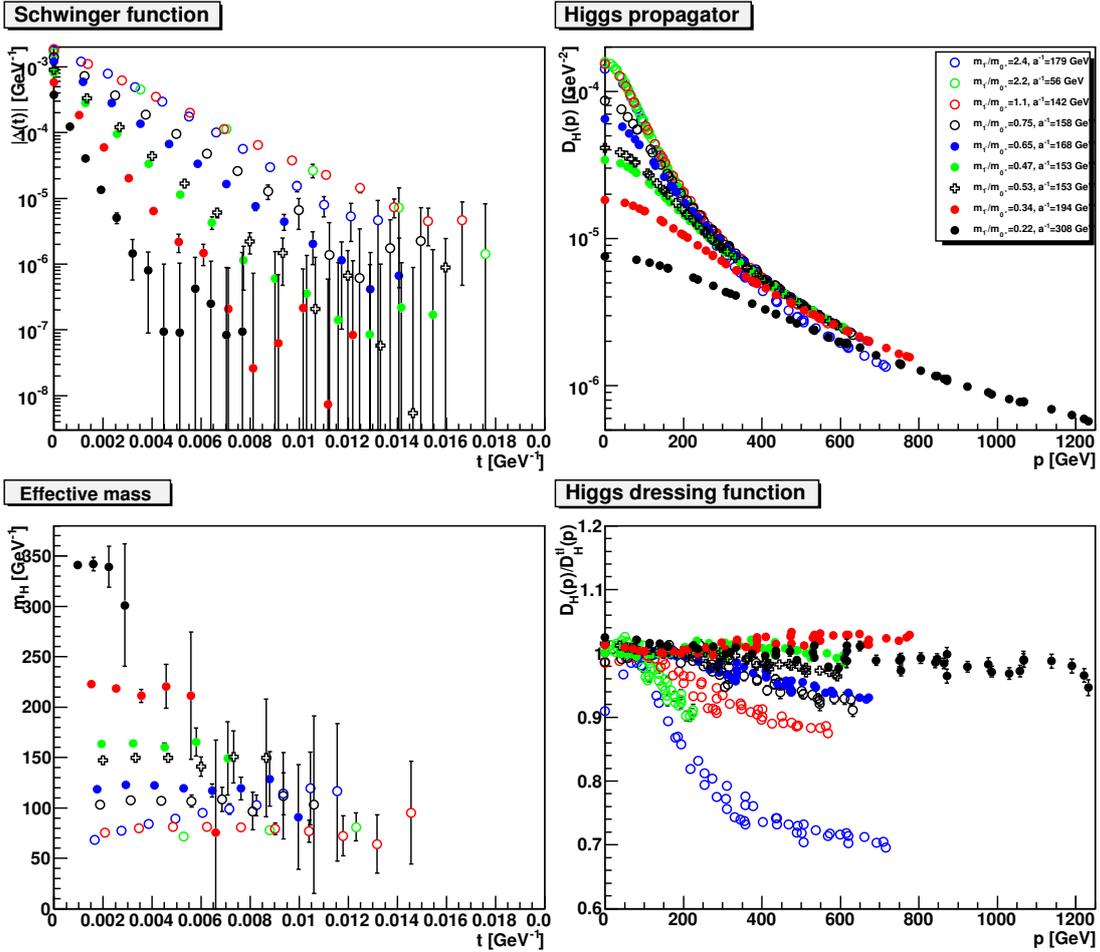

Figure 3.9: The Higgs propagator (top-right panel), dressing function (bottom-left panel), space-time function (top-left panel), and effective mass (bottom-left panel) for different mass ratios m_{1^-}/m_{0^+} on 24^4 lattices. All propagators are renormalized in the pole scheme.
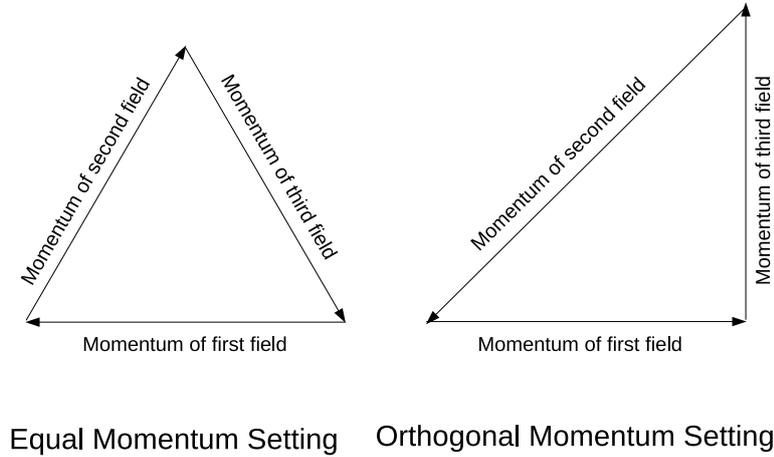
Figure 3.10: Different momentum settings for fields in vertices, Equal momentum setting (left) and Orthogonal momentum setting (right), are shown in the figure.

Two momentum settings are selected for the analysis of three point vertices, equal momentum setting (EMS) and orthogonal momentum setting (OMS). In EMS, all the momenta of the three fields involved in the correlation functions have equal momentum. For this situation, the only way they can conserve momentum is to have 60° as the minimum angle between the momentum vectors of all the fields. Pictorially, if these momenta are plotted as vectors, they will make an equilateral triangle. For the case of OMS, two of the fields involved in the correlation functions make a 90° angle with each other as the name implies. In order to conserve momentum, these fields have momentum components in such a way that if their momenta are plotted as vectors on a diagram, they will make a right triangle. Figure 3.10 is a pictorial way to explain the two settings [3].

In comparison, for the case of propagators these momentum settings were not a problem. The reason is that, loosely speaking, they are only two point vertices which means that two independent momentum selection can be made for two fields in one correlation function, and when the conservation of momentum is taken into account it will introduce one constraint on the two previously independent momentum values. Hence there is only one momentum for the two point functions calculated in above.

The dressing functions for the computed vertices have already been explained. It is the central part in understanding vertices, with respect to the projection of vertices (here tree level

---

[3]The third momentum setting, when in OMS the momenta along perpendicular and base of the right triangle are equal, is implicitly included. It is the situation when the two internal angles in right triangle are equal.
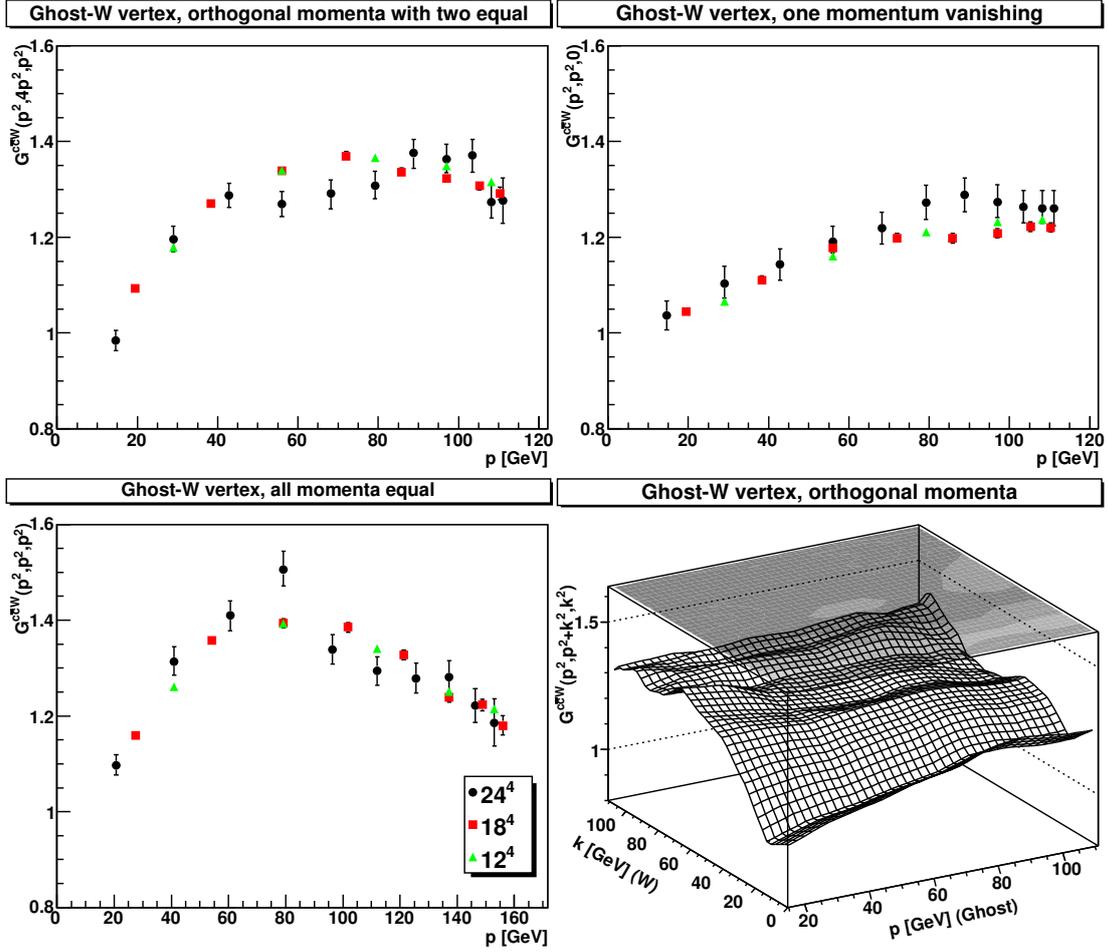
Figure 3.11: The ghost-W vertex. The top-left panel shows the case of equal ghost and W vertex, orthogonal to each other. The top-right panel shows the case for vanishing W momentum. The bottom-left panel shows the symmetric configuration. The bottom-right panel is a three-dimensional plot of the possible ghost and W momenta orthogonal to each other. The mass ratio is $m_{1^-}/m_{0^+} = 2.2$. The results are not renormalized.

expressions). Hence, from now on vertex and dressing function will be used interchangeably.

3.6.1 Ghost- Gauge Fields Vertices

The ghost-gauge field vertices are statistically the most easily, though not trivially, computable vertices [24]. Since the gauge selected is (minimal) Landau gauge there is also a ghost-anti-ghost symmetry [54]. Therefore, the momentum dependency for anti ghost field can be inferred from ghost field, and vice versa. For different Physics situation (different lines of constant Physics) the vertices are given in the figures 3.11-3.13.

Lets start with the QLD Physics. Figure 3.11 shows the ghost-gauge field vertices for different momentum settings. As the figure shows, there is a clear bump for the case when all momenta are equal. For this momentum setting, higher momentum values are accessible com-

Figure 3.12: The ghost-W vertex. The top-left panel shows the case of equal ghost and W vertex, orthogonal to each other. The top-right panel shows the case for vanishing W momentum. The bottom-left panel shows the symmetric configuration. The bottom-right panel is a three-dimensional plot of the possible ghost and W momenta orthogonal to each other. The mass ratio is $m_{1^-}/m_{0^+} = 0.65$. The results are is not renormalized.
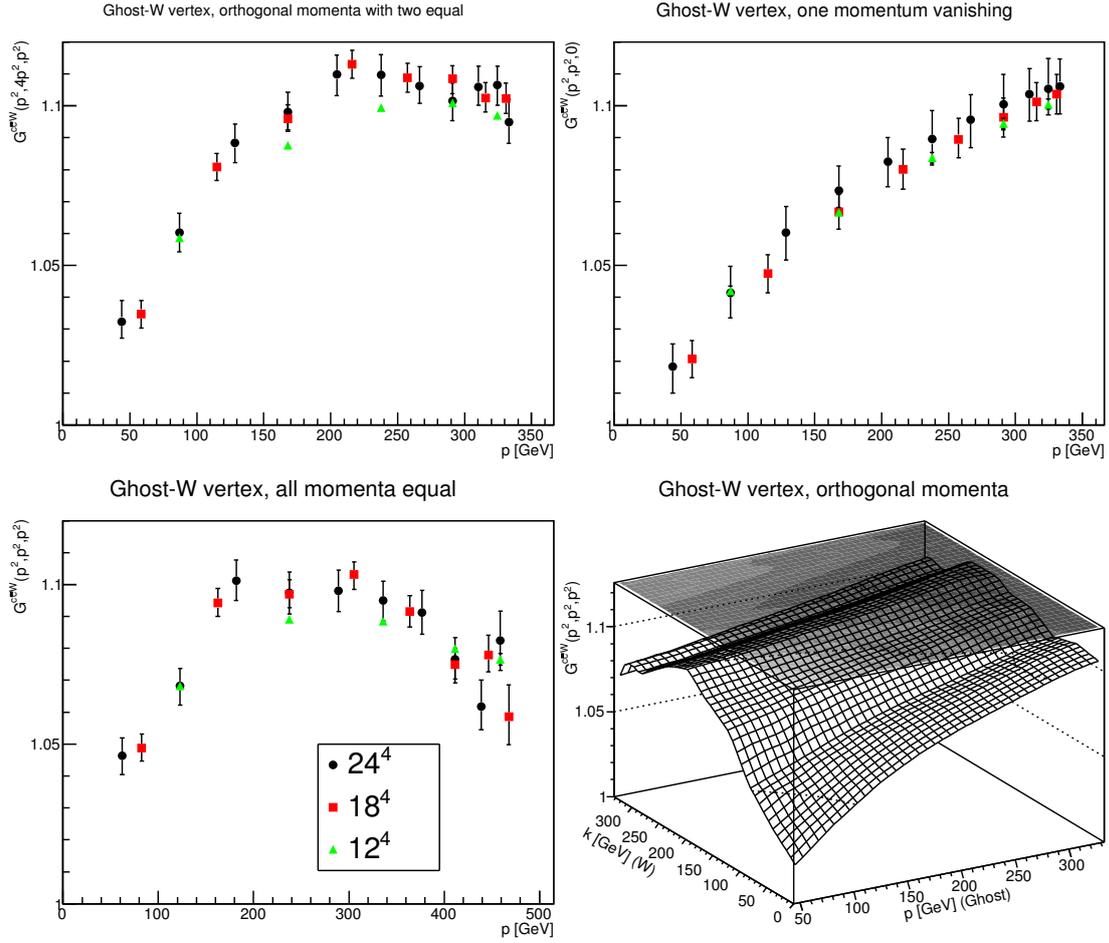
Figure 3.13: The ghost-W vertex. The top-left panel shows the case of equal ghost and W vertex, orthogonal to each other. The top-right panel shows the case for vanishing W momentum. The bottom-left panel shows the symmetric configuration. The bottom-right panel is a three-dimensional plot of the possible ghost and W momenta orthogonal to each other. The mass ratio is $m_{1^-}/m_{0^+} = 0.31$. The results are not renormalized.
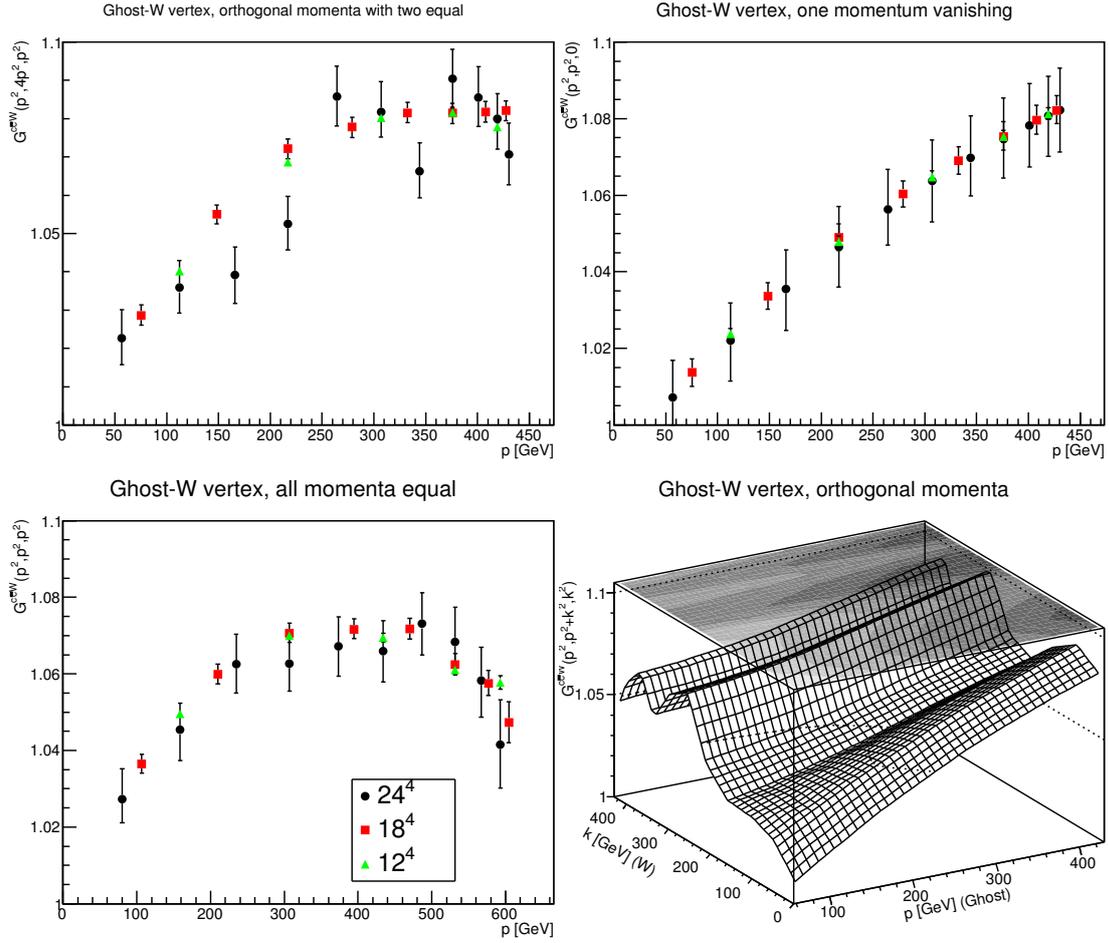
pared with other settings hence the bump in the figure is clearly visible for this setting. Other than this, it is not unfair to say that the vertex is rather flat while the bump is around the lightest bound state in the YMH theory. There is a similarity with SU(2) Yang-Mills theory [22, 54–58].

For the case of HLD, as in figures 3.12 and 3.13, the bump seems to be less prominent while at the same time it is also shifted towards higher momentum side around the values which is roughly two times the mass of the 0^+. It is also apparent from the equation 3.21 which comes from the relation between the ghost-gauge field vertex renormalization and the gauge and ghost propagators [59].

3.6.2   Three Gauge Fields Vertices

The three point vertices of 3 gauge fields are shown in figures 3.14-3.16. In comparison with gauge-ghost fields vertices, they are more effected by statistical fluctuations as in the figures. It is also observed in YM theory [55]. These fluctuations increase with momentum and grow considerably large to an extent that the results are not reliable after some momentum value as shown in the figures.

For the case of QLD, as in figure 3.14, there is some suppression in infrared momentum region, and shows some sign of zero crossing at some value of momentum. In comparison to YM theory, this behavior has already been observed [22, 55, 56, 58]. For the case of YM theory, the results in lower dimensions [55, 60, 61] show zero crossing, while for the case of four dimensions [55] the volumes are not large enough to make a conclusive statement. As the simulations are performed in four dimensions for YMH theory, the same problem is faced as in the results of YM theory in four dimensions. Hence, it remains to clearly observe the behavior in deep infrared region.

The vertices in HLD are shown in figures 3.15-3.16. The first observation is that for both values of 0^+ mass, there is no such suppression in the infrared region as in the case of QLD, though a slight tendency is still found which is surely not as clear as in the case of QLD. However, it remains to be seen what happens for larger lattices, which will give us a chance to go further in infrared region. Furthermore, there seems to be a slight dependency on the mass of 0^+ but with the current statistics, it is not possible to clarify it.

3.6.3   Scalar- Gauge Fields Vertices

In comparison to Yang-Mills theory, Higgs-gauge field vertex is the additional vertex which we get from the YMH theory. Not only is it important for understanding of YMH theory and Higgs effect [3], it is also important for studies of confinement in QLD [62]. Already there have been some speculations regarding this vertex and it remained to actually compute it and see how this vertex actually behaves. YMH theory provides a good laboratory for this vertex. However, it turns out to be the noisiest among the three point vertices in the theory and demands very

Figure 3.14: The three-W vertex. The top-left panel shows the case of equal ghost and W vertex, orthogonal to each other. The top-right panel shows the case for vanishing W momentum. The bottom-left panel shows the symmetric configuration. The bottom-right panel is a three-dimensional plot of the possible ghost and W momenta orthogonal to each other. The mass ratio is $m_{1^-}/m_{0^+} = 2.2$. The results are not renormalized.
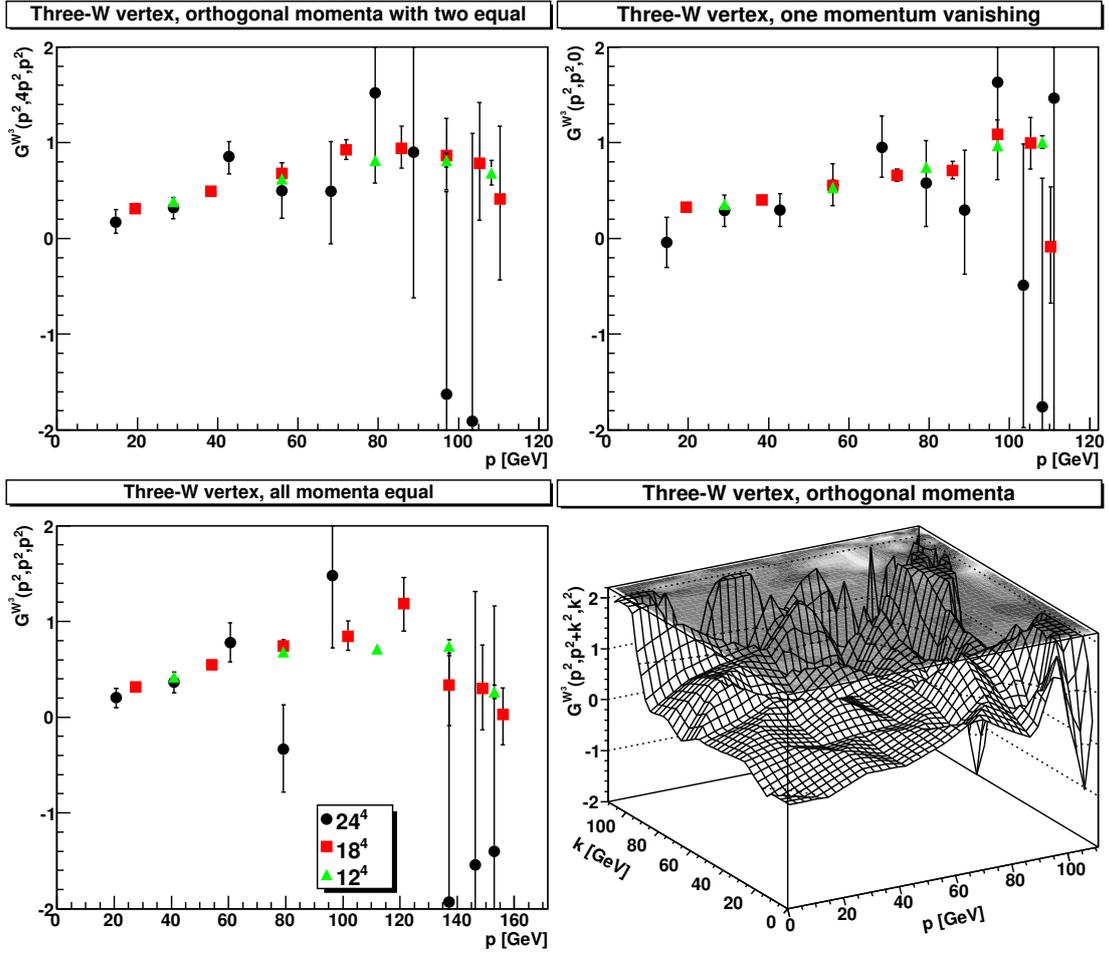
Figure 3.15: The three-W vertex. The top-left panel shows the case of equal ghost and W vertex, orthogonal to each other. The top-right panel shows the case for vanishing W momentum. The bottom-left panel shows the symmetric configuration. The bottom-right panel is a three-dimensional plot of the possible ghost and W momenta orthogonal to each other. The mass ratio is $m_{1^-}/m_{0^+} = 0.65$. The results are is not renormalized.

Figure 3.16: The three-W vertex. The top-left panel shows the case of equal ghost and W vertex, orthogonal to each other. The top-right panel shows the case for vanishing W momentum. The bottom-left panel shows the symmetric configuration. The bottom-right panel is a three-dimensional plot of the possible ghost and W momenta orthogonal to each other. The mass ratio is $m_{1^-}/m_{0^+} = 0.31$. The results are not renormalized.
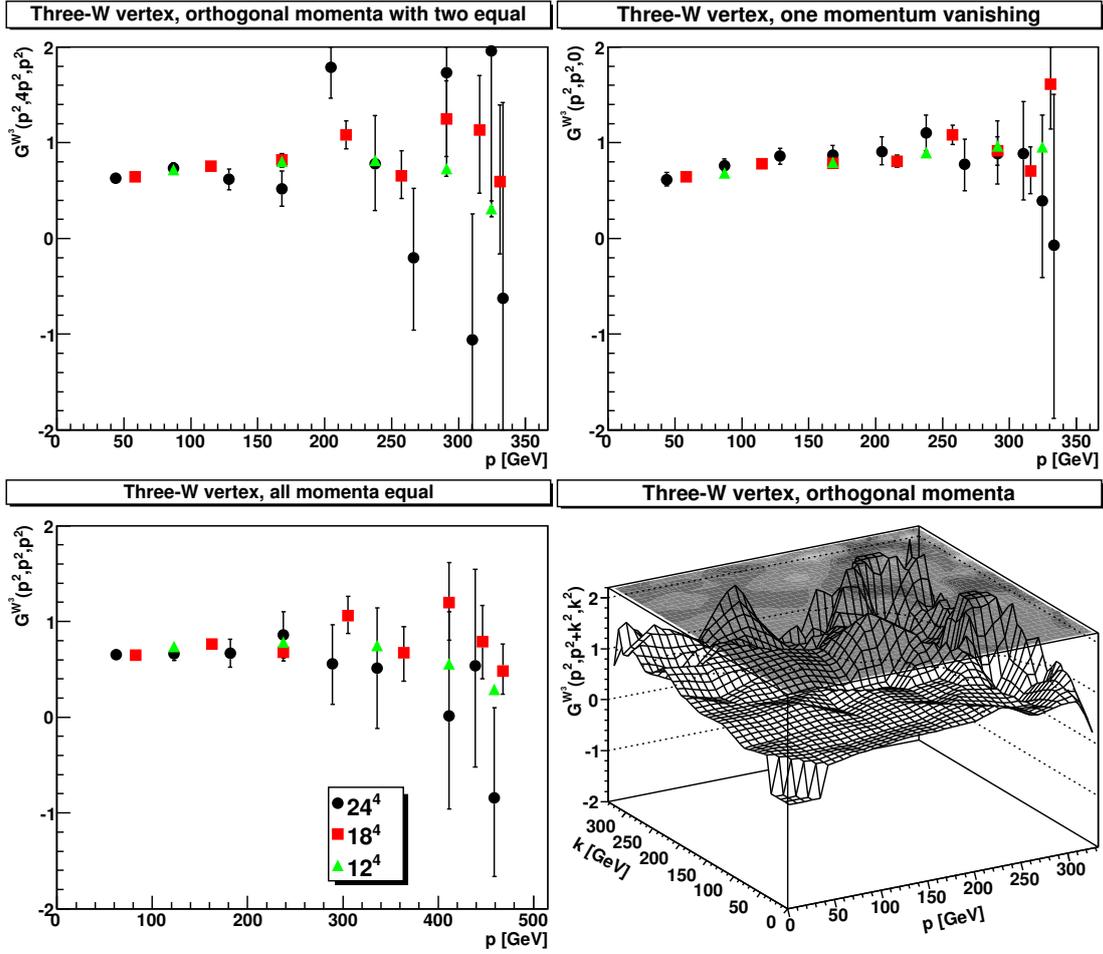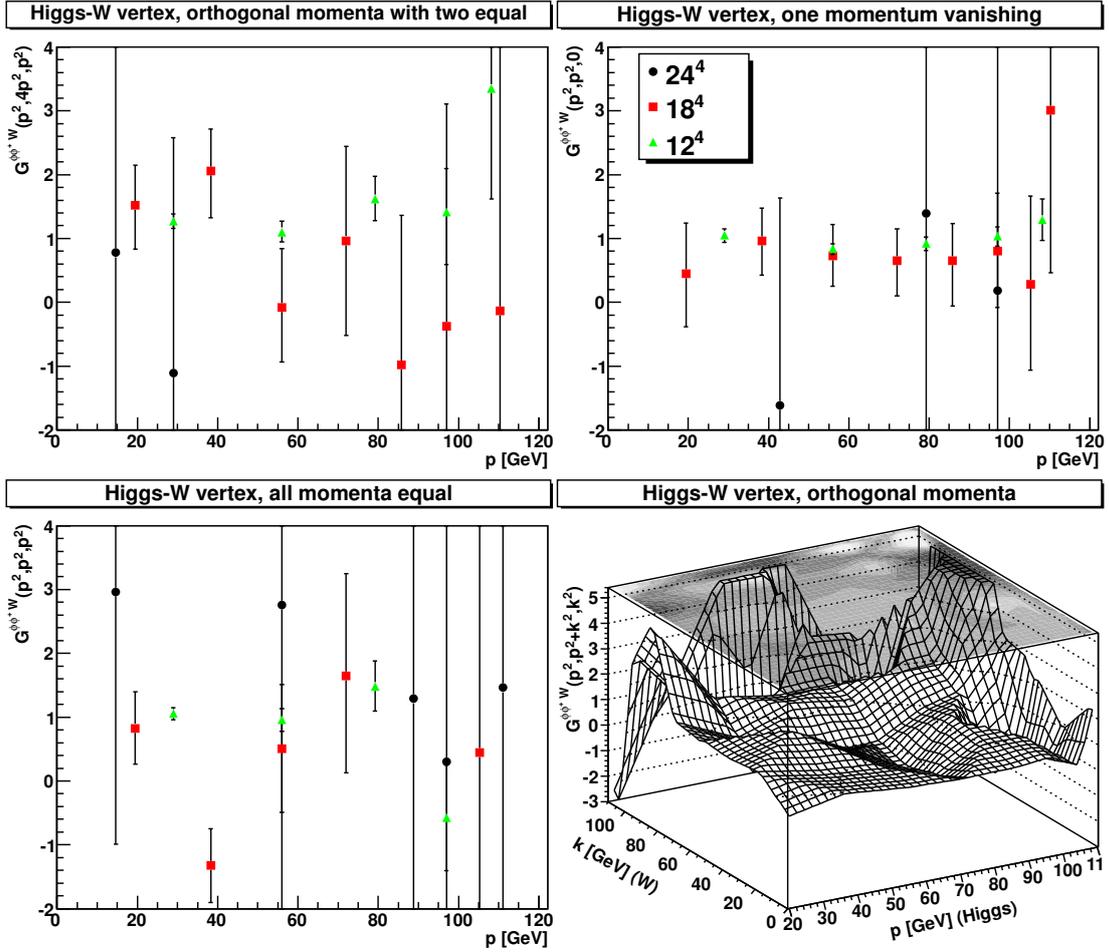
Figure 3.17: The Higgs-W vertex. The top-left panel shows the case of equal ghost and W vertex, orthogonal to each other. The top-right panel shows the case for vanishing W momentum. The bottom-left panel shows the symmetric configuration. The bottom-right panel is a three-dimensional plot of the possible ghost and W momenta orthogonal to each other. The mass ratio is $m_{1^-}/m_{0^+} = 2.2$. The results are not renormalized.
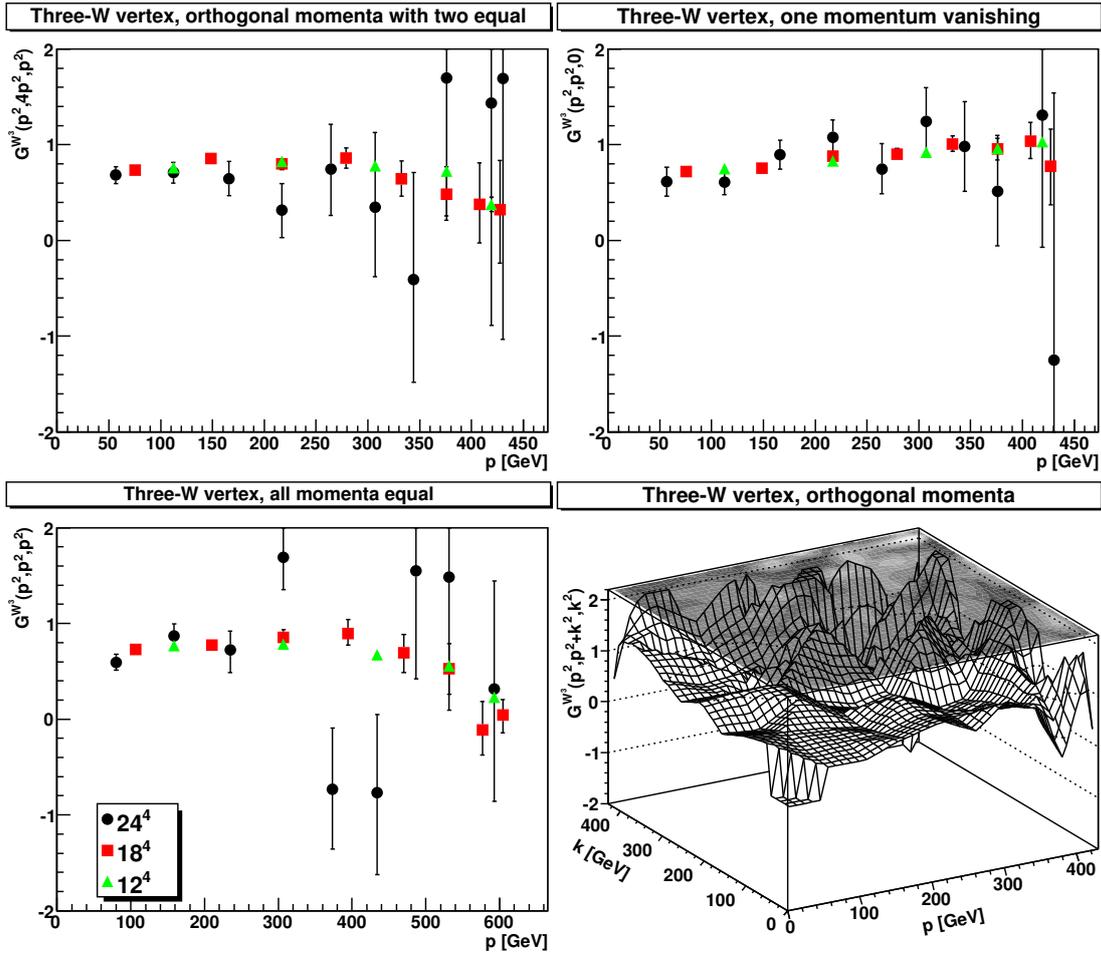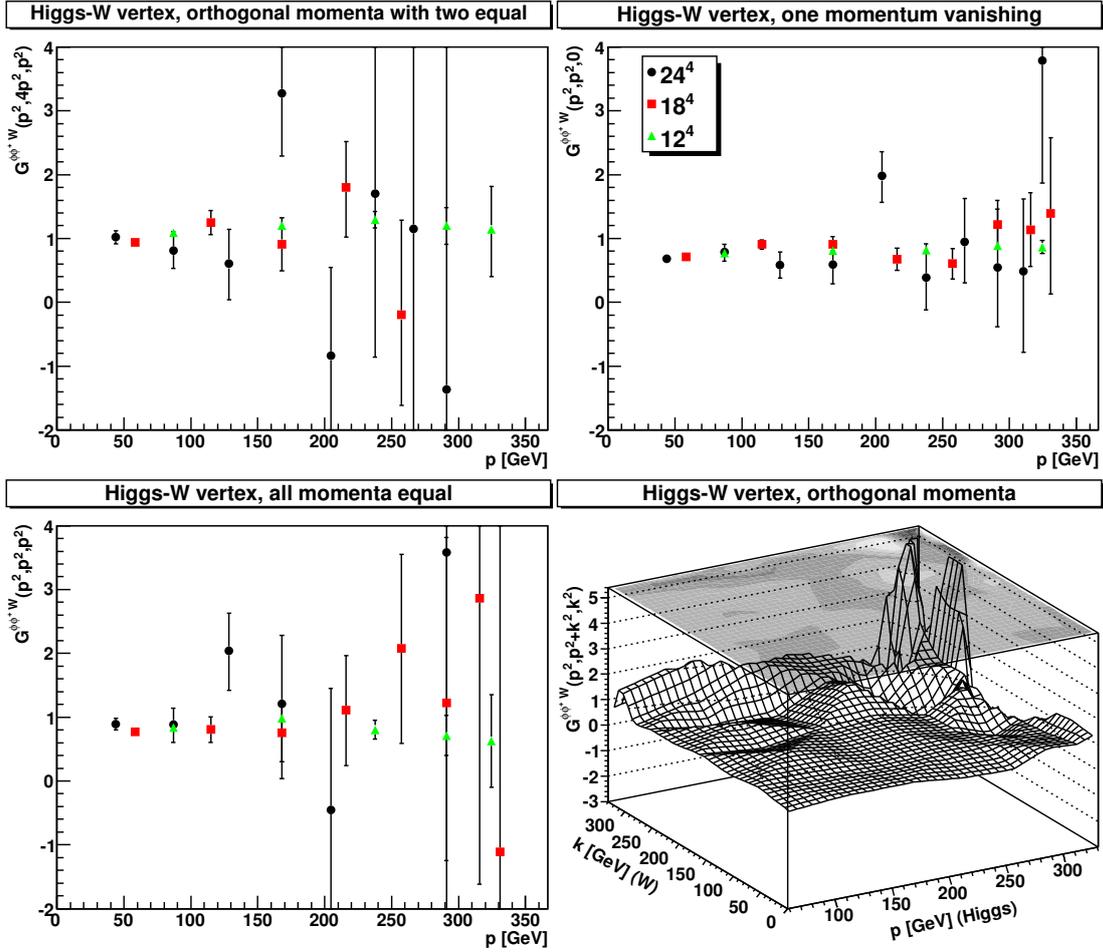
Figure 3.18: The Higgs-W vertex. The top-left panel shows the case of equal ghost and W vertex, orthogonal to each other. The top-right panel shows the case for vanishing W momentum. The bottom-left panel shows the symmetric configuration. The bottom-right panel is a three-dimensional plot of the possible ghost and W momenta orthogonal to each other. The mass ratio is $m_{1^-}/m_{0^+} = 0.65$. The results are is not renormalized.

Figure 3.19: The Higgs-W vertex. The top-left panel shows the case of equal ghost and W vertex, orthogonal to each other. The top-right panel shows the case for vanishing W momentum. The bottom-left panel shows the symmetric configuration. The bottom-right panel is a three-dimensional plot of the possible ghost and W momenta orthogonal to each other. The mass ratio is $m_{1^-}/m_{0^+} = 0.31$. The results are not renormalized.
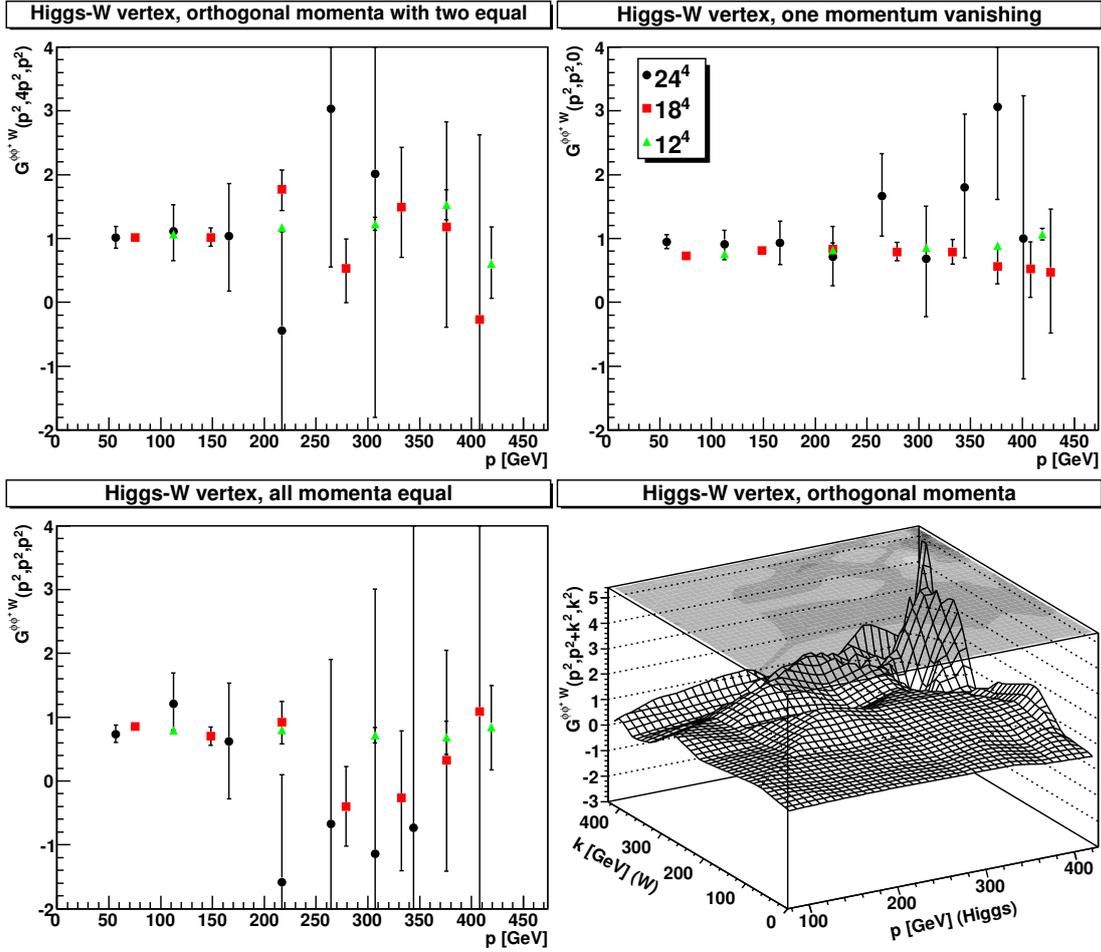
high statistics as already apparent in figures 3.17-3.19. Hence the results are shown as far as they make any sense at all. As in the figures, statistical noise increases with momentum, hence the points not shown in the results are for the high momentum values.

For the case of QLD Physics, the vertex is most effected by statistics, see figure 3.17. Though it is already very hard to conclude anything from the results, within statistical errors the dressing function seems to have a constant function around the value 1 against momentum for all cases. It implies that the Higgs-Gauge field vertex is very close to the tree level expression for the vertex. Hence the non-perturbative contribution for this vertex seems to be very small if any. However, it remains to confirm it by much more statistics which is undoubtedly a challenging task in terms of resources for computation. Since the dressing function seems to be a constant function of momentum, no infrared divergence or suppression is observed.

For the case of HLD Physics, the situation remains more or less the same. The dressing function is again very close to 1 and it behaves like a constant function. The only good news is that as the mass of 0^+ state increases (the ratio m_{1^-}/m_{0^+} decreases), the vertex becomes slightly less noisy as shown in figures 3.18 and 3.19. For HLD, no infrared divergence or suppression is observed.

For the quenched case, such flat behavior of functions have been observed and no angular dependence is observed [63] and [64].

To sum up, in all the explored three lines lines of constant Physics the dressing function seems like a constant function with no different behavior in the infrared region, and appears to preclude any possibility to obtain a strong contribution to the intermediate distance string tension from a single W exchange, as discussed for QCD [54, 65].

3.7 Running Gauge Coupling

The propagators, along with vertices, have already been discussed by now. Using only the gauge and ghost propagators, running gauge coupling can be defined in the miniMOM scheme [49, 59] as

$$\alpha(p^2) = \alpha(\mu^2)p^6 D_{Gh}(p^2,\mu^2)^2 D_w(p^2,\mu^2) \tag{3.36}$$

where $D_{Gh}(p^2,\mu^2)$ and $D_w(p^2,\mu^2)$ are ghost field and gauge field propagators, respectively. The scale μ^2 is the momentum value where the experimental input value for the running coupling is selected. Lets note here that running gauge coupling is a gauge dependent quantity and in PDG [30] the coupling is available at the Z mass in a different scheme. Since $\alpha(p^2)$ acts as merely a normalization constant, the ratio $\frac{\alpha(p^2)}{\alpha(\mu^2)}$ is considered for plotting in the figure 3.20. It is easy to anticipate that lattice artifacts on ghost and gauge field propagators enter directly into the running gauge coupling.

As in figure 3.20, for larger values of momentum all the plotted running gauge couplings
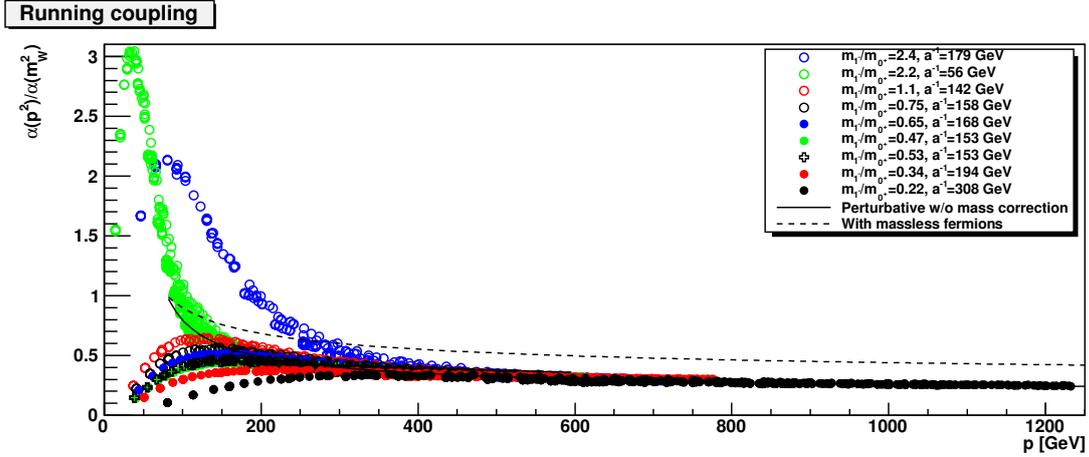
Figure 3.20: The running coupling for different mass ratios m_{1^-}/m_{0^+} on 24^4 lattices. Renormalization has been performed such as to agree with the perturbative running coupling at large momenta. See the text for details on the latter.

agree very well with the leading order massless running gauge coupling given by [13]

$$\frac{\alpha(p^2)}{\alpha(\mu^2)} = \frac{1}{1 + \frac{1}{4\pi}\beta_0 ln(\frac{p^2}{\mu^2})}$$

(3.37)

where β_0 is $\frac{43}{6}$ in this theory which is the the first coefficient of the $\beta-$function. There is a remarkable difference from that case with the 12 species of the SM fermions included, for which $\beta_0 = \frac{19}{6}$. For the case of YMH theory, the running gauge coupling is considerably weaker than the one with SM in which fermions are included, as remarked in [66].

For the momentum values of the order of the bound state masses between 50 and 250 GeV, a strong quantitative difference between the QLD like and HLD Physics is found. In QLD, the running gauge coupling shows a pronounced peak, like in YM theory [22]. In HLD, though it is by construction infrared and ultraviolet vanishing running coupling, only remnants of the peak does remain.

In our gauge, which is a non-aligned gauge [16], there is no three Higgs vertex, while currently no simple relations as the one for $\alpha(p^2)$ exist so that the 4 Higgs coupling could be computed. As stated already, the statistical noise is also a serious factor to be considered for any Higgs related coupling.

Chapter 4

Conclusions

The investigation discussed above gave us considerable insight into the YMH theory, while at the same time provided us the quantities which can be used for further studies. At the same time, it also raised a number of questions to consider for further investigation.

With the investigation conducted, some part of the parameter space of YMH theory is classified and it is known whether they belong to HLD or QLD, hence the Physics concerned with several regions in parameter space is further known [26]. In these explored regions there is also some information at hand how lattice artifacts effect, at least the explored, gauge invariant quantities in the theory. Despite the fact that still a lot of exploration needs to be done for finding lines of constant Physics, some more *approximate* LCPs are known to us now. Since now we already know some of the regions where it is possible to do Spectroscopy in an attempt to compare the results with experimentally known results, results from two sets of parameters have already been presented in chapter 2, along with other situations which are more interesting from theoretical point of view. Not only is the information about phenomenology is available at hand, we also have cases when it is actually possible to study transitions between channels, as an example is already included in chapter 2. It presented an opportunity to see how the theory behaves with a heavy state in 0^+ channel. It is also known from simulations how a gauge dependent quantity, which is not an observable, can mimic a gauge invariant quantity, which is also an observable. Based upon spectra from different parameters in both HLD and QLD, overall YMH theory appeared to behave like a weakly interacting theory.

For the gauge dependent quantities, one of the most important information comes for the vertices between gauge and scalar fields. YMH theory served as a laboratory to test how these vertices behave and if there is any extra ordinary feature of this vertex specially for the case of QCD like Physics. Despite that collecting reasonable statistics had been a very serious issue, at least from relatively smaller lattices we know how these vertices behave, and at the same time it also gave us at least a clue that there is no sign of suppression or divergence towards ultraviolet and infrared region, as far as we could explore on the momentum scale.

Another extraordinary finding was that the gauge field behaves like in Yang-Mills theory in QLD, which means that inclusion of the scalar field did not have any drastic effect on the gauge field. In general it is not expected since the simulations performed do not strictly forbid the fields from influencing each other in a Monte Carlo simulation. These similarities raises the question whether inclusion of more scalar fields will have any effect on such observed similarities.

One aspect of our findings is that for the case of heavy Higgs in HLD, all propagators and vertices are clearly in disagreement with their tree level counterparts, as in chapter 3. It clearly means that were the experimentally found Higgs particle heavier enough, it would not be accessible by perturbation theory at all [3]. Hence we should consider ourselves very lucky with a relatively light Higgs so that we could have a possibility to compare the results from perturbative and non-perturbative calculations.

Our findings are also very useful for investigating the theory, calculation approaches and computation techniques. The whole investigation was an effort towards finding new correlation functions which is a crucial requirement for DSEs, and also FRGs. For the DSEs, with these correlation functions known, they can serve as input to DSEs rather than as ansatzes for DSEs, and new correlation functions can be calculated which are either not calculated, or difficult to deal with by other non-perturbative approaches. Note that from lattice calculations, no analytical results are obtained, and it remains always a question how reliable any interpolation or extrapolation is.

At the moment, the immediate step is to have more statistics in order to be able to conclusively observe if there is any new state which is not what we naively expected. Finding a new state will surely be a great achievement since it will also show that there is more in nature than what we could naively expect while assuming that the YMH theory is a weakly interacting theory. If bound states really exist in nature, and they are theoretically found and experimentally discovered, it will surely help us in cataloging the findings during the searches for new Physics. At the same time, they will also open the door for Spectroscopy which is interesting both from the point of view of phenomenology as well as experiments.

It also remains to be seen what happens in the extreme infrared region. For this purpose, larger lattice sizes need to be considered with lattice calculations. It also remains to find more LCPs and more points on the already known LCPs which will eventually take us very close to the continuum if it exists. Furthermore, it will also help us in conclusively finding the renormalization scheme which is crucially important for calculations.

From the side of completely understanding the theory itself, other channels are also to be thoroughly explored which will also result in a much richer Spectroscopy than it is with only two channels explored [31]. Already knowledge from another channel was used while exploring the LCPs. It clearly implies how important such explorations are.

The results from computation of quantities and their analysis are very encouraging to explore the theory further. Besides the computation and understanding of Physics, they can be used as input for other non-perturbative calculation methods, such as DSEs. However, there are a number of problems in the theory which really need to be addressed in order to fully understand the theory. The first, and perhaps the most important one, is the triviality of the theory in non-perturbative sense. As it is already stated before, there is no conclusive proof for the triviality of the theory, it remains to be seen whether the theory is truly a non-trivial theory. The second problem is to check if there are possible lattice artifacts when the lattice size is increased and/or finer lattices are used. Furthermore, the remormalization of, particularly, scalar propagator needs to be understood.

For an extension of the work done, the first non-trivial extension of YMH theory is to include the QED sector in the theory so that degeneracy in gauge boson masses is lifted, and fermions are added in the theory. It will turn this relatively simpler theory into the theory which could describe nature more completely. It may bring changes in the quantities already computed but as a theory which could be a true description of the nature, it will allow us to make predictions with more confidence which is, in the author's opinion, the ultimate goal of scientific research.

Ehrenwörtliche Erklärung

Ich erkläre hiermit ehrenwörtlich, dass ich die vorliegende Arbeit selbstständig, ohne unzulässige Hilfe Dritter und ohne Benutzung anderer als der angegebenen Hilfsmittel und Literatur angefertigt habe. Die aus anderen Quellen direkt oder indirekt übernommenen Daten und Konzepte sind unter Angabe der Quelle gekennzeichnet. Ergebnisse, die in Zusammenarbeit mit den Mitgliedern des Lehrstuhles für Quantenfeldtheorie in Jena und anderen Kooperationen entstanden sind, sind in der Arbeit entsprechend benannt.

Weitere Personen waren an der inhaltlich-materiellen Erstellung der vorliegenden Arbeit nicht beteiligt. Insbesondere habe ich hierfür nicht die entgeltliche Hilfe von Vermittlungs- bzw. Beratungsdiensten (Promotionsberatern und andere Personen) in Anspruch genommen. Niemand hat von mir unmittelbar oder mittelbar geldwerte Leistungen für Arbeiten erhalten, die im Zusammenhang mit dem Inhalt der vorgelegten Dissertation stehen.

Die Arbeit wurde bisher weder im In- noch im Ausland in gleicher oder ähnlicher Form einer anderen Prüfungsbehörde vorgelegt.

Die geltende Promotionsordnung der Physikalisch-Astronomischen Fakultät ist mir bekannt. Ich versichere ehrenwörtlich, dass ich nach bestem Wissen die reine Wahrheit gesagt und nichts verschwiegen habe.

Jena, 06.12.2014

Tajdar Mufti

Bibliography

[1] Riazuddin Fayyazuddin. *A Modern Introduction to Particle Physics, Second Edition*. World Scientific Publishing, P.O.Box 128, Farrer Road, Singapore 912805, 2000. Singapore: World Scientific Publishing (2000) 737 p.

[2] G. 't Hooft. The making of the standard model. *Nature*, 448:271–273, 2007.

[3] M. Bohm, Ansgar Denner, and H. Joos. *Gauge theories of the strong and electroweak interaction*. Teubner, Stuttgart, 2001. Stuttgart, Germany: Teubner (2001) 784 p.

[4] Pierre Binetruy. *Supersymmetry Theory, Experiment, and Cosmology*. Oxford Graduate Texts, Oxford, 2006. Oxford Press.

[5] CMS Collaboration. Search for Displaced SUSY in Dilepton Final States. 2014.

[6] Dezsö Horváth. Search for the Higgs boson: a statistical adventure of exclusion and discovery. *J.Phys.Conf.Ser.*, 510:012001, 2014.

[7] G. Aad et al. Charged-particle multiplicities in pp interactions at $\sqrt{s} = 900$ GeV measured with the ATLAS detector at the LHC. *Phys.Lett.*, B688:21–42, 2010.

[8] M. Fanti. Combination of all searches and extraction of properties of the Higgs boson (ATLAS and CMS). *PoS*, Photon2013:076, 2014.

[9] Reinhard Alkofer and J. Greensite. Quark Confinement: The Hard Problem of Hadron Physics. *J.Phys.*, G34:S3, 2007.

[10] Eric S. Swanson. A Primer on Functional Methods and the Schwinger-Dyson Equations. *AIP Conf.Proc.*, 1296:75–121, 2010.

[11] Holger Gies. Introduction to the functional RG and applications to gauge theories. *Lect.Notes Phys.*, 852:287–348, 2012.

[12] Heinz J. Rothe. *Lattice Gauge Theories, An Introduction*. World Scientific, London, 1996. London, UK: world Scientific (1996) 381 p.

[13] Axel Maas and Tajdar Mufti. Two-and three-point functions in Landau gauge Yang-Mills-Higgs theory. *JHEP*, 10.1007/JHEP04(2014):006, 2014.

[14] Axel Maas. Some more details of minimal-Landau-gauge Yang-Mills propagators. 2014.

[15] Martin Lüscher. Signatures of unstable particles in finite volume. *Nucl.Phys.*, B364:237–254, 1991.

[16] Axel Maas. (non-)aligned gauges and global gauge symmetry breaking. *Mod. Phys. Lett. A*, 27(38):1250222, 2012.

[17] Bernard F. Schutz. *A First Course in General Relativity.* Cambridge University Press, Cambridge, 1985. Cambridge, UK: Cambridge University Press (1985) 388 p.

[18] Menahem Schiffer Ronald Adler, Maurice Bazin. *Introduction to General Relativity.* 1965.

[19] Christof Gattringer and Christian B Lang. *Quantum Chromodynamics on the Lattice.* Springer, Berlin, 2010. Heidelberg, Germany: Springer (2010) 343 p.

[20] S.F. Novaes. Standard model: An Introduction. 1999.

[21] David J.E. Callaway. Triviality Pursuit: Can Elementary Scalar Particles Exist? *Phys.Rept.*, 167:241, 1988.

[22] Axel Maas. Describing gauge bosons at zero and finite temperature. *Phys. Rep.*, 524:203, 2013.

[23] Axel Maas. Accessing directly the properties of fundamental scalars in the confinement and Higgs phase. *Eur. Phys. J.*, C71:1548, 2011.

[24] Attilio Cucchieri, Axel Maas, and Tereza Mendes. Exploratory study of three-point Green's functions in Landau-gauge Yang-Mills theory. *Phys. Rev.*, D74:014503, 2006.

[25] W. Langguth, I. Montvay, and P. Weisz. MONTE CARLO STUDY OF THE STANDARD SU(2) HIGGS MODEL. *Nucl. Phys.*, B277:11, 1986.

[26] J. Jersak, C. B. Lang, T. Neuhaus, and G. Vones. PROPERTIES OF PHASE TRANSITIONS OF THE LATTICE SU(2) HIGGS MODEL. *Phys. Rev.*, D32:2761, 1985.

[27] Axel Maas. Bound-state/elementary-particle duality in the Higgs sector and the case for an excited 'Higgs' within the standard model. *Mod.Phys.Lett.*, A28:1350103, 2013.

[28] C. B. Lang H G Evertz, J. Jersak and T.Neuhaus. SU(2) Higgs Boson and Vector Boson Masses on the Lattice. *Phys. lett. B*, 171:2, 1986.

[29] O. Philipsen, M. Teper, and H. Wittig. On the mass spectrum of the SU(2) Higgs model in (2+1)- dimensions. *Nucl.Phys.*, B469:445–472, 1996.

[30] J. Beringer et al. (Particle Data Group). *Phys. Rev. D*, 86:010001, 2012.

[31] Axel Maas and Tajdar Mufti. Unpublished.

[32] M. Luscher. Volume Dependence of the Energy Spectrum in Massive Quantum Field Theories. 2. Scattering States. *Commun.Math.Phys.*, 105:153–188, 1986.

[33] Xu Feng, Karl Jansen, and Dru B. Renner. A new moving frame to extract scattering phases in lattice QCD. *PoS*, LATTICE2010:104, 2010.

[34] V.N. Gribov. Quantization of Nonabelian Gauge Theories. *Nucl.Phys.*, B139:1, 1978.

[35] I.M. Singer. Some Remarks on the Gribov Ambiguity. *Commun.Math.Phys.*, 60:7–12, 1978.

[36] Daniel Zwanziger. Fundamental modular region, Boltzmann factor and area law in lattice gauge theory. *Nucl.Phys.*, B412:657–730, 1994.

[37] F. Karsch and J. Rank. Landau gauge fixing and finite temperature gluon propagator in SU(2) lattice gauge theory. *Nucl. Phys. Proc. Suppl.*, 42:508–510, 1995. Polyakov loop and the gluon propagator.

[38] Axel Maas. On the structure of the residual gauge orbit. *PoS*, QCD-TNT-II:028, 2011.

[39] Axel Maas. Local and global gauge-fixing. *PoS*, ConfinementX:034, 2012.

[40] Axel Maas. More on Gribov copies and propagators in Landau-gauge Yang-Mills theory. *Phys. Rev.*, D79:014505, 2009.

[41] Eduardo H. Fradkin and Stephen H. Shenker. Phase Diagrams of Lattice Gauge Theories with Higgs Fields. *Phys. Rev.*, D19:3682–3697, 1979.

[42] Francesco Knechtli and Rainer Sommer. String breaking in SU(2) gauge theory with scalar matter fields. *Phys. Lett.*, B440:345–352, 1998.

[43] Francesco Knechtli. Determining lines of constant physics in the confinement phase of the SU(2) Higgs model. *Phys. Lett.*, B478:387–393, 2000.

[44] C. Bonati, G. Cossu, M. D'Elia, and A. Di Giacomo. Phase diagram of the lattice SU(2) Higgs model. *Nucl. Phys.*, B828:390–403, 2010.

[45] W. Langguth and I. Montvay. TWO STATE SIGNAL AT THE CONFINEMENT HIGGS PHASE TRANSITION IN THE STANDARD SU(2) HIGGS MODEL. *Phys. Lett.*, B165:135, 1985.

[46] Christian S. Fischer, Axel Maas, and Jan M. Pawlowski. On the infrared behavior of Landau gauge Yang-Mills theory. *Annals Phys.*, 324:2408–2437, 2009.

[47] Patrick O. Bowman et al. Scaling behavior and positivity violation of the gluon propagator in full QCD. *Phys. Rev.*, D76:094505, 2007.

[48] Reinhard Alkofer, W. Detmold, C. S. Fischer, and P. Maris. Analytic properties of the Landau gauge gluon and quark propagators. *Phys. Rev.*, D70:014014, 2004.

[49] Lorenz von Smekal, Kim Maltman, and Andre Sternbeck. The strong coupling and its running to four loops in a minimal MOM scheme. *Phys. Lett.*, B681:336–342, 2009. mini-MOM.

[50] Attilio Cucchieri and Tereza Mendes. Constraints on the IR behavior of the ghost propagator in Yang-Mills theories. *Phys. Rev.*, D78:094503, 2008. Large lattice.

[51] I. L. Bogolubsky, E. M. Ilgenfritz, M. Müller-Preussker, and A. Sternbeck. Lattice gluodynamics computation of Landau gauge Green's functions in the deep infrared. *Phys. Lett.*, B676:69–73, 2009. Large lattices.

[52] A. Sternbeck, L. von Smekal, D. B. Leinweber, and A. G. Williams. Comparing SU(2) to SU(3) gluodynamics on large lattices. *PoS*, LAT2007:340, 2007.

[53] Jeff Greensite, Štefan Olejník, and Daniel Zwanziger. Coulomb energy, remnant symmetry, and the phases of non- Abelian gauge theories. *Phys. Rev.*, D69:074506, 2004.

[54] Reinhard Alkofer and Lorenz von Smekal. The infrared behavior of QCD Green's functions: Confinement, dynamical symmetry breaking, and hadrons as relativistic bound states. *Phys. Rept.*, 353:281, 2001.

[55] Attilio Cucchieri, Axel Maas, and Tereza Mendes. Three-point vertices in Landau-gauge Yang-Mills theory. *Phys. Rev.*, D77:094510, 2008.

[56] Markus Q. Huber and Lorenz von Smekal. On the influence of three-point functions on the propagators of Landau gauge Yang-Mills theory. *JHEP*, 1304:149, 2013.

[57] Leonard Fister and Jan M. Pawlowski. Yang-mills correlation functions at finite temperature. 2011.

[58] Marcela Pelaez, Matthieu Tissier, and Nicolas Wschebor. Three-point correlation functions in Yang-Mills theory. *Phys.Rev.*, D88:125003, 2013.

[59] Lorenz von Smekal, Andreas Hauck, and Reinhard Alkofer. A solution to coupled Dyson-Schwinger equations for gluons and ghosts in Landau gauge. *Ann. Phys.*, 267:1, 1998.

[60] Axel Maas. Two- and three-point Green's functions in two-dimensional Landau-gauge Yang-Mills theory. *Phys. Rev.*, D75:116004, 2007.

[61] Markus Q. Huber, Axel Maas, and Lorenz von Smekal. Two- and three-point functions in two-dimensional Landau-gauge Yang-Mills theory: Continuum results. *JHEP*, 1211:035, 2012.

[62] Leonard Fister, Reinhard Alkofer, and Kai Schwenzer. On the Infrared Behavior of Landau Gauge Yang-Mills Theory with a Fundamentally Charged Scalar Field. *Phys. Lett.*, B688:237–243, 2010.

[63] Axel Maas. Scalar-matter-gluon interaction. *PoS*, FacesQCD:033, 2011.

[64] A. Maas. *Quenched fundamental and adjoint Higgs 2-point and 3-point functions, unpublished*.

[65] Reinhard Alkofer, Christian S. Fischer, Felipe J. Llanes-Estrada, and Kai Schwenzer. The quark-gluon vertex in Landau gauge QCD: Its role in dynamical chiral symmetry breaking and quark confinement. *Annals Phys.*, 324:106–172, 2009.

[66] Axel Maas and Tajdar Mufti. Exploring Higgs Sector Spectroscopy. *PoS*, LATTICE 2013:056, 2013.